Bessel correlations and Bessel beams

VRIJE UNIVERSITEIT

Bessel correlations and Bessel beams

ACADEMISCH PROEFSCHRIFT

ter verkrijging van de graad Doctor aan
de Vrije Universiteit Amsterdam,
op gezag van de rector magnificus
prof.dr. V. Subramaniam,
in het openbaar te verdedigen
ten overstaan van de promotiecommissie
van de Faculteit der Exacte Wetenschappen
op dinsdag 20 Juni 2017 om 15.45 uur
in de aula van de universiteit,
De Boelelaan 1105

door

Yangyundou Wang

geboren te Jishan, Shanxi, China

promotor: prof.dr. T.D. Visser

Samenstelling leescommissie:

prof.dr. W.M.G. Ubachs,	Vrije Universiteit, Amsterdam, The Netherlands
prof.dr. B.J. Hoenders,	Universiteit Groningen, The Netherlands
prof.dr. G.J. Gbur,	University of North Carolina at Charlotte, USA
prof.dr. P.S. Carney,	University of Illinois at Urbana-Champaign, USA
dr. H.F. Schouten,	Vrije Universiteit, Amsterdam, The Netherlands

This work was financially supported by Northwestern Polytechnical University, Xi'an, China.

Contents

Contents **7**

1 Introduction **11**
- 1.1 Introduction 11
- 1.2 Elements of optical coherence 12
  - 1.2.1 Complex analytic signals 12
  - 1.2.2 Correlation functions in the space-time domain . . . 13
  - 1.2.3 Correlations in the space-frequency domain 19
  - 1.2.4 How correlations propagate 23
- 1.3 Elements of optical scattering 29
- 1.4 Outline of this thesis 32
  - 1.4.1 Publications 34

2 Dynamic control of light scattering using spatial coherence **35**
- 2.1 Introduction 36
- 2.2 Partially coherent sources 37
- 2.3 Scattering by a Gaussian-correlated sphere 39
- 2.4 Gaussian Schell-model sources 41
- 2.5 Uncorrelated annular sources 43
- 2.6 Uncorrelated, infinitely thin annular sources 45
- 2.7 Conclusions 47
- Appendix A - Derivation of Eq. (2.25) 48
- Appendix B - Derivation of Eq. (2.31) 50
- Appendix C - Derivation of Eq. (2.34) 52

3 Tuneable, anomalous Mie scattering using partial coherence 55
3.1 Introduction 56
3.2 Mie scattering with partially coherent fields 57
3.3 J_0-correlated fields 60
3.4 Changing the coherence length 64
3.5 Total scattered power 65
3.6 Conclusions 67

4 Strong suppression of forward or backward Mie scattering by using spatial coherence 69
4.1 Introduction 70
4.2 Scalar Mie scattering 71
4.3 Mie scattering with J_0 Bessel-correlated fields 73
4.4 Suppression of forward scattering 74
4.5 Suppression of backward scattering 78
4.6 Conclusions 79
Appendix A - Derivation of Eq. (4.13) 80

5 Creating von Laue patterns in crystal scattering with partially coherent sources 83
5.1 Introduction 85
5.2 Scattering from crystalline structures 86
5.3 Orthorhombic crystals 90
5.4 Gaussian Schell-model sources 92
5.5 Uncorrelated, infinitely thin annular sources 97
5.6 Conclusions 101

6 The electromagnetic field produced by a refractive axicon 105
6.1 Introduction 106
6.2 Geometrical rays 107
6.3 Scalar fields 109
6.3.1 The axial intensity 114
6.3.2 The transverse intensity 114
6.4 Electromagnetic fields 117
6.4.1 Linear polarization 117
6.4.2 Radial Polarization 122

6.4.3 Azimuthal Polarization 123
6.5 The electromagnetic field of an axicon 124
6.5.1 The axial intensity 124
6.5.2 The effective wavelength on axis 126
6.5.3 The transverse intensity 126
6.5.4 The far-zone intensity 129
6.6 Conclusions 132
Appendix A - Derivation of Eq. (6.23) 133
Appendix B - Derivation of Eq. (6.89) 134

Bibliography **137**

Summary in Dutch **147**

Chapter 1

Introduction

1.1 Introduction

Light scattering is perhaps the most fundamental of optical processes. It is encountered in many branches of the natural sciences, for example in astronomy, meteorology, atomic physics, and in solid-state physics. An important example is scattering by a spherical object. Descartes described the rainbow in terms of refraction and reflection of light rays by spherical water droplets almost 400 years ago [Haussmann, 2016]. But it was not until 1908 that Mie [Mie, 1908] provided a rigorous (but very complicated) solution to the problem of scattering of light by spherical particles. Since then, Mie's theory has been applied to fields like quantum scattering, non-linear optics, and atmospheric scattering [Hergert and Wriedt (eds.), 2012]. In this thesis, we will make extensive use of scalar Mie theory.

Another topic of this thesis is optical coherence theory. Its general framework has been described in numerous publications [Beran and Parrent, 1964; Born and Wolf, 1995; Goodman, 1985; Mandel and Wolf, 1995; Marathay, 1982; Perina, 1985; Schouten and Visser, 2008; Troup, 1985; Wolf, 2007; Gbur and Visser, 2010]. Coherence is essentially a consequence of correlations between some components of the fluctuating electric field at two (or more) points in space or in time, and is manifested by the sharpness of fringes in Young's interference experiment. The basic tools of coherence theory are correlation functions and correlation matrices which, unlike some directly measurable quantities such as the spectrum of light, obey precise propagation laws. With the help of these laws one may determine, for example, spectral and polarization changes that occur as the light propagates.

In this thesis we study the effects of coherence on scattering. We therefore begin by briefly reviewing these two topics.

1.2 Elements of optical coherence

In physics one can distinguish two types of processes: those that are *deterministic*, and those that are *random*. Deterministic processes are predictable. In classical mechanics, for example, knowledge of the present position of an object, together with its mass, velocity and the forces that act upon it, completely determines its future position and velocity. Random processes, on the other hand, are inherently non-predictable. An example is provided by quantum mechanics, which holds as a central tenet the stochastic nature of an event like spontaneous emission. Such random or *non-deterministic* processes can be characterized by their statistical behavior. This behavior describes the average value of a process, how much it fluctuates, and how fast or slow these fluctuations occur in space and time. In other words, we can describe random processes by their mean, their standard deviation, and their correlation functions. We begin this informal description of random optical processes by briefly reviewing fundamental concepts such as the complex analytic signal representation, ensembles, ergodicity and stationarity. This will allow us to introduce correlation functions in both the space-time domain (Section 1.2.2) and the space-frequency domain (Section 1.2.3). The propagation of correlation functions is governed by precise laws, as is discussed in Section 1.2.4.

1.2.1 Complex analytic signals

Although optical fields are real-valued, it is often more convenient to use complex-valued quantities. We therefore begin our mathematical description of wave fields by introducing their so-called *complex analytic signal representation* [Mandel and Wolf, 1995, Sec. 3.1]. Let us write a scalar optical field $u(\mathbf{r}, t)$, where $\mathbf{r}$ denotes a position in space and t is a moment in time, as a temporal Fourier transform, namely

$$u(\mathbf{r}, t) = \int_{-\infty}^{\infty} \tilde{u}(\mathbf{r}, \omega)\, e^{-\mathrm{i}\omega t}\, \mathrm{d}\omega. \tag{1.1}$$

Because $u(\mathbf{r}, t)$ is real-valued, we have that

$$\tilde{u}(\mathbf{r}, -\omega) = \tilde{u}^*(\mathbf{r}, \omega). \tag{1.2}$$

This result implies that the negative frequency components ($\omega < 0$) do not contain any information that is not present in the positive frequency components ($\omega > 0$). We can therefore associate with the field a new function

$$V(\mathbf{r}, t) = \int_{0}^{\infty} \tilde{u}(\mathbf{r}, \omega)\, e^{-\mathrm{i}\omega t}\, \mathrm{d}\omega, \tag{1.3}$$

where the integral now ranges from zero to infinity. The field $V(\mathbf{r}, t)$ is called the complex analytic signal representation of the real field $u(\mathbf{r}, t)$. One can readily show that

$$u(\mathbf{r}, t) = 2\,\mathrm{Re}\, V(\mathbf{r}, t). \tag{1.4}$$

In words, the real-valued field $u(\mathbf{r}, t)$ is equal to two times the real part of its associated complex analytic signal $V(\mathbf{r}, t)$.

An optical wave field $u(\mathbf{r}, t)$ has a temporal mean that is zero: the probability that it takes on a positive value is equal to the probability that it is negative, i.e.,

$$\langle u(\mathbf{r}, t) \rangle \equiv \lim_{T\to\infty} \frac{1}{2T} \int_{-T}^{+T} u(\mathbf{r}, t)\, \mathrm{d}t = 0. \tag{1.5}$$

A proof that the analytic signal representation of $u(\mathbf{r}, t)$ is also a zero-mean function can be found in [Mandel and Wolf, 1995, Sec. 3.1.3]. We will continue our discussion of optical fields by using the function V, rather than u.

1.2.2 Correlation functions in the space-time domain

An experiment to determine the time average of any process would involve keeping track of its behavior over a very, very long period of time.

According to Eq. (1.5) one would have to take, in principle at least, an infinite numbers of readings of the same system. Suppose now that we have, instead of a single system, a very large set (called an *"ensemble"*) of copies of this system and that we take just a single measurement of each of these so-called *realizations* of the system, and then calculate their average. If each realization of the ensemble carries the same statistical information, then the outcome of this procedure, which gives an *ensemble average*, is equal to the *time average* produced by observing a single system. If this is the case the system is said to be *ergodic.* In the following we will always assume ergodicity. An extensive overview of this concept can be found in [Papoulis, 1991].

As remarked in the previous section, the fact that the real field $u(\mathbf{r},t)$ has a time average of zero, Eq. (1.5), implies that its complex analytic signal representation $V(\mathbf{r},t)$ is also a zero-mean function:

$$\langle V(\mathbf{r},t)\rangle \equiv \lim_{T\to\infty}\frac{1}{2T}\int_{-T}^{+T} V(\mathbf{r},t)\,\mathrm{d}t = 0. \tag{1.6}$$

Many different mechanisms, like the before-mentioned spontaneous emission, but also electronic noise, thermal fluctuations, mechanical vibrations, or the dynamic use of spatial light modulators, will cause the field to fluctuate randomly. The statistical character of these fluctuations can be described by the field's *cross-correlation function*

$$\Gamma(\mathbf{r}_1,\mathbf{r}_2,t_1,t_2) = \langle V^*(\mathbf{r}_1,t_1)V(\mathbf{r}_2,t_2)\rangle. \tag{1.7}$$

This function represents the *covariance* of the two zero-mean processes $V(\mathbf{r}_1,t_1)$ and $V(\mathbf{r}_2,t_2)$. It expresses the correlation between the field at position $\mathbf{r}_1$ at time t_1 and the field at position $\mathbf{r}_2$ at time t_2.

In many cases the source that generates the fields will be *stationary.*[1] This means that the cross-correlation $\Gamma(\mathbf{r}_1,\mathbf{r}_2,t_1,t_2)$ depends on t_1 and t_2 only through their difference $\tau = t_2 - t_1$. We then have

$$\begin{aligned}\Gamma(\mathbf{r}_1,\mathbf{r}_2,\tau) &= \langle V^*(\mathbf{r}_1,t)V(\mathbf{r}_2,t+\tau)\rangle, &(1.8)\\ &= \lim_{T\to\infty}\frac{1}{2T}\int_{-T}^{+T} V^*(\mathbf{r}_1,t)V(\mathbf{r}_2,t+\tau)\,\mathrm{d}t. &(1.9)\end{aligned}$$

[1]Strictly speaking, what is assumed here is *wide-sense stationarity.* For a fuller discussion we refer to [Mandel and Wolf, 1995].

The function $\Gamma(\mathbf{r}_1, \mathbf{r}_2, \tau)$ is called the *mutual coherence function*. The notion of *temporal coherence* refers to the situation where the two observation points coincide, i.e. $\mathbf{r}_1 = \mathbf{r}_2 = \mathbf{r}$. We can define the *coherence time* Δt as the duration after which $\Gamma(\mathbf{r}, \mathbf{r}, \tau)$ decreases by a factor $1/e$ from its maximum value, which occurs at $\tau = 0$:

$$\Gamma(\mathbf{r}, \mathbf{r}, \Delta t) = \Gamma(\mathbf{r}, \mathbf{r}, 0)/e. \tag{1.10}$$

The field that is observed at the same position $\mathbf{r}$ at two moments in time, is said to be correlated if the time difference is less than Δt. If the time difference exceeds Δt the field is said to be uncorrelated.

The *longitudinal coherence length* is the distance that light travels during the coherence time, i.e., this length equals $c\Delta t$, with c the speed of light.

In a similar manner, the *spatial coherence length* $\Delta\mathbf{r}$ of the field is defined by setting the time difference $\tau = 0$, and considering the separation distance between $\mathbf{r}_1$ and $\mathbf{r}_2$ for which $\Gamma(\mathbf{r}_1, \mathbf{r}_2, 0)$ decreases by a factor $1/e$ from its maximum value, which occurs at $\mathbf{r}_1 = \mathbf{r}_2 = \mathbf{r}$:

$$\Gamma(|\mathbf{r}_1 - \mathbf{r}_2| = \Delta\mathbf{r}, 0) = \Gamma(\mathbf{r}, \mathbf{r}, 0)/e. \tag{1.11}$$

When, at the same moment in time, the field is observed at two points that are separated by a distance that is less than $\Delta\mathbf{r}$, the field is correlated. If the separation is larger than $\Delta\mathbf{r}$, the field is uncorrelated.

The three arguments of the mutual coherence function suggest that we cannot always distinguish between temporal coherence (where $\mathbf{r}_1 = \mathbf{r}_2$), and spatial coherence (where $\tau = 0$). In general, we are dealing with the correlation of the field at two different points, with a non-zero time difference between them. It is therefore said that $\Gamma(\mathbf{r}_1, \mathbf{r}_2, \tau)$ describes the *spatio-temporal coherence* properties of the field.

The *instantaneous intensity* at a position $\mathbf{r}$ at time t may be defined as the squared modulus of the field, i.e.,

$$I(\mathbf{r}, t) = V^*(\mathbf{r}, t)V(\mathbf{r}, t). \tag{1.12}$$

It is clear from Eq. (1.9) that the *average intensity* at $\mathbf{r}$ equals

$$I(\mathbf{r}) = \langle I(\mathbf{r}, t)\rangle = \langle V^*(\mathbf{r}, t)V(\mathbf{r}, t)\rangle = \Gamma(\mathbf{r}, \mathbf{r}, 0). \tag{1.13}$$

It will be convenient to use a normalized version of the mutual coherence function by defining

$$\gamma(\mathbf{r}_1, \mathbf{r}_2, \tau) = \frac{\Gamma(\mathbf{r}_1, \mathbf{r}_2, \tau)}{[\Gamma(\mathbf{r}_1, \mathbf{r}_1, 0)\Gamma(\mathbf{r}_2, \mathbf{r}_2, 0)]^{1/2}}. \tag{1.14}$$

This so-called *complex degree of coherence* can be shown to satisfy the inequalities [Mandel and Wolf, 1995, Sec. 4.3.1]

$$0 \leq |\gamma(\mathbf{r}_1, \mathbf{r}_2, \tau)| \leq 1. \tag{1.15}$$

The lower bound corresponds to a complete lack of coherence, whereas the upper bound indicates full coherence. For intermediate values the field is said to be *partially coherent*.

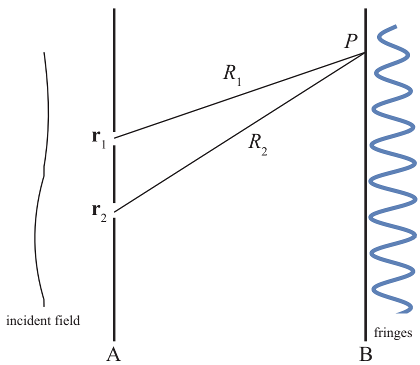

Figure 1.1: Young's two pinhole experiment. A partially coherent field is incident on an opaque screen A that contains two identical small apertures ("pinholes") at $\mathbf{r}_1$ and $\mathbf{r}_2$. The light that is transmitted forms interference fringes on a second, parallel screen B, and is observed at P.

The function $\gamma(\mathbf{r}_1, \mathbf{r}_2, \tau)$ has a clear physical meaning, as we will now discuss. The state of coherence of a wave field determines its possibility to form *interference patterns*. This is illustrated by examining Young's experiment with partially coherent light. Consider the setup sketched in Fig. 1.1. An optical field is incident on an opaque screen A that has two identical small apertures, which are located at $\mathbf{r}_1$ and $\mathbf{r}_2$. The light that passes through the apertures forms an interference pattern on a second, parallel screen B. Since the two pinholes both emit spherical waves, the total field at a point P on the observation screen can be written as[2]

$$V(P,t) = V(\mathbf{r}_1, t - R_1/c)\frac{e^{\mathrm{i}kR_1}}{R_1} + V(\mathbf{r}_2, t - R_2/c)\frac{e^{\mathrm{i}kR_2}}{R_2}, \tag{1.16}$$

where R_1 and R_2 are the distances from the two pinholes to P. According to Eq. (1.13), the average intensity at P equals

$$\begin{aligned} I(P) &= \langle V^*(P,t)V(P,t)\rangle, & (1.17)\\ &= \frac{I(\mathbf{r}_1)}{R_1^2} + \frac{I(\mathbf{r}_2)}{R_2^2} + \frac{2}{R_1R_2}\mathrm{Re}\left\{e^{\mathrm{i}k(R_2-R_1)}\Gamma(\mathbf{r}_1,\mathbf{r}_2,\tau)\right\}, & (1.18)\end{aligned}$$

with the time difference $\tau = (R_2 - R_1)/c$. Let us first assume that the point P is so far away from the two apertures that we may use the approximation

$$\frac{1}{R_1} \approx \frac{1}{R_2} = \frac{1}{R}. \tag{1.19}$$

We next assume that the average intensity at the two pinholes is the same, i.e.

$$I(\mathbf{r}_1) = I(\mathbf{r}_2) = I(\mathbf{r}). \tag{1.20}$$

Substitution of these two assumptions in Eq. (3.38) yields the expressions

$$\begin{aligned} I(P) &= \frac{2I(\mathbf{r})}{R^2} + \frac{2}{R^2}\mathrm{Re}\left\{e^{\mathrm{i}k(R_2-R_1)}\Gamma(\mathbf{r}_1,\mathbf{r}_2,\tau)\right\}, & (1.21)\\ &= \frac{2I(\mathbf{r})}{R^2}\left\{1 + |\gamma(\mathbf{r}_1,\mathbf{r}_2,\tau)|\cos[k(R_2-R_1) + \phi(\mathbf{r}_1,\mathbf{r}_2,\tau)]\right\}, & (1.22)\end{aligned}$$

where we have used the definition (1.14) of the complex degree of coherence, and written

$$\gamma(\mathbf{r}_1,\mathbf{r}_2,\tau) = |\gamma(\mathbf{r}_1,\mathbf{r}_2,\tau)|e^{\mathrm{i}\phi(\mathbf{r}_1,\mathbf{r}_2,\tau)}, \tag{1.23}$$

[2]We make use of a simplified form of the so-called propagator function [Born and Wolf, 1995, Sec. 8.2]. However, this will not affect our result.

with $\phi(\mathbf{r}_1, \mathbf{r}_2, \tau)$ the phase (or "argument") of $\gamma(\mathbf{r}_1, \mathbf{r}_2, \tau)$. Let us now imagine that the observation point P is slightly moved across the screen B (i.e., up or down in Fig. 1.1). The factor $R_2 - R_1$ then changes, which causes the last term in Eq. (1.22) to vary between $|\gamma(\mathbf{r}_1, \mathbf{r}_2, \tau)|$ and $-|\gamma(\mathbf{r}_1, \mathbf{r}_2, \tau)|$. That means that the maximum intensity and the minimum intensity in the immediate neighborhood of P are given by

$$I_{\max} = \frac{2I(\mathbf{r})}{R^2}(1 + |\gamma(\mathbf{r}_1, \mathbf{r}_2, \tau)|), \tag{1.24}$$

$$I_{\min} = \frac{2I(\mathbf{r})}{R^2}(1 - |\gamma(\mathbf{r}_1, \mathbf{r}_2, \tau)|), \tag{1.25}$$

respectively. The local *sharpness* or *visibility* $\mathcal{V}$ of the fringe pattern in Young's experiment is defined as

$$\mathcal{V} \equiv \frac{I_{\max} - I_{\min}}{I_{\max} + I_{\min}}. \tag{1.26}$$

If we substitute from Eqs. (1.24) and (1.25) into (1.26), we get the result that

$$\mathcal{V} = |\gamma(\mathbf{r}_1, \mathbf{r}_2, \tau)|. \tag{1.27}$$

So we find that the visibility of the interference fringes that are produced in Young's experiment is equal to the modulus of the complex degree of coherence of the field that is incident at the two pinholes. This is illustrated in Fig. 1.2 where the interference fringes are plotted for three different values of $|\gamma(\mathbf{r}_1, \mathbf{r}_2, \tau)|$. On the left this modulus is 1, which means that the field is fully coherent, and that the intensity minimums are zero. The situation for a partially coherent field, with $|\gamma(\mathbf{r}_1, \mathbf{r}_2, \tau)| = 0.5$, is shown in the middle. The modulation of the intensity with position is now significantly less. When the field at the two pinholes is completely uncorrelated, i.e. when $|\gamma(\mathbf{r}_1, \mathbf{r}_2, \tau)| = 0$, a constant, unmodulated intensity pattern is formed, with zero visibility. This situation is shown on the right-hand side of the figure.

The physical meaning of the phase ϕ of the complex quantity $\gamma(\mathbf{r}_1, \mathbf{r}_2, \tau)$ follows from Eq. (1.22). This phase determines the shift of the fringes with respect to the case when the incident field is fully coherent and *co-phasal*, i.e., when $\gamma(\mathbf{r}_1, \mathbf{r}_2, \tau) = 1$.

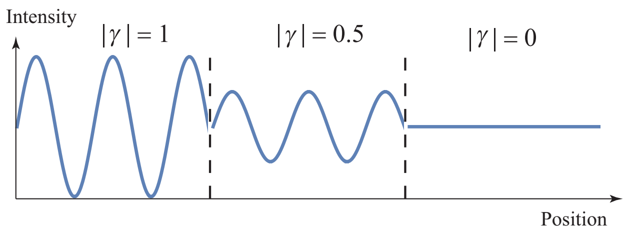

Figure 1.2: Interference fringes in Young's experiment for three different values of the modulus of the complex degree of coherence $\gamma(\mathbf{r}_1, \mathbf{r}_2, \tau)$. On the left $|\gamma(\mathbf{r}_1, \mathbf{r}_2, \tau)| = 1$ and the fringes have what is called *perfect visibility*, with the intensity minimums being zero. In the middle panel $|\gamma(\mathbf{r}_1, \mathbf{r}_2, \tau)| = 0.5$ and it is seen that the minima are non-zero. On the right, $\gamma(\mathbf{r}_1, \mathbf{r}_2, \tau) = 0$. This means that the intensity pattern has a constant value without any spatial modulation.

It should be noted that the assumption of stationarity is crucial for the derivation of the results in this Section. An important example of a field that is *not* stationary, is the output of a pulsed laser. In the description of the coherence properties of such a field both time arguments t_1 and t_2 that appear in Eq. (1.7) have to be retained. A thorough description of non-stationary fields can be found in the work by Bertolotti and coworkers [Bertolotti *et al.*, 1995; Bertolotti *et al.*, 1997].

1.2.3 Correlations in the space-frequency domain

Until now we have studied the coherence properties of optical fields in the space-time domain. In many cases, however, it is much easier to work in the space-frequency domain. Consider, for example, the situation in which a light wave is scattered at several points, at different times. In the space-time domain we need to keep track of all these events and take their relative time difference into account in order to calculate the resulting scattered field. No such need exists in the space-frequency domain where time has been "transformed away", and only a single frequency component of the field is considered.

So, in order to study correlations in the space-frequency domain, we begin by introducing the *cross-spectral density function* by taking the temporal Fourier transform of the mutual coherence function:

$$W(\mathbf{r}_1, \mathbf{r}_2, \omega) = \frac{1}{2\pi} \int_{-\infty}^{\infty} \Gamma(\mathbf{r}_1, \mathbf{r}_2, \tau) e^{\mathrm{i}\omega\tau} \, \mathrm{d}\tau. \tag{1.28}$$

The question now arises if $W(\mathbf{r}_1, \mathbf{r}_2, \omega)$ can, just like its space-time counterpart $\Gamma(\mathbf{r}_1, \mathbf{r}_2, \tau)$, be interpreted as an ensemble average of the product of two random fields. The answer is yes, and for the somewhat complicated derivation the reader is referred to [Mandel and Wolf, 1995, Sec. 4.7.2], where it is shown that

$$W(\mathbf{r}_1, \mathbf{r}_2, \omega) = \langle U^*(\mathbf{r}_1, \omega) U(\mathbf{r}_2, \omega) \rangle. \tag{1.29}$$

Here $U(\mathbf{r}, \omega)$ represents a monochromatic wave field at position $\mathbf{r}$ with frequency ω. Each realization of this field has a random phase and amplitude. When the two spatial arguments of the cross-spectral density coincide ($\mathbf{r}_1 = \mathbf{r}_2 = \mathbf{r}$) this function becomes the *power spectrum* of the field. The so-called *spectral density* is therefore defined as

$$S(\mathbf{r}, \omega) = W(\mathbf{r}, \mathbf{r}, \omega) = \langle U^*(\mathbf{r}, \omega) U(\mathbf{r}, \omega) \rangle. \tag{1.30}$$

Just like for the mutual coherence function, it is advantageous to introduce a normalized version of the cross-spectral density function, called the *spectral degree of coherence*, by defining

$$\mu(\mathbf{r}_1, \mathbf{r}_2, \omega) = \frac{W(\mathbf{r}_1, \mathbf{r}_2, \omega)}{[S(\mathbf{r}_1, \omega) S(\mathbf{r}_2, \omega)]^{1/2}}. \tag{1.31}$$

One can show [Mandel and Wolf, 1995, Sec. 4.3.2] that it satisfies the two inequalities

$$0 \leq |\mu(\mathbf{r}_1, \mathbf{r}_2, \omega)| \leq 1. \tag{1.32}$$

The lower bound corresponds to the absence of coherence of the field at $\mathbf{r}_1$ and $\mathbf{r}_2$ at frequency ω, whereras the upper bound indicates complete coherence. For intermediate values of $|\mu(\mathbf{r}_1, \mathbf{r}_2, \omega)|$ the field is said to be partially coherent. The physical meaning of the spectral degree of coherence can be explained by considering a modified version of Young's experiment, as shown in Fig. 1.3. Both pinholes are now covered by a narrow-band spectral filter with central frequency ω.

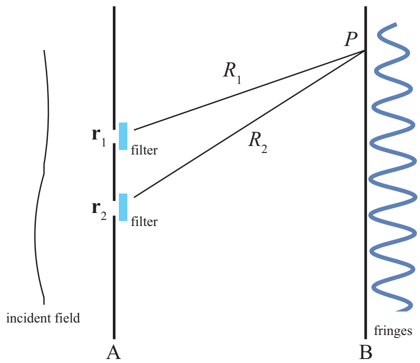

Figure 1.3: A modified version of Young's two pinhole experiment. A field is incident on an opaque screen A that contains two pinholes. Both pinholes are covered by a narrow-band spectral filter that transmits only fields with a frequency around ω. This light then forms interference fringes on the observation screen B.

The field at an observation point P is again the sum of the two spherical waves emanating from the pinholes:

$$U(P,\omega) = U(\mathbf{r}_1,\omega)\frac{e^{\mathrm{i}kR_1}}{R_1} + U(\mathbf{r}_2,\omega)\frac{e^{\mathrm{i}kR_2}}{R_2}. \tag{1.33}$$

It follows from Eqs. (1.30) and (1.33) that the spectral density at P is given by the expression

$$S(P,\omega) = \frac{S(\mathbf{r}_1,\omega)}{R_1^2} + \frac{S(\mathbf{r}_2,\omega)}{R_2^2} + \frac{2}{R_1R_2}\mathrm{Re}\{e^{\mathrm{i}k(R_2-R_1)}W(\mathbf{r}_1,\mathbf{r}_2,\omega)\}. \tag{1.34}$$

Let us again assume that

$$\frac{1}{R_1} \approx \frac{1}{R_2} = \frac{1}{R}, \tag{1.35}$$

and that the spectral density of the light that is incident at the two pinholes is the same, i.e.,

$$S(\mathbf{r}_1,\omega) = S(\mathbf{r}_2,\omega) = S(\mathbf{r},\omega). \tag{1.36}$$

On making use of these two assumptions in Eq. (1.34), we find that

$$S(P,\omega) = \frac{2S(\mathbf{r},\omega)}{R^2}\left[1 + \mathrm{Re}\{e^{\mathrm{i}k(R_2-R_1)}\mu(\mathbf{r}_1,\mathbf{r}_2,\omega)\}\right]. \tag{1.37}$$

An important consequence of Eq. (1.37) is that *only* in the special case when $\mu(\mathbf{r}_1,\mathbf{r}_2,\omega) = 0$ will the spectrum that is observed on screen B be proportional to the spectrum $S(\mathbf{r},\omega)$ that is incident on the two pinholes. In general, though, the observed spectrum will be different from that at the two pinholes, because it is modified by the term containing the spectral degree of coherence. This is an example of so-called *coherence-induced spectral changes*, meaning that the spectrum of the light that is observed is not necessarily identical to the spectrum of the source, because of its random nature. An extensive review of this subject, sometimes called the *Wolf effect*, is given in [Wolf and James, 1996]. Spectral changes that are caused by coherence are to be distinguished from those that are *diffraction-induced* and occur, e.g., in the focusing of spatially coherent, polychromatic light [Gbur *et al.*, 2002; Visser and Wolf, 2003].

Let us next write

$$\mu(\mathbf{r}_1,\mathbf{r}_2,\omega) = |\mu(\mathbf{r}_1,\mathbf{r}_2,\omega)|\, e^{\mathrm{i}\delta}, \tag{1.38}$$

where δ denotes the phase of the spectral degree of coherence (for brevity the arguments of δ are not displayed). We then have that

$$S(P,\omega) = \frac{2S(\mathbf{r},\omega)}{R^2}\left[1 + |\mu(\mathbf{r}_1,\mathbf{r}_2,\omega)|\mathrm{Re}\left\{e^{\mathrm{i}k(R_2-R_1)}e^{\mathrm{i}\delta}\right\}\right]. \tag{1.39}$$

If the position of the observation point P is gradually changed, then the spectral density will take on values between its maximum and minimum, namely

$$S_{\mathrm{max}} = \frac{2S(\mathbf{r},\omega)}{R^2}\left[1 + |\mu(\mathbf{r}_1,\mathbf{r}_2,\omega)|\right], \tag{1.40}$$

$$S_{\mathrm{min}} = \frac{2S(\mathbf{r},\omega)}{R^2}\left[1 - |\mu(\mathbf{r}_1,\mathbf{r}_2,\omega)|\right]. \tag{1.41}$$

In analogy with Eq. (1.26) we define the local *spectral visibility* of the fringes as

$$\mathcal{V}_{\mathrm{spec}} \equiv \frac{S_{\mathrm{max}} - S_{\mathrm{min}}}{S_{\mathrm{max}} + S_{\mathrm{min}}}. \tag{1.42}$$

If we substitute from Eqs. (1.40) and (1.41) into (1.42), we get the result that

$$\mathcal{V}_{\text{spec}} = |\mu(\mathbf{r}_1, \mathbf{r}_2, \omega)|. \tag{1.43}$$

So, we can identify the visibility of the fringes in Young's experiment with spectral filters as the modulus of the spectral degree of coherence. It is seen from Eq. (1.39) that the phase δ plays a role that is analogous to that of the phase of the complex degree of coherence: a change in this phase results in a transverse shift of the interference pattern.

We end this section by noting that although the mutual coherence function $\Gamma(\mathbf{r}_1, \mathbf{r}_2, \tau)$ and the cross-spectral density function $W(\mathbf{r}_1, \mathbf{r}_2, \omega)$ are each other's Fourier transform, this is, in general, not the case for their normalized versions $\gamma(\mathbf{r}_1, \mathbf{r}_2, \tau)$ and $\mu(\mathbf{r}_1, \mathbf{r}_2, \omega)$. This is due to the terms in the denominatior of their respective definitions.

1.2.4 How correlations propagate

We next adress the fundamental question of how the coherence properties of a source influence the state of coherence of the field that it produces. Let us begin by examining a very simple system, namely two uncorrelated, random point sources, S_1 and S_2. The fields that they generate are observed at two points P_1 and P_2, as sketched in Fig. 1.4. We will arrive at the somewhat counter-intuitive conclusion that the total field of these sources acquires a high degree of coherence on propagation.

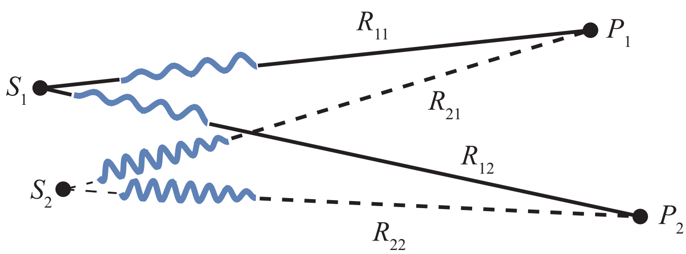

Figure 1.4: Two random point sources, S_1 and S_2, emit uncorrelated wave trains that are observed at P_1 and P_2.

Let $V_1(P_1, t)$ and $V_1(P_2, t)$ be the fields at P_1 and P_2 due to S_1, and let $V_2(P_1, t)$ and $V_2(P_2, t)$ be the fields at P_1 and P_2 that are caused by

S_2. Furthermore, R_{ij} , with $i, j = 1, 2$, denotes the distance from S_i to P_j. If the path difference $|R_{11} - R_{12}|$ is less than the longitudinal coherence length of source S_1, we can make the approximation

$$V_1(P_1, t) \approx V_1(P_2, t). \tag{1.44}$$

Similarly, if $|R_{21} - R_{22}|$ is less than the longitudinal coherence length of source S_2, we also have that

$$V_2(P_1, t) \approx V_2(P_2, t). \tag{1.45}$$

The total fields at P_1 and P_2, denoted by $V(P_1, t)$ and $V(P_2, t)$, are both the sum of the contributions of S_1 and S_2, i.e.,

$$V(P_1, t) \quad = V_1(P_1, t) + V_2(P_1, t), \tag{1.46}$$

$$V(P_2, t) \quad = V_1(P_2, t) + V_2(P_2, t). \tag{1.47}$$

But it is clear from using Eqs. (1.44) and (1.45) in Eqs. (1.46) and (1.47) that

$$V(P_1, t) \approx V(P_2, t). \tag{1.48}$$

This last expression shows that, in spite of the fact that the wave trains that are emitted by S_1 and S_2 are completely uncorrelated, their superpositions at P_1 and P_2 are quite similar, and are therefore strongly correlated. This example demonstrates how coherence can build up on propagation. It is precisely this mechanism that is the underlying principle of the celebrated experiments carried out by Michelson and Pease [Wolf, 2007, Sec. 3.3.1]. They found that light from distant stars, when observed on Earth, gives rise to interference fringes with a clear visibility. According to Eq. (1.27) this means that this light has acquired a non-zero degree of coherence on propagation, even though we may consider the stars to be composed of a huge collection of completely uncorrelated atomic point sources.

The evolution of coherence functions on propagation can be described in a more rigorous fashion, as we now discuss. The field $V(\mathbf{r}, t)$ satisfies the wave equation, i.e.,

$$\left(\nabla^2 - \frac{1}{c^2}\frac{\partial^2}{\partial t^2}\right) V(\mathbf{r}, t) = 0, \tag{1.49}$$

where

$$\nabla^2 \equiv \frac{\partial^2}{\partial x^2} + \frac{\partial^2}{\partial y^2} + \frac{\partial^2}{\partial z^2} \tag{1.50}$$

denotes the Laplacian. If we now take the complex conjugate of this expression and multiply it with the field at another point $\mathbf{r}_2$ at time t_2, we get

$$\nabla_1^2 V^*(\mathbf{r}_1, t_1) V(\mathbf{r}_2, t_2) = \frac{1}{c^2} \frac{\partial^2}{\partial t_1^2} V^*(\mathbf{r}_1, t_1) V(\mathbf{r}_2, t_2). \tag{1.51}$$

Here the subscript 1 of the Laplacian indicates differentiation with respect to $\mathbf{r}_1$. We can take the ensemble average of both sides and interchange the order of differentiation and averaging to obtain

$$\nabla_1^2 \langle V^*(\mathbf{r}_1, t_1) V(\mathbf{r}_2, t_2)\rangle = \frac{1}{c^2} \frac{\partial^2}{\partial t_1^2} \langle V^*(\mathbf{r}_1, t_1) V(\mathbf{r}_2, t_2)\rangle. \tag{1.52}$$

If the field is statistically stationary, then

$$\langle V^*(\mathbf{r}_1, t_1) V(\mathbf{r}_2, t_2)\rangle = \Gamma(\mathbf{r}_1, \mathbf{r}_2, \tau), \tag{1.53}$$

with the time difference $\tau = t_2 - t_1$, and $\Gamma(\mathbf{r}_1, \mathbf{r}_2, \tau)$ the mutual coherence function that we defined earlier in Eq. (1.9). Clearly, $\partial^2/\partial t_1^2 = \partial^2/\partial \tau^2$. That means that we can re-write Eq. (1.52) as

$$\nabla_1^2 \Gamma(\mathbf{r}_1, \mathbf{r}_2, \tau) = \frac{1}{c^2} \frac{\partial^2}{\partial \tau^2} \Gamma(\mathbf{r}_1, \mathbf{r}_2, \tau). \tag{1.54}$$

This result shows that, just like the field itself, the mutual coherence function also satisfies the wave equation. Armed with this knowledge, we can calculate precisely how the correlation of a random optical field evolves on propagation through free space. Equation (1.54) is often applied in coherence theory to investigate the properties of the field that is generated by a source with a known (or prescribed) state of coherence.

By a completely similar approach as above, it can be derived that

$$\nabla_2^2 \Gamma(\mathbf{r}_1, \mathbf{r}_2, \tau) = \frac{1}{c^2} \frac{\partial^2}{\partial \tau^2} \Gamma(\mathbf{r}_1, \mathbf{r}_2, \tau). \tag{1.55}$$

In this equation the spatial differentiation is with respect to the variable $\mathbf{r}_2$, rather than $\mathbf{r}_1$.

After this discussion it will perhaps not come as a surprise that the cross-spectral density function, the space-frequency counterpart of the mutual coherence function, satisfies a pair of Helmholtz equations, namely

$$\left(\nabla_1^2 + k^2\right) W(\mathbf{r}_1, \mathbf{r}_2, \omega) \quad = 0, \tag{1.56}$$
$$\left(\nabla_2^2 + k^2\right) W(\mathbf{r}_1, \mathbf{r}_2, \omega) \quad = 0. \tag{1.57}$$

Together the four formulas (1.54)–(1.57) are known as the *Wolf equations*, after their discoverer Emil Wolf. It is fair to say that they form the basis of the modern theory of optical coherence. One way these expressions can be applied is to study how the correlation functions evolve on propagation from a source plane on which the state of coherence is known. To illustrate this, let us consider a field $U^{(0)}(\mathbf{r}, \omega)$ in a plane $z = 0$, that propagates into the half space $z > 0$. According to the Fresnel-Huygens principle, at an arbitrary point of observation $P(\mathbf{r})$ the field equals

$$U(\mathbf{r}, \omega) = \iint_{z=0} U^{(0)}(\mathbf{r}', \omega) G(\mathbf{r}, \mathbf{r}', \omega)\, \mathrm{d}^2 r', \tag{1.58}$$

with $G(\mathbf{r}, \mathbf{r}', \omega)$ the free-space Green's function pertaining to the Helmholtz equation:

$$G(\mathbf{r}, \mathbf{r}', \omega) = \frac{e^{\mathrm{i}kR}}{R}, \tag{1.59}$$

where $R = |\mathbf{r}' - \mathbf{r}|$. We next assume the point P to be far away from the source, and that its location is specified by $\mathbf{r} = r\mathbf{s}$, where $\mathbf{s}$ is a unit directional vector as sketched in Fig. 1.5. We can then approximate the distance R in the exponent by the distance r minus the projection of the position vector $\mathbf{r}'$ onto the vector $\mathbf{s}$, i.e.,

$$R = |\mathbf{r}' - \mathbf{r}| \approx r - \mathbf{r}' \cdot \mathbf{s}. \tag{1.60}$$

If we also use that $R^{-1} \approx r^{-1}$, we find the asymptotic form of the Green's function as

$$G(\mathbf{r}, \mathbf{r}', \omega) \sim \frac{e^{\mathrm{i}kr}}{r} e^{-\mathrm{i}k\mathbf{r}' \cdot \mathbf{s}}. \tag{1.61}$$

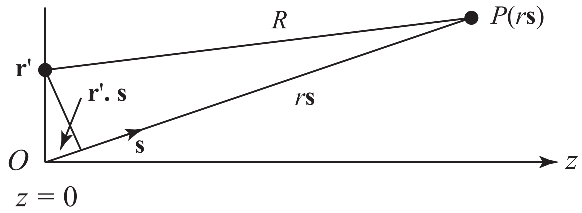

Figure 1.5: Illustrating the far-zone form of the Green's function.

On using this expression in Eq. (1.58) the field can be written as

$$U^{(\infty)}(r\mathbf{s},\omega) = \frac{e^{\mathrm{i}kr}}{r}\iint_{z=0} U^{(0)}(\mathbf{r}',\omega)e^{-\mathrm{i}k\mathbf{r}'\cdot\mathbf{s}}\,\mathrm{d}^2r', \tag{1.62}$$

where the superscript (∞) indicates that we are dealing with an observation point in the far zone. If we next define

$$\begin{aligned}
\mathbf{r}' &= (x', y', z'), &(1.63)\\
\boldsymbol{\rho}' &= (x', y'), &(1.64)\\
\mathbf{s} &= (s_x, s_y, s_z), &(1.65)\\
\mathbf{s}_\perp &= (s_x, s_y), &(1.66)
\end{aligned}$$

we get the result that

$$U(r\mathbf{s},\omega) = \frac{e^{\mathrm{i}kr}}{r}\iint_{z=0} U^{(0)}(\boldsymbol{\rho}',0,\omega)e^{-\mathrm{i}k\boldsymbol{\rho}'\cdot\mathbf{s}_\perp}\,\mathrm{d}x'\mathrm{d}y'. \tag{1.67}$$

If we define the two-dimensional Fourier transform of a function $g(\boldsymbol{\rho})$ as

$$\tilde{g}(\mathbf{u}) = \frac{1}{(2\pi)^2}\int g(\boldsymbol{\rho})e^{-\mathrm{i}\mathbf{u}\cdot\boldsymbol{\rho}}\,\mathrm{d}^2\rho, \tag{1.68}$$

we can re-write Eq. (1.67) as

$$U(r\mathbf{s},\omega) = (2\pi)^2\frac{e^{ikr}}{r}\tilde{U}(k\mathbf{s}_\perp,\omega). \tag{1.69}$$

This equation will be recognized as the central result of *Fraunhofer diffraction.* It states that the far-zone field is, apart from a prefactor, equal to the two-dimensional spatial Fourier transform of the field in the source plane. We can use Eq. (1.67) to calculate the cross-spectral density function of the field in the far zone. According to its definition, given by (1.29), we have

$$W^{(\infty)}(r_1\mathbf{s}_1, r_2\mathbf{s}_2, \omega) = \langle U^{(\infty)*}(r_1\mathbf{s}_1, \omega)U^{(\infty)}(r_2\mathbf{s}_2, \omega)\rangle, \quad (1.70)$$

$$= \frac{e^{\mathrm{i}k(r_2-r_1)}}{r_1 r_2}\langle \iiiint_{z=0} U^{(0)*}(\boldsymbol{\rho}_1', 0, \omega)U^{(0)}(\boldsymbol{\rho}_2', 0, \omega) \times e^{-\mathrm{i}k(\boldsymbol{\rho}_2'\cdot\mathbf{s}_{2\perp}-\boldsymbol{\rho}_1'\cdot\mathbf{s}_{1\perp})}\,\mathrm{d}x_1'\mathrm{d}y_1'\mathrm{d}x_2'\mathrm{d}y_2'.\rangle \quad (1.71)$$

Interchanging the order of integration and ensemble averaging yields the expression

$$W^{(\infty)}(r_1\mathbf{s}_1, r_2\mathbf{s}_2, \omega) = \frac{e^{\mathrm{i}k(r_2-r_1)}}{r_1 r_2}\iiiint_{z=0} W^{(0)}(\boldsymbol{\rho}_1', 0, \boldsymbol{\rho}_2', 0, \omega) \times e^{-\mathrm{i}k(\boldsymbol{\rho}_2'\cdot\mathbf{s}_{2\perp}-\boldsymbol{\rho}_1'\cdot\mathbf{s}_{1\perp})}\,\mathrm{d}x_1'\mathrm{d}y_1'\mathrm{d}x_2'\mathrm{d}y_2'. \quad (1.72)$$

If we now define the four-dimensional Fourier transform of a function $f(\boldsymbol{\rho}_1, \boldsymbol{\rho}_2)$ as

$$\tilde{f}(\mathbf{u}, \mathbf{v}) = \frac{1}{(2\pi)^4}\iiiint f(\boldsymbol{\rho}_1, \boldsymbol{\rho}_2)e^{-\mathrm{i}(\mathbf{u}\cdot\boldsymbol{\rho}_1+\mathbf{v}\cdot\boldsymbol{\rho}_2)}\,\mathrm{d}^2\rho_1\mathrm{d}^2\rho_2, \quad (1.73)$$

and compare this with Eq. (1.72), it is seen that

$$W^{(\infty)}(r_1\mathbf{s}_1, r_2\mathbf{s}_2, \omega) = \frac{(2\pi)^4 e^{\mathrm{i}k(r_2-r_1)}}{r_1 r_2}\tilde{W}^{(0)}(-k\mathbf{s}_{1\perp}, k\mathbf{s}_{2\perp}, \omega). \quad (1.74)$$

We thus find the important result that the cross-spectral density in the far zone is proportional to the four-dimensional spatial Fourier transform of the same function in the source plane. The striking analogy between Eqs. (1.74) and (1.69) is a direct consequence of the fact that both the field itself and its correlation function satisfy the Helmholtz equation.

We saw earlier from Eq. (1.30) that the spectral density is given by the cross-spectral density function evaluated at two identical positions. From Eq. (1.74) it therefore follows immediately that the far-zone spectral density is given by the expression

$$S^{(\infty)}(r\mathbf{s}, \omega) = W^{(\infty)}(r\mathbf{s}, r\mathbf{s}, \omega), \quad (1.75)$$

$$= \frac{(2\pi)^4}{r^2}\tilde{W}^{(0)}(-k\mathbf{s}_\perp, k\mathbf{s}_\perp, \omega). \quad (1.76)$$

From this equation we see that the spectrum in the far zone of a source is determined by the correlation function in the source plane. This is the underlying cause of the aforementioned Wolf effect: the spectrum that is observed away from the source can be substantially different from the spectrum of the source. For more details and experimental confirmation of this effect we refer to the review presented in [Wolf and James, 1996].

Another implication of Eq. (1.76) is that it shows the spectrum $S^{(\infty)}(r\mathbf{s}, \omega)$ to be a *secondary* quantity that is derived from knowledge of the correlation function $W^{(\infty)}(r_1\mathbf{s}_1, r_2\mathbf{s}_2, \omega)$ evaluated at two coincident points. The cross-spectral density function in the far zone can be calculated by "propagating" the correlation function of the source using Eq. (1.74). All this is a consequence of the fact that the cross-spectral density function obeys a pair of precise propagation laws, namely the two Helmholtz equations given by Eqs. (1.56) and (1.57). No such propagation law exists for the spectral density.

1.3 Elements of optical scattering

In this section we describe the first-order Born approximation for the case of a partially coherent, incident field on a partially coherent scatterer.

Let us begin by considering the scattering of a monochromatic wave

$$V^{(\mathrm{inc})}(\mathbf{r}, t) = U^{(\mathrm{inc})}(\mathbf{r}, \omega) e^{-\mathrm{i}\omega t}, \tag{1.77}$$

that is incident upon a linear scatterer, which occupies a finite domain D in free space as shown in Fig. 1.6. Here $\mathbf{r}$ denotes an arbitrary point either outside or inside the scatterer, t denotes the time and ω denotes the frequency. We assume that the scatterer has a refractive index $n(\mathbf{r}, \omega)$. Let

$$V(\mathbf{r}, t) = U(\mathbf{r}, \omega) e^{-\mathrm{i}\omega t}, \tag{1.78}$$

be the total field at a point $\mathbf{r}$. $U(\mathbf{r}, \omega)$ then satisfies the Helmholtz equation

$$\nabla^2 U(\mathbf{r}, \omega) + k^2 n^2(\mathbf{r}, \omega) U(\mathbf{r}, \omega) = 0, \tag{1.79}$$

where ∇^2 denotes the Laplacian, and k is the free-space wave number associated with frequency ω, i.e.

$$k = \omega / c, \tag{1.80}$$

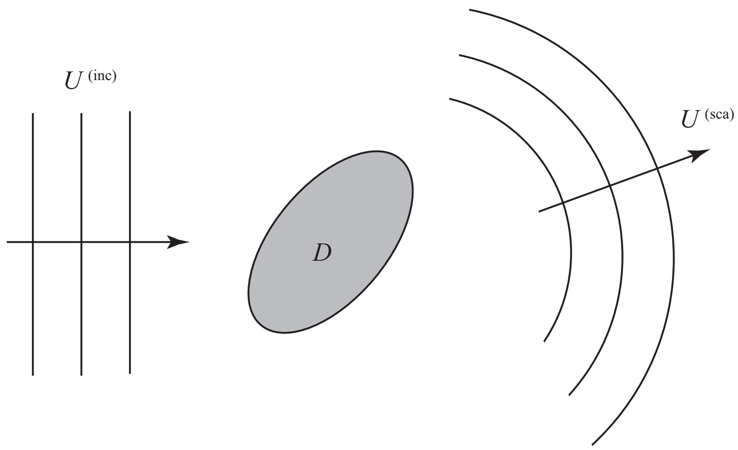

Figure 1.6: The scattering of a monochromatic wave by a scatterer occupying a domain D.

c being the speed of light in vacuum. We can rewrite Eq. (1.79) as

$$\nabla^2 U(\mathbf{r},\omega) + k^2 U(\mathbf{r},\omega) = -4\pi F(\mathbf{r},\omega) U(\mathbf{r},\omega), \tag{1.81}$$

where the quantity

$$F(\mathbf{r},\omega) = \frac{1}{4\pi} k^2 [n^2(\mathbf{r},\omega) - 1] \tag{1.82}$$

is called the scattering potential of the medium.

Let us represent the field $U(\mathbf{r},\omega)$ as the sum of the incident field $U^{(\text{inc})}(\mathbf{r},\omega)$ and the scattered field $U^{(\text{sca})}(\mathbf{r},\omega)$, i.e.,

$$U(\mathbf{r},\omega) = U^{(\text{inc})}(\mathbf{r},\omega) + U^{(\text{sca})}(\mathbf{r},\omega). \tag{1.83}$$

The incident field is assumed to satisfy the free-space Helmholtz equation

$$(\nabla^2 + k^2) U^{(\text{inc})}(\mathbf{r},\omega) = 0, \tag{1.84}$$

everywhere. By making use of the outgoing Green's function pertaining to the Helmholtz equation, it can be shown that the total field obeys the equation [Born and Wolf, 1995, Sec. 3.1.1]

$$U(\mathbf{r},\omega) = U^{(\mathrm{inc})}(\mathbf{r},\omega) + \int_D F(\mathbf{r}',\omega)U(\mathbf{r}',\omega)G(|\mathbf{r}-\mathbf{r}'|,\omega)\mathrm{d}^3r', \tag{1.85}$$

with

$$G(R,\omega) = e^{\mathrm{i}kR}/R, \tag{1.86}$$

with $R = |\mathbf{r} - \mathbf{r}'|$. Eq. (1.85), together with Eq. (1.83), is the basic expression for the scattered field. It is usually called the integral equation of potential scattering.

In general, it is not possible to solve Eq. (1.85) in a closed form. However, when the scattering is weak, an important approximation can be made. Let us assume that the magnitude $U^{(\mathrm{sca})}$ of the scattered field is much smaller than the magnitude $U^{(\mathrm{inc})}$ of the incident field:

$$|U^{(\mathrm{sca})}(\mathbf{r},\omega)| \ll |U^{(\mathrm{inc})}(\mathbf{r},\omega)| \tag{1.87}$$

throughout the scatterer. It is seen from Eqs. (1.82) and (1.85) that this will be the case if the refractive index is close to unity. We can then replace the total field U by the incident field $U^{(\mathrm{inc})}$ in Eq. (1.85), i.e. write that

$$U(\mathbf{r},\omega) \approx U^{(\mathrm{inc})}(\mathbf{r},\omega) + \int_D F(\mathbf{r}',\omega)U^{(\mathrm{inc})}(\mathbf{r}',\omega)G(|\mathbf{r}-\mathbf{r}'|,\omega)\mathrm{d}^3r'. \tag{1.88}$$

This formula is known as the first-order Born approximation.

We will now consider the more complicated situation when the light incident on a deterministic scatterer is not monochromatic but is partially coherent. Let $W^{(\mathrm{inc})}(\mathbf{r}_1,\mathbf{r}_2,\omega)$ be the cross-spectral density function of the incident field. As before,

$$W^{(\mathrm{inc})}(\mathbf{r}_1,\mathbf{r}_2,\omega) = \langle U^{(\mathrm{inc})*}(\mathbf{r}_1,\omega)U^{(\mathrm{inc})}(\mathbf{r}_2,\omega)\rangle. \tag{1.89}$$

In a similar fashion, the scattered field may be written as

$$W^{(\mathrm{sca})}(\mathbf{r}_1,\mathbf{r}_2,\omega) = \langle U^{(\mathrm{sca})*}(\mathbf{r}_1,\omega)U^{(\mathrm{sca})}(\mathbf{r}_2,\omega)\rangle. \tag{1.90}$$

If we substitute from Eq. (1.88) into Eq. (1.90) we obtain the formula

$$W^{(\mathrm{sca})}(\mathbf{r}_1, \mathbf{r}_2, \omega) = \int_D \int_D W^{(\mathrm{inc})}(\mathbf{r}_1, \mathbf{r}_2, \omega) F^*(\mathbf{r}'_1, \omega) F(\mathbf{r}'_2, \omega) \\ \times G^*(|\mathbf{r}_1 - \mathbf{r}'_1|, \omega)\, G(|\mathbf{r}_2 - \mathbf{r}'_2|, \omega)\, \mathrm{d}^3 r'_1 \mathrm{d}^3 r'_2. \qquad (1.91)$$

Until now we have assumed that the scatterer is deterministic. The scattering potential $F(\mathbf{r}, \omega)$ is then a well-defined function of position. Frequently, however, this is not so; the scattering potential is then a random function of position. An example is the turbulent atmosphere in which the refractive index varies randomly both in time and in space. From Eq. (1.91), we obtain

$$W^{(\mathrm{sca})}(\mathbf{r}_1, \mathbf{r}_2, \omega) = \int_D \int_D W^{(\mathrm{inc})}(\mathbf{r}_1, \mathbf{r}_2, \omega) C_F(\mathbf{r}'_1, \mathbf{r}'_2, \omega) \\ \times G^*(|\mathbf{r}_1 - \mathbf{r}'_1|, \omega) G(|\mathbf{r}_2 - \mathbf{r}'_2|, \omega) \mathrm{d}^3 r'_1 \mathrm{d}^3 r'_2. \qquad (1.92)$$

where

$$C_F(\mathbf{r}'_1, \mathbf{r}'_2, \omega) = \langle F^*(\mathbf{r}'_1, \omega) F(\mathbf{r}'_2, \omega) \rangle \qquad (1.93)$$

is the correlation function of the scattering potential and the angled brackets indicate the average taken over an ensemble of realizations of the scattering potential at position $\mathbf{r}_1$ and $\mathbf{r}_2$. We will make use of Eq. (1.92) in Chapter 2.

The special case of scattering by a homogeneous, deterministic sphere, so-called Mie scattering, is treated in many standard text books [van de Hulst, 1981], [Born and Wolf, 1995], [Hergert and Wriedt (eds.), 2012]. In Chapters 3 and 4 we will apply several expressions found in these sources.

1.4 Outline of this thesis

The second Chapter [Wang *et al.*, 2015b] of this work discusses how to control the scattered field dynamically by spatial coherence. Using a scalar field model and applying the first-order Born approximation, the angular distribution of the scattered field is examined. In particular, we study both a Gaussian-correlated field and a Bessel-correlated field which are incident on a Gaussian-correlated spherical particle. It is shown that, unlike the maximum forward scattered field which is generated by the Gaussian-correlated field, the angular distribution of the scattered field which is produced by the Bessel-correlated field, can be tuned to gradually suppress the forward scattering intensity, and even create a cone-like scattered field.

In the third Chapter [Wang *et al.*, 2015a] a tuneable, anomalously scattered field is obtained by using a J_0 Bessel-correlated beam which is incident on a homogeneous sphere. We found that the direction of maximum scattering can be shifted by changing the spatial coherence length. In this process the total power that is scattered remains constant.

The fourth Chapter [Wang *et al.*, 2016b] is about how to strongly suppress the forward or backward Mie scattering by using spatial coherence. We derived analytic expressions relating Mie scattering with partially coherent fields in the forward and backward directions to scattering with fully coherent fields. It is found that the angle θ_{max} in the forward direction is quite insensitive to the precise value of the refractive index. Moreover, for a large sphere, the angle θ_{max} is very well approximated to the value in a simpler but related situation, namely the scattering of J_0-correlated light by a Gaussian random scatterer while using the first-order Born approximation. Our results show that the use of spatial coherence offers a new tool to actively steer the Mie scattered field.

Chapter 5 [Wang *et al.*, 2016a] deals with the scattering of a partially coherent field by a periodic potential. Scattering from such crystalline structures produces highly directional peaks, that are called von Laue spots. We analyze the von Laue pattern that is generated by a wide-band, partially coherent source that is located in the far zone of the crystal. In particular, we derive an analytic expression for the scattering by an orthorhombic structure of identical point scatterers. When the incident field is Gaussian correlated, the von Laue spots get more diffuse. When the incident field is J_0-Bessel correlated, the von Laure pattern changes drastically. In the forward direction, multi-colored ellipses are produced. In the backward direction the scattering generates overlapping, near monochromatic rings.

In Chapter 6 [Wang *et al.*, 2017] we turn our attention from Bessel-correlated fields to beams with a Bessel intensity distribution. These so-called non-diffracting beams have been the subject of intense investigation during the last few years. However, most of the work was done within the framework of scalar diffraction theory. We have analyzed the electromagnetic field that is produced by a paraxial axicon lens. We found, among other things, that the axicon field is strongly dependent on the polarization of the incident beam. When this beam is linearly polarized, both the on-axis and the transverse intensity are in good agreement with the predictions of scalar theory. However, when the incident beam is radially or azimuthally polarized, the field distribution changes dramatically.

We end this thesis with a summary in Dutch of our results.

1.4.1 Publications

This thesis is based on the following publications:

- Yangyundou Wang, Shenggang Yan, David Kuebel, and Taco D. Visser, "Dynamic control of light scattering using spatial coherence," Physical Review A, vol. 92, 013806 (2015).

- Yangyundou Wang, Hugo F. Schouten, and Taco D. Visser, "Tunable, anomalous Mie scattering using spatial coherence," Optics Letters, vol. 40, pp. 4779–4782 (2015).

- Yangyundou Wang, Hugo F. Schouten, and Taco D. Visser, "Strong suppression of forward or backward Mie scattering by using spatial coherence," Journal of the Optical Society of America A, vol. 33, pp. 513–518 (2016).

- Yangyundou Wang, David Kuebel, Taco D. Visser, and Emil Wolf, "Creating new von Laue patterns in crystal scattering with partially coherent sources," Physical Review A, vol. 94, 033812 (2016).

- Yangyundou Wang, Shenggang Yan, Ari T. Friberg, David Kuebel, and Taco D. Visser, "The electromagnetic field produced by a refractive axicon," to be submitted.

Chapter 2

Dynamic control of light scattering using spatial coherence

This Chapter is based on

- Yangyundou Wang, Shenggang Yan, David Kuebel and Taco D. Visser, "Dynamic control of light scattering using spatial coherence," Physical Review A, vol. 92, 013806 (2015).

Abstract
The scattering of light is perhaps the most fundamental of optical processes. However, active, and dynamic control of the directionality of a scattered light field has until now remained elusive. Here we show that with an easily generated, Bessel-correlated field, this goal can be achieved, at least partially. In particular, the angular distribution of a field scattered by a random spherical particle can be tuned to gradually suppress the forward scattering intensity, and even create a cone-like scattered field. Our method provides a tool for the dynamic control of scattering patterns, both macroscopically and microscopically.

2.1 Introduction

The scattering of wave fields is a process that is encountered in many branches of science, such as astronomy, atmospheric studies, solid state physics, and optics. Because both of its fundamental importance and its many applications, it is highly desirable to achieve active control over the strength and directionality of the scattered field. When a wave is incident on a spherical object, typically a substantial portion of the field is scattered in the forward and in the backward direction. Examples of strong forward scattering are the Mie effect [Born and Wolf, 1995, Sec. 14.5], and the Arago-Poisson spot [van de Hulst, 1981, Sec. 8.1]. Kerker *et al.* [Kerker *et al.*, 1983] seem to have been the first to examine under what conditions this angular distribution of the scattered field is modified. Ever since their work, many researchers have analyzed how the composition or geometry of a particle can be chosen such that the scattering in certain directions is suppressed, see, e.g., [Alu and Engheta, 2010; Nieto-Vesperina *et al.*, 2011; Garcia-Camara *et al.*, 2011; Geffrin *et al.*, 2012; Person *et al.*, 2013; Xie *et al.*, 2015; Korotkova, 2015; Naraghi *et al.*, 2015]. Here we demonstrate a completely different approach to control the scattering process. By using a scalar field model and applying the first-order Born approximation, we show that dynamic manipulation of the source that generates the incident field, rather than of the scattering object, offers a simple tool to control the angular distribution of the scattered field.

Over the years, many studies have been dedicated to the effects of spatial coherence on the scattering process [Carter and Wolf, 1988; Jannson *et al.*, 1988; Gori *et al.*, 1990; Carney and Wolf, 1998; Cabaret *et al.*, 1998; Visser *et al.*, 2006; Greffet *et al.*, 2003; van Dijk *et al.*, 2010; Fischer *et al.*, 2012]. One typically finds that the scattering remains predominantly in the forward direction, but becomes more diffuse when the spatial coherence of the incident field decreases. However, these studies were limited to Gaussian-correlated fields. Here we report the result that Bessel-correlated fields, which can readily be generated as reported in [Raghunathan *et al.*, 2010], allow one to dynamically vary the scattering amplitude, making it possible to gradually suppress scattering in the forward direction, and eventually even create a cone-like scattered field. We examine scalar fields that are generated by partially coherent, planar sources, and use the first-order Born approximation to study the scattered field that arises when a Gaussian-correlated sphere is placed in the far zone. We compare so-called Gaussian Schell-model sources and uncorrelated annular sources that produce Bessel-correlated fields.

2.2 Partially coherent sources

Let us consider a secondary, partially coherent, planar source that is situated in the plane $z = 0$, as shown in Fig. 2.1. The symbol $\boldsymbol{\rho} = (x, y)$ denotes a transverse vector. The coherence properties of the source field at two points $\boldsymbol{\rho}_1$, and $\boldsymbol{\rho}_2$ at frequency ω can be characterized by the cross-spectral density function [Mandel and Wolf, 1995, Sec. 4.3.2]

$$W^{(0)}(\boldsymbol{\rho}_1, \boldsymbol{\rho}_2, \omega) = \langle U^{(0)^*}(\boldsymbol{\rho}_1, \omega) U^{(0)}(\boldsymbol{\rho}_2, \omega)\rangle, \tag{2.1}$$

where the angled brackets indicate the average taken over an ensemble of realizations of source fields $U^{(0)}(\boldsymbol{\rho}, \omega)$. The cross-spectral density in the far zone of the source, denoted by $W^{(\infty)}$, is given by the formula [Mandel and Wolf, 1995, Eq. 5.3-4]

$$\begin{aligned} W^{(\infty)}(r_1\mathbf{u}_1, r_2\mathbf{u}_2, \omega) = {} & \left(\frac{k}{2\pi}\right)^2 \frac{\exp[ik(r_2 - r_1)]}{r_1 r_2} \cos\alpha_1 \cos\alpha_2 \\ & \times \iint_{z=0} W^{(0)}(\boldsymbol{\rho}_1, \boldsymbol{\rho}_2, \omega) \\ & \times \exp[-ik(\mathbf{u}_{2\perp} \cdot \boldsymbol{\rho}_2 - \mathbf{u}_{1\perp} \cdot \boldsymbol{\rho}_1)]\, \mathrm{d}^2\rho_1 \mathrm{d}^2\rho_2, \end{aligned} \tag{2.2}$$

where $\mathbf{u}_{1\perp}$ and $\mathbf{u}_{2\perp}$ are the projections, considered as two-dimensional vectors, of the three-dimensional directional unit vectors $\mathbf{u}_1$ and $\mathbf{u}_2$ onto the source plane. α_1 and α_2 denote the angles which the vectors $\mathbf{u}_1$ and $\mathbf{u}_2$ make with the positive z axis. A sphere with volume D is located in the far zone of the source, at a distance Δz. If the linear dimensions of the scatterer are assumed to be small compared to Δz, then the angle subtended at the origin O by the scatterer is small, and $\cos\alpha_1 \approx \cos\alpha_2 \approx 1$. Furthermore, the factor $k(r_2 - r_1)$ where $r_i = |(\boldsymbol{\rho}_i, z_i)|$, with $i = 1$ or 2, can then be expressed as

$$\begin{aligned} k(r_2 - r_1) &\approx k[z_2(1 + \rho_2^2/2z_2^2) - z_1(1 + \rho_1^2/2z_1^2)], \qquad (2.3) \\ &\approx k(z_2 - z_1), \qquad (2.4) \end{aligned}$$

where we have used the fact that ρ_1 and ρ_2 are both bounded by the transverse size of the scatterer. In addition, the small size of the scatterer implies that the factor $1/r_1r_2$ does not vary appreciably over its domain D, i.e., $1/r_1r_2 \approx 1/(\Delta z)^2$. On making use of these approximations in Eq. (2.2) we obtain the expression

$$\begin{aligned} W^{(\infty)}(r_1\mathbf{u}_1, r_2\mathbf{u}_2, \omega) = &\left(\frac{k}{2\pi\Delta z}\right)^2 \exp[ik(z_2 - z_1)] \\ &\times \iint_{z=0} W^{(0)}(\boldsymbol{\rho}_1, \boldsymbol{\rho}_2, \omega) \\ &\times \exp[-ik(\mathbf{u}_{2\perp} \cdot \boldsymbol{\rho}_2 - \mathbf{u}_{1\perp} \cdot \boldsymbol{\rho}_1)]\, \mathrm{d}^2\rho_1 \mathrm{d}^2\rho_2. \end{aligned} \tag{2.5}$$

It is worth noting that the factor $\exp[ik(z_2 - z_1)]$ implies that the far-zone field is longitudinally fully coherent [Mandel and Wolf, 1995, Sec. 5.2.1]. Before we can use Eq. (2.5) as an expression for the cross-spectral density of the field that is incident on the scatterer, it must be expressed in terms of the primed variables defined in Fig. 2.1. This is done by noting that

$$\mathbf{r}_i = r_i\mathbf{u}_i = (\boldsymbol{\rho}_i, z_i) = (\boldsymbol{\rho}'_i, z_i), \quad i = 1, 2, \tag{2.6}$$

and hence

$$\mathbf{u}_{i\perp} = \boldsymbol{\rho}'_i / r_i \approx \boldsymbol{\rho}'_i / \Delta z. \tag{2.7}$$

This allows us to re-write Eq. (2.5) as

$$\begin{aligned} W^{(\mathrm{inc})}(\mathbf{r}'_1, \mathbf{r}'_2, \omega) = &\left(\frac{k}{2\pi\Delta z}\right)^2 \exp[ik(z'_2 - z'_1)] \\ &\times \iint_{z=0} W^{(0)}(\boldsymbol{\rho}_1, \boldsymbol{\rho}_2, \omega) \\ &\times \exp[-ik(\boldsymbol{\rho}'_2 \cdot \boldsymbol{\rho}_2 - \boldsymbol{\rho}'_1 \cdot \boldsymbol{\rho}_1)/\Delta z]\, \mathrm{d}^2\rho_1 \mathrm{d}^2\rho_2, \end{aligned} \tag{2.8}$$

where the superscript "inc" indicates the incident field. We will make use of Eq. (2.8) to determine the cross-spectral density of the field incident on the scattering volume D for different kinds of sources.

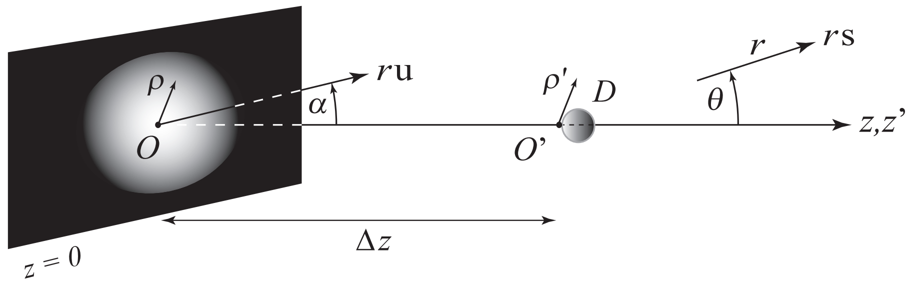

Figure 2.1: A secondary, partially coherent source is situated in the plane $z = 0$. A sphere occupying a domain D is located in the far zone, at a distance Δz. The directional unit vector $\mathbf{u}$ and the position z are defined with respect to the origin $O = (0, 0, 0)$. The directional unit vector $\mathbf{s}$ and the position z' are defined with respect to a second origin $O' = (0, 0, \Delta z)$. The transverse vectors $\boldsymbol{\rho} = (x, y)$ and $\boldsymbol{\rho}' = (x', y')$ denote two-dimensional positions.

2.3 Scattering by a Gaussian-correlated sphere

Suppose first that a deterministic field $U^{(\mathrm{inc})}(\mathbf{r}, \omega)$ is incident on a deterministic scatterer. The space-dependent part of the scattered field $U^{(\mathrm{sca})}(\mathbf{r}, \omega)$ is, within the accuracy of the first-order Born approximation, given by the expression [Born and Wolf, 1995, Sec. 13.1.2]

$$U^{(\mathrm{sca})}(\mathbf{r}, \omega) = \int_D F(\mathbf{r}', \omega) U^{(\mathrm{inc})}(\mathbf{r}', \omega) G(\mathbf{r}, \mathbf{r}', \omega)\, \mathrm{d}^3 r', \tag{2.9}$$

where

$$F(\mathbf{r}, \omega) = \frac{k^2}{4\pi}[n^2(\mathbf{r}, \omega) - 1] \tag{2.10}$$

denotes the scattering potential of the medium, $n(\mathbf{r}, \omega)$ being its refractive index, and

$$G(\mathbf{r}, \mathbf{r}', \omega) = \frac{\exp(ik|\mathbf{r} - \mathbf{r}'|)}{|\mathbf{r} - \mathbf{r}'|} \tag{2.11}$$

is the outgoing free-space Green's function of the Helmholtz operator.
We choose the origin O' of a second Cartesian coordinate system at the front face of the scatterer and consider the field at a point $\mathbf{r}$ in its far

zone, as sketched in Fig. 2.1. Setting $\mathbf{r} = r\mathbf{s}$, with $\mathbf{s}$ a unit directional vector, the Green's function in the far zone may be approximated by the expression

$$G(\mathbf{r}, \mathbf{r}', \omega) \sim \frac{\exp(ikr)}{r} \exp(-ik\mathbf{s} \cdot \mathbf{r}'). \tag{2.12}$$

For a random scatterer the scattering potential is a random function of position. Let

$$C_F(\mathbf{r}_1', \mathbf{r}_2', \omega) = \langle F^*(\mathbf{r}_1', \omega) F(\mathbf{r}_2', \omega) \rangle_F \tag{2.13}$$

be its correlation function. The angled brackets denote the average, taken over an ensemble of realizations of the scattering potential. We will consider scattering from a Gaussian-correlated, homogeneous, isotropic sphere. Then

$$C_F(\mathbf{r}_1', \mathbf{r}_2', \omega) = C_0 \exp\left[-(\mathbf{r}_2' - \mathbf{r}_1')^2 / 2\sigma_F^2\right], \tag{2.14}$$

where C_0 is a positive constant, and the coherence length σ_F is assumed to be small compared with the linear dimensions of the scattering volume. This assumption will later allow us to extend the domain of integration to $\mathbb{R}^3$. Next we assume that the incident field is partially coherent. Because of the random nature of both the incident field and the scatterer, the scattered field will, of course, also be random. Its cross-spectral density function is defined, in complete analogy with Eq. (2.1), as

$$W^{(\text{sca})}(\mathbf{r}_1, \mathbf{r}_2, \omega) = \langle U^{(\text{sca})*}(\mathbf{r}_1, \omega) U^{(\text{sca})}(\mathbf{r}_2, \omega) \rangle, \tag{2.15}$$

where the angled brackets indicate the average, taken over an ensemble of realizations of the scattered field. On substituting from Eqs. (2.9) and (2.13) into Eq. (2.15) and interchanging the order of integration and ensemble averaging, we find the formula

$$\begin{aligned} W^{(\text{sca})}(\mathbf{r}_1, \mathbf{r}_2, \omega) = \iint_D & W^{(\text{inc})}(\mathbf{r}_1', \mathbf{r}_2', \omega) C_F(\mathbf{r}_1', \mathbf{r}_2', \omega) \\ & \times G^*(\mathbf{r}_1, \mathbf{r}_1', \omega) G(\mathbf{r}_2, \mathbf{r}_2', \omega)\, \mathrm{d}^3 r_1' \mathrm{d}^3 r_2'. \end{aligned} \tag{2.16}$$

The spectral density of the scattered field, $S^{(\mathrm{sca})}(\mathbf{r},\omega)$, is obtained by setting the two positions $\mathbf{r}_1$ and $\mathbf{r}_2$ equal, i.e.,

$$S^{(\mathrm{sca})}(\mathbf{r},\omega) = W^{(\mathrm{sca})}(\mathbf{r},\mathbf{r},\omega), \tag{2.17}$$

$$= \frac{C_0}{r^2}\iint_D W^{(\mathrm{inc})}(\mathbf{r}_1',\mathbf{r}_2',\omega)\exp\left[-(\mathbf{r}_2'-\mathbf{r}_1')^2/2\sigma_F^2\right] \times \exp[-ik\mathbf{s}\cdot(\mathbf{r}_2'-\mathbf{r}_1')]\,\mathrm{d}^3r_1'\mathrm{d}^3r_2', \tag{2.18}$$

where we have used Eqs. (2.12) and (2.14). Before proceeding, we note that Eq. (2.18) relates the cross-spectral density of the incident field, $W^{(\mathrm{inc})}$, with the distribution of the scattered field in the far zone, $S^{(\mathrm{sca})}$. This relation has the form of a Fourier transform of the cross-spectral density, weighed with a Gaussian factor. In view of Eq. (2.8), which is also a Fourier transform, one might then suspect, on the basis of the van Cittert-Zernike theorem [Mandel and Wolf, 1995, Sec. 4.4.4], that the shape of a delta-correlated source is somehow mimicked by the scattered field. This observation was the motivation for this study.

Next we will analyze the consequences of Eq. (2.18) for incident fields generated by sources with different coherence properties. To simplify the notation we suppress the ω dependence of the various quantities from now on.

2.4 Gaussian Schell-model sources

Let us first assume that the source is of the Gaussian Schell-model type. Such sources have a cross-spectral density of the form [Wolf, 2007, Sec. 5.3.1]

$$W^{(0)}(\boldsymbol{\rho}_1,\boldsymbol{\rho}_2) = [S^{(0)}(\boldsymbol{\rho}_1)]^{1/2}[S^{(0)}(\boldsymbol{\rho}_2)]^{1/2}\mu^{(0)}(\boldsymbol{\rho}_1-\boldsymbol{\rho}_2,), \tag{2.19}$$

with

$$S^{(0)}(\boldsymbol{\rho}) = A^2\exp\left(-\rho^2/2\sigma_S^2\right), \tag{2.20}$$

$$\mu^{(0)}(\boldsymbol{\rho}_1-\boldsymbol{\rho}_2) = \exp[-(\boldsymbol{\rho}_2-\boldsymbol{\rho}_1)^2/2\sigma_\mu^2], \tag{2.21}$$

representing the spectral density and the spectral degree of coherence of the source field, respectively, the constants A, σ_S and σ_μ being positive quantities. On substituting from Eqs. (2.19)–(2.21) into Eq. (2.8) we obtain the formula

$$\begin{aligned} W^{(\mathrm{inc})}(\mathbf{r}_1', \mathbf{r}_2',) = &\left(\frac{kA\sigma_S\sigma_{\mathrm{eff}}}{\Delta z}\right)^2 \exp[ik(z_2'-z_1')] \\ &\times \exp\left[\frac{-k^2\sigma_S^2(\boldsymbol{\rho}_2'-\boldsymbol{\rho}_1')^2}{2(\Delta z)^2}\right] \\ &\times \exp\left[\frac{-k^2\sigma_{\mathrm{eff}}^2(\boldsymbol{\rho}_2'+\boldsymbol{\rho}_1')^2}{8(\Delta z)^2}\right], \end{aligned} \tag{2.22}$$

where

$$\frac{1}{\sigma_{\mathrm{eff}}^2} = \frac{1}{4\sigma_S^2} + \frac{1}{\sigma_\mu^2}. \tag{2.23}$$

On making use of Eq. (2.22) in expression (2.18) we find that the normalized distribution of the scattered intensity is given by the expression

$$S_N^{(\mathrm{sca})}(\theta) = S^{(\mathrm{sca})}(\theta)/S^{(\mathrm{sca})}(\theta=0), \tag{2.24}$$

$$= \exp\left[-k^2\sigma_F^2(1-\cos\theta)^2/2\right]\exp\left[-k^2\sin^2\theta/4\Gamma\right], \tag{2.25}$$

where

$$\Gamma = \frac{k^2\sigma_S^2}{2\Delta z^2} + \frac{1}{2\sigma_F^2}, \tag{2.26}$$

and θ denotes the scattering angle, shown in Fig. 2.1. A detailed derivation of Eq. (2.25) is presented in Appendix A. It is seen from Eq. (2.25) that the scattered field depends on the two length scales σ_S and σ_F. Notice that there is no dependence on the correlation length σ_μ of the source. This is a consequence of the fact that the scattering volume is located in the far zone, which means that the field in the vicinity of the z' axis has become essentially transversely coherent, as is discussed in [Mandel and Wolf, 1995, Sec. 5.6.4]. In Fig. 2.2 the spectral density of the scattered field is shown for different values of σ_F, the effective correlation length of the scatterer. It is seen that the scattering becomes more directional when σ_F increases. However, in all cases the scattering reaches its maximum value in the forward direction ($\theta = 0$). The scattered intensity for angles larger than 0.08 is negligible.

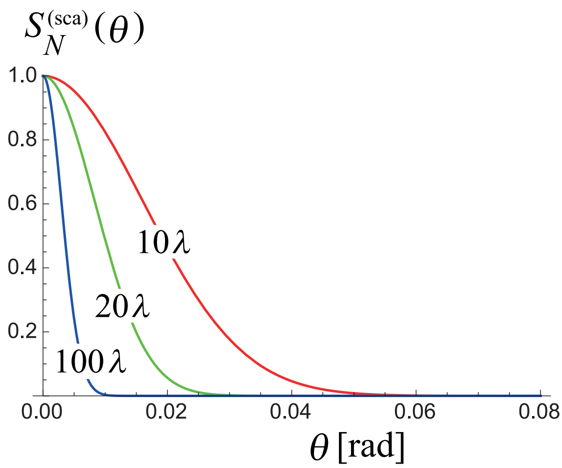

Figure 2.2: The normalized spectral density of the scattered field for selected values of the effective correlation length of the sphere: $\sigma_F = 10\lambda$ (red), 20λ (green) and 100λ (blue). In these examples the wavelength $\lambda = 0.6328$ μm, $\sigma_S = 1$ cm, and $\Delta z = 4$ m.

2.5 Uncorrelated annular sources

Next we consider a completely incoherent (i.e., delta-correlated), ring-shaped source with a uniform spectral density, and with inner radius a and outer radius b. The realization of such a source was reported in [Raghunathan *et al.*, 2010]. In this case the spectral density and the spectral degree of coherence in the source plane are

$$S^{(0)}(\boldsymbol{\rho}) = A^2 \left[\mathrm{circ}(\rho/b) - \mathrm{circ}(\rho/a)\right], \tag{2.27}$$

$$\mu^{(0)}(\boldsymbol{\rho}_1, \boldsymbol{\rho}_2) = \delta^2(\boldsymbol{\rho}_2 - \boldsymbol{\rho}_1), \tag{2.28}$$

where δ^2 denotes the two-dimensional Dirac delta function, and $\mathrm{circ}(x)$ the circle function, $\mathrm{circ}(x) = 1$ if $x \leq 1$, and 0 otherwise. Hence

$$\begin{aligned} W^{(0)}(\boldsymbol{\rho}_1, \boldsymbol{\rho}_2) = A^2 &\left[\mathrm{circ}(\rho_1/b) - \mathrm{circ}(\rho_1/a)\right]^{1/2} \\ &\times \left[\mathrm{circ}(\rho_2/b) - \mathrm{circ}(\rho_2/a)\right]^{1/2} \delta^2(\boldsymbol{\rho}_2 - \boldsymbol{\rho}_1). \end{aligned} \tag{2.29}$$

On substituting from this formula into Eq. (2.8) we find that

$$W^{(\mathrm{inc})}(\mathbf{r}_1', \mathbf{r}_2') = \frac{kA^2}{2\pi\Delta z} \exp[ik(z_2' - z_1')] \times \left[\frac{bJ_1\left(kb|\boldsymbol{\rho}_2' - \boldsymbol{\rho}_1'|/\Delta z\right)}{|\boldsymbol{\rho}_2' - \boldsymbol{\rho}_1'|} - \frac{aJ_1\left(ka|\boldsymbol{\rho}_2' - \boldsymbol{\rho}_1'|/\Delta z\right)}{|\boldsymbol{\rho}_2' - \boldsymbol{\rho}_1'|}\right], \quad (2.30)$$

where J_1 denotes the Bessel function of the first kind of order 1. On using Eq. (2.30) in Eq. (2.18) we obtain for the scattered intensity the expression

$$S^{(\mathrm{sca})}(\theta) = C \exp\left[-\frac{k^2\sigma_F^2(1-\cos\theta)^2}{2}\right] \times \int_0^\infty \left[bJ_1\left(\frac{kb\rho}{\Delta z}\right) - aJ_1\left(\frac{ka\rho}{\Delta z}\right)\right] \times J_0(k\rho\sin\theta)\exp\left(-\frac{\rho^2}{2\sigma_F^2}\right)\mathrm{d}\rho. \quad (2.31)$$

where C is a constant, independent of the angle θ. A specified derivation of Eq. (2.31) can be found in Appendix B. The results of a numerical evaluation of Eq. (2.31) are shown in Fig. 2.3. When the inner radius $a = 0$, meaning that the source is circular, the scattered field has a broad distribution that is centered on the forward direction $\theta = 0$. When $a =$ 2 mm, the forward scattered field has a decreased intensity that is only 45% of the maximum value which occurs near $\theta = 0.01$. Increasing the inner radius a to 2 cm produces a scattered field that is essentially zero in the forward direction and reaches a peak near $\theta = 0.025$. The effects of further increasing the inner radius a are illustrated in Fig. 2.4. The scattered field distribution becomes gradually narrower, and the direction of maximum intensity increases, eventually reaching a value of 8 degrees. This cone-like scattering that is obtained with a Bessel-correlated field is in marked contrast with the diffuse forward scattering that arises from a Gaussian-correlated field as was shown in Fig. 2.2.

It is to be noted that although we have presented examples at optical frequencies and scatterers with dimensions of $\sim 100\lambda$, we expect this method to work equally well at at longer wavelengths and for larger objects.

Finally, the question how zero forward scattering can be compatible with the optical theorem has been raised several years ago [Alu and

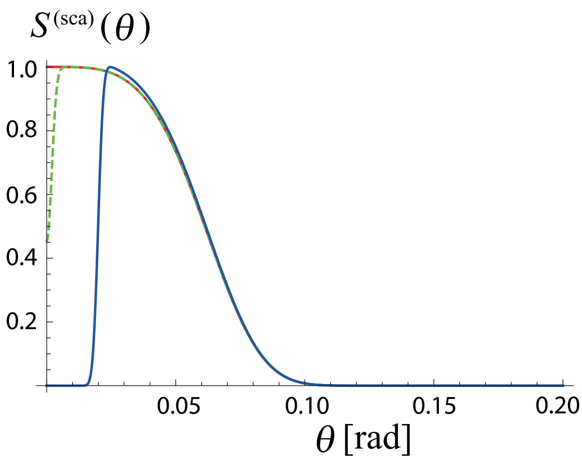

Figure 2.3: Angular distribution of the scattered field for various choices of the inner radius a of an annular source: $a = 0$ (red), 2 mm (dashed green), and 2 cm (blue). The curves are normalized to unity. In this example $\lambda = 0.6328$ μm, $\Delta z = 1$ m, $\sigma_F = 100$ λ, and the outer radius $b = 15$ cm.

Engheta, 2010]. Since this theorem holds only for deterministic scatterers that are illuminated by a fully coherent, monochromatic plane wave [Carney *et al.*, 1997], and because both conditions are not satisfied here, it clearly does not apply to the present case.

2.6 Uncorrelated, infinitely thin annular sources

It is instructive to consider the idealized case of a completely incoherent, infinitely thin "delta-ring" source. If this ring has a uniform spectral density A^2 and a radius c, then the cross-spectral density of the field in the source plane is given by the expression

$$W^{(0)}(\boldsymbol{\rho}_1, \boldsymbol{\rho}_2) = A^2\delta(\rho_1 - c)\delta^2(\boldsymbol{\rho}_1 - \boldsymbol{\rho}_2). \tag{2.32}$$

On substituting from this formula into Eq. (2.8) we find that

$$W^{(\mathrm{inc})}(\mathbf{r}'_1, \mathbf{r}'_2) = \frac{c}{2\pi}\left(\frac{Ak}{\Delta z}\right)^2 \exp[ik(z'_2 - z'_1)]J_0\left(\frac{kc|\boldsymbol{\rho}'_2 - \boldsymbol{\rho}'_1|}{\Delta z}\right). \tag{2.33}$$

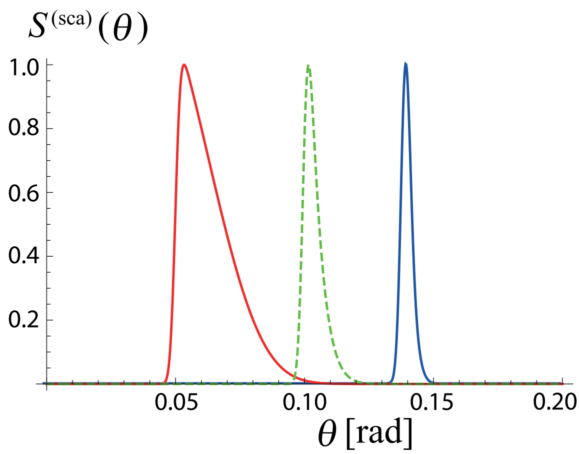

Figure 2.4: Angular distribution of the scattered field for various choices of the inner radius a of an annular source: $a = 5$ cm (red), 10 cm (dashed green), and 14 cm (blue). The curves are normalized to unity. The parameters are the same as in Fig. 2.3.

On making use of expression (2.33) in Eq. (2.18) we find (see Appendix C for details) that the distribution of the scattered intensity is now given by the formula

$$S^{(\mathrm{sca})}(\theta) = \exp\left[-\frac{k^2\sigma_F^2(1-\cos\theta)^2}{2}\right] \times \int_0^\infty J_0[k\rho\sin\theta] J_0\left(\frac{kc\rho}{\Delta z}\right)\exp\left(-\frac{\rho^2}{2\sigma_F^2}\right)\rho\,\mathrm{d}\rho. \qquad (2.34)$$

The product of the two oscillating J_0 functions will tend to cancel on integration, leading to a zero result. Except, however, when the arguments of the two functions are identical ($k\rho\sin\theta = kc\rho/\Delta z$). This means that we expect a scattered field that is negligibly small in all directions, with exception of the angle θ_{max} given by

$$\theta_{\mathrm{max}} \approx \sin\theta_{\mathrm{max}} = c/\Delta z. \qquad (2.35)$$

On numerically evaluating Eq. (2.34) we see that the scattered field is indeed concentrated in a very narrow interval around the direction θ_{max},

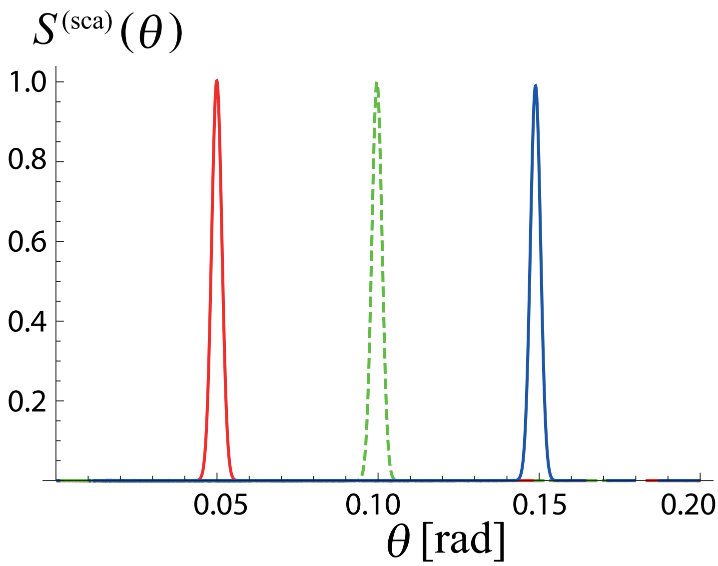

Figure 2.5: Normalized angular distribution of the scattered field for various choices of the radius c of an infinitely thin annular source: $c = 5$ cm (red), 10 cm (dashed green), and 15 cm (blue). The predicted values of $\theta_{\max}$ are 0.05, 0.10 and 0.15, respectively. The parameters are the same as in Fig. 2.3.

as can be seen from Fig. 2.5. Notice that $\theta_{\max}$ is also the semi-angle that is subtended by the source at the location of the scatterer.

2.7 Conclusions

We have demonstrated how the angular distribution of a field that is scattered by a random, Gaussian-correlated sphere can be manipulated using spatial coherence. Three types of sources were examined: Gaussian-Schell model sources, incoherent annular sources, and incoherent, infinitely thin annular sources. The first produces a Gaussian-correlated field, the rest a Bessel-correlated field. Using the first-order Born approximation, it was found that a Gaussian-correlated field gives rise to scattering that is predominantly in the forward direction. In stark contrast, the Bessel-correlated field was shown to lead to a decreased forward scattering. By simply varying the size of an uncorrelated annular source, the scattering distribution can be tuned, and can even take on a cone-like form without any forward scattering. Unlike using specially designed scatterers which produce a single, static field distribution, our approach can be used to dynamically alter the scattered field. We believe that our approach offers a new tool for the many uses of light scattering [Hergert and Wriedt (eds.), 2012]. For example, this method may be used to selectively address detectors that are positioned at different angles, or in cloaking [Alu and Engheta, 2009].

Appendix A - Derivation of Eq. (2.25)

Just as for the derivation of Eq. (2.22), it is advantageous to introduce sum and difference variables by defining

$$\boldsymbol{\rho}_+ = (\boldsymbol{\rho}'_1 + \boldsymbol{\rho}'_2)/2, \tag{A-1}$$
$$\boldsymbol{\rho}_- = \boldsymbol{\rho}'_2 - \boldsymbol{\rho}'_1, \tag{A-2}$$
$$z_+ = (z'_1 + z'_2)/2, \tag{A-3}$$
$$z_- = z'_2 - z'_1. \tag{A-4}$$

The Jacobian of this transformation is unity. Next we express all quantities in Eq. (2.18) in terms of these new variables. For the cross-spectral density given by Eq. (2.22) this gives

$$\begin{aligned} W^{(\mathrm{inc})}(\boldsymbol{\rho}_+, z_+, \boldsymbol{\rho}_-, z_-) = \beta \exp(ikz_-) \exp\left(-\frac{k^2\sigma_S^2\rho_-^2}{2(\Delta z)^2}\right) \\ \times \exp\left(-\frac{k^2\sigma_{\mathrm{eff}}^2\rho_+^2}{2(\Delta z)^2}\right), \end{aligned} \tag{A-5}$$

where

$$\beta = \left(\frac{kA\sigma_S\sigma_{\mathrm{eff}}}{\Delta z}\right)^2. \tag{A-6}$$

For the correlation function of the scattering potential, Eq. (2.14), we now get

$$C_F(\boldsymbol{\rho}_-, z_-) = C_0 \exp\left[-(\rho_-^2 + z_-^2)/2\sigma_F^2\right], \tag{A-7}$$

and the product of the two Green's functions becomes

$$\frac{\exp[-ik\mathbf{s}\cdot(\mathbf{r}_2'-\mathbf{r}_1')]}{r^2} = \frac{1}{r^2}\exp(-ik\mathbf{s}_\perp\cdot\boldsymbol{\rho}_-)\exp(-iks_z z_-). \tag{A-8}$$

Here $\mathbf{s} = (\mathbf{s}_\perp, s_z)$, $\mathbf{s}_\perp$ being the two-dimensional projection, considered as a vector, of the unit directional vector $\mathbf{s}$ onto the xy plane. Substitution from Eqs. (A-2), (A-3) and (A-4) into Eq. (2.18) yields

$$\begin{aligned} S^{(\mathrm{sca})}(r\mathbf{s}) = {} & \frac{C_0\beta}{r^2}\int \mathrm{d}z_+ \int \exp\left[-\frac{k^2\sigma_{\mathrm{eff}}^2\rho_+^2}{2(\Delta z)^2}\right]\mathrm{d}^2\rho_+ \\ & \times \int \exp\left(-\frac{z_-^2}{2\sigma_F^2}\right)\exp\left[-ik(s_z-1)z_-\right]\mathrm{d}z_- \\ & \times \int \exp\left\{-\rho_-^2\left[\frac{k^2\sigma_S^2}{2(\Delta z)^2}+\frac{1}{2\sigma_F^2}\right]\right\}\exp\left(-ik\mathbf{s}_\perp\cdot\boldsymbol{\rho}_-\right)\mathrm{d}^2\rho_-. \end{aligned} \tag{A-9}$$

The first two integrals, those over z_+ and ρ_+, do not depend on the direction of scattering $\mathbf{s}$. We let M denote their product. Making use of the assumption that σ_F is small compared to the scatterer size, the integrals over z_- and $\boldsymbol{\rho}_-$ may be extended to infinity. They are then both seen to be a Fourier transform of a Gaussian distribution, whose evaluation yields

$$\begin{aligned} & \int_{-\infty}^{\infty}\exp\left(-\frac{z_-^2}{2\sigma_F^2}\right)\exp\left[-ik(s_z-1)z_-\right]\mathrm{d}z_-, \\ & = \sqrt{2\pi}\sigma_F\exp\left[-\frac{k^2\sigma_F^2(1-s_z)^2}{2}\right], \end{aligned} \tag{A-10}$$

and

$$\begin{aligned} & \int_{-\infty}^{\infty}\exp\left\{-\rho_-^2\left[\frac{k^2\sigma_S^2}{2(\Delta z)^2}+\frac{1}{2\sigma_F^2}\right]\right\}\exp\left(-ik\mathbf{s}_\perp\cdot\boldsymbol{\rho}_-\right)\mathrm{d}^2\rho_-, \\ & = \frac{\pi}{\Gamma}\exp\left(-\frac{k^2 s_\perp^2}{4\Gamma}\right), \end{aligned} \tag{A-11}$$

where

$$\Gamma = \frac{k^2\sigma_S^2}{2(\Delta z)^2}+\frac{1}{2\sigma_F^2}. \tag{A-12}$$

Thus we obtain

$$S^{(\mathrm{sca})}(r\mathbf{s}) = \frac{C_0 \beta M \sigma_F \sqrt{2}\pi^{3/2}}{\Gamma r^2} \exp\left[-\frac{k^2\sigma_F^2(1-s_z)^2}{2}\right] \times \exp\left(-\frac{k^2 s_\perp^2}{4\Gamma}\right). \tag{A-13}$$

Using that $s_z = \cos\theta$ and $s_\perp^2 = \sin^2\theta$, we find that the normalized distribution of the spectral density of the scattered field is given by the expression

$$S_N^{(\mathrm{sca})}(\theta) = S^{(\mathrm{sca})}(\theta)/S^{(\mathrm{sca})}(\theta=0), \tag{A-14}$$

$$= \exp\left[-k^2\sigma_F^2(1-\cos\theta)^2/2\right] \exp\left[-k^2\sin^2\theta/4\Gamma\right], \tag{A-15}$$

which is Eq. (2.25).

Appendix B - Derivation of Eq. (2.31)

On making use of the sum and difference variables that were introduced in Appendix A, and then substituting from Eq. (2.30) into Eq. (2.18) we obtain the formula

$$\begin{aligned} S^{(\mathrm{sca})}(r\mathbf{s}) = {} & \frac{C_0 A^2 k}{2\pi r^2 \Delta z} \int \mathrm{d}z_+ \int \mathrm{d}^2\rho_+ \\ & \times \int \exp\left(-\frac{z_-^2}{2\sigma_F^2}\right) \exp\left[ikz_-(1-s_z)\right] \mathrm{d}z_- \\ & \times \int \left[\frac{bJ_1\left(kb\rho_-/\Delta z\right)}{\rho_-} - \frac{aJ_1\left(ka\rho_-/\Delta z\right)}{\rho_-}\right] \\ & \times \exp\left(-\frac{\rho_-^2}{2\sigma_F^2}\right) \exp\left(-ik\mathbf{s}_\perp \cdot \boldsymbol{\rho}_-\right) \mathrm{d}^2\rho_-. \end{aligned} \tag{B-1}$$

The first two integrals, those over z_+ and ρ_+, yield the volume of the scatterer, which we denote by V.

Using the assumption that σ_F is much smaller than the size of the particle, the integration over z_- may be extended to infinity. The integral is then seen to be a Fourier transform of a Gaussian distribution, for which we find

$$\int_{-\infty}^{\infty} \exp\left(-\frac{z_-^2}{2\sigma_F^2}\right) \exp\left[ik(1-s_z)z_-\right] \mathrm{d}z_- \\ = \sqrt{2\pi}\sigma_F \exp\left[-\frac{k^2\sigma_F^2(1-s_z)^2}{2}\right]. \tag{B-2}$$

The remaining integral over $\boldsymbol{\rho}_-$ can be re-written as

$$\int \left[\frac{bJ_1\left(kb\rho_-/\Delta z\right)}{\rho_-} - \frac{aJ_1\left(ka\rho_-/\Delta z\right)}{\rho_-}\right] \\ \times \exp\left(-\frac{\rho_-^2}{2\sigma_F^2}\right) \exp\left(-ik\mathbf{s}_\perp \cdot \boldsymbol{\rho}_-\right) \mathrm{d}^2\rho_-, \\ = \int_0^{\infty} \int_0^{2\pi} \exp\left(-iks_\perp \rho\cos\gamma\right) \left[bJ_1\left(kb\rho/\Delta z\right) - aJ_1\left(ka\rho/\Delta z\right)\right] \\ \times \exp\left(-\frac{\rho^2}{\sigma_F^2}\right) \mathrm{d}\gamma \mathrm{d}\rho. \tag{B-3}$$

Since

$$\int_0^{2\pi} \exp\left(-iks_\perp\rho\cos\gamma\right) \mathrm{d}\gamma = 2\pi J_0(k\rho s_\perp), \tag{B-4}$$

we obtain the formula

$$2\pi \int_0^{\infty} J_0(k\rho s_\perp) \left[bJ_1\left(kb\rho/\Delta z\right) - aJ_1\left(ka\rho/\Delta z\right)\right] \\ \times \exp\left(-\frac{\rho^2}{\sigma_F^2}\right) \mathrm{d}\rho. \tag{B-5}$$

This integral can be evaluated numerically. Combining these results, while using that $s_z = \cos\theta$ and $s_\perp = \sin\theta$, we finally find that

$$S^{(\mathrm{sca})}(\theta) = C \exp\left[-\frac{k^2\sigma_F^2(1-\cos\theta)^2}{2}\right] \\ \times \int_0^{\infty} \left[bJ_1\left(\frac{kb\rho}{\Delta z}\right) - aJ_1\left(\frac{ka\rho}{\Delta z}\right)\right] J_0(k\rho\sin\theta) \exp\left(-\frac{\rho^2}{2\sigma_F^2}\right) \mathrm{d}\rho, \tag{B-6}$$

with

$$C = \frac{C_0 A^2 k V \sqrt{2\pi}\sigma_F}{r^2 \Delta z}, \tag{B-7}$$

which is Eq. (2.31).

Appendix C - Derivation of Eq. (2.34)

On making use of the sum and difference variables that were introduced in Appendix A, and then substituting from Eq. (2.33) into Eq. (2.18) we obtain the expression

$$\begin{aligned} S^{(\text{sca})}(r\mathbf{s}) = {} & \frac{cC_0 A^2 k^2}{2\pi(\Delta z)^2 r^2} \int \mathrm{d}z_+ \int \mathrm{d}^2\rho_+ \\ & \times \int \exp\left(-\frac{z_-^2}{2\sigma_F^2}\right) \exp\left[-ik(s_z - 1)z_-\right] \mathrm{d}z_- \\ & \times \int J_0\left(\frac{kc}{\Delta z}|\boldsymbol{\rho}_-|\right) \exp\left(-\frac{\rho_-^2}{\sigma_F^2}\right) \exp\left(-ik\mathbf{s}_\perp \cdot \boldsymbol{\rho}_-\right) \mathrm{d}^2\rho_-. \end{aligned} \tag{C-1}$$

The first two integrals, those over z_+ and ρ_+, yield the volume of the scatterer, which we denote by V.

Using the assumption that σ_F is much smaller than the size of the particle, the integration over z_- may be extended to infinity. The integral is then seen to be a Fourier transform of a Gaussian distribution, for which we find

$$\begin{aligned} & \int_{-\infty}^{\infty} \exp\left(-\frac{z_-^2}{2\sigma_F^2}\right) \exp\left[ik(1 - s_z)z_-\right] \mathrm{d}z_-, \\ & = \sqrt{2\pi}\sigma_F \exp\left[-\frac{k^2\sigma_F^2(1 - s_z)^2}{2}\right]. \end{aligned} \tag{C-2}$$

Likewise, the remaining integral over $\boldsymbol{\rho}_-$ can be re-written as

$$\begin{aligned} & \int_{-\infty}^{\infty} J_0\left(\frac{kc|\boldsymbol{\rho}_-|}{\Delta z}\right) \exp\left(-\frac{\rho_-^2}{\sigma_F^2}\right) \exp\left(-ik\mathbf{s}_\perp \cdot \boldsymbol{\rho}_-\right) \mathrm{d}^2\rho_- \\ & = \int_0^{\infty} \int_0^{2\pi} \exp\left(-ik|\mathbf{s}_\perp|\rho\cos\gamma\right) J_0\left(\frac{kc\rho}{\Delta z}\right) \exp\left(-\frac{\rho^2}{\sigma_F^2}\right) \rho\, \mathrm{d}\gamma \mathrm{d}\rho. \end{aligned} \tag{C-3}$$

Since

$$\int_0^{2\pi} \exp\left(-iks_\perp \rho \cos\gamma\right) \mathrm{d}\gamma = 2\pi J_0(k\rho s_\perp), \tag{C-4}$$

we find for the integral over $\boldsymbol{\rho}_-$

$$2\pi \int_0^\infty J_0\left(\frac{kc\rho}{\Delta z}\right) J_0(k|\mathbf{s}_\perp|\rho) \exp\left(-\frac{\rho^2}{2\sigma_F^2}\right) \rho \, \mathrm{d}\rho. \tag{C-5}$$

This integral can be evaluated numerically. Combining these results, while using that $s_z = \cos\theta$ and $s_\perp = \sin\theta$, we finally obtain the formula

$$\begin{aligned} S^{(sca)}(\theta) = {} & C \exp\left[-\frac{k^2\sigma_F^2(1-\cos\theta)^2}{2}\right] \\ & \times \int_0^\infty J_0\left(\frac{kc\rho}{\Delta z}\right) J_0(k\rho\sin\theta) \exp\left(-\frac{\rho^2}{2\sigma_F^2}\right) \rho \, \mathrm{d}\rho, \end{aligned} \tag{C-6}$$

with

$$C = \frac{cC_0 A^2 V k^2 \sqrt{2\pi}\sigma_F}{r^2(\Delta z)^2}, \tag{C-7}$$

which is Eq. (2.34).

Chapter 3

Tuneable, anomalous Mie scattering using partial coherence

This Chapter is based on

- Yangyundou Wang, Hugo F. Schouten, and Taco D. Visser, "Tunable, anomalous Mie scattering using spatial coherence," Optics Letters, vol. 40, pp. 4779-4782 (2015).

Abstract
We demonstrate that a J_0 Bessel-correlated beam that is incident on a homogeneous sphere, produces a highly unusual distribution of the scattered field, with the maximum no longer occurring in the forward direction. Such a beam can be easily generated using a spatially incoherent, annular source. Moreover, the direction of maximal scattering can be shifted by changing the spatial coherence length. In this process the total power that is scattered remains constant. This new tool to control scattering directionality may be used to steer the scattered field away from the forward direction and selectively adress detectors situated at different angles.

3.1 Introduction

Mie scattering, which is the scattering of an optical field by a spherical object, has a long and venerable history [Mie, 1908; Born and Wolf, 1995; van de Hulst, 1981]. In its classical form it deals with the scattering of a fully coherent, monochromatic plane wave by a homogeneous, deterministic sphere. Its many applications in, e.g., spectroscopy, optical trapping, astronomy and atmospheric studies [Bohren and Huffman, 2004; Hergert and Wriedt (eds.), 2012], have led to a large literature, a substantial part of which can be divided into two broad categories. The first one, inspired by the seminal work of Kerker *et al.* [Kerker *et al.*, 1983], consists of efforts to design objects with a prescribed scattering profile, such as a suppressed scattering in the forward or backward directions [Nieto-Vesperina *et al.*, 2011; Garcia-Camara *et al.*, 2011; Geffrin *et al.*, 2012; Person *et al.*, 2013; X-ie *et al.*, 2015; Korotkova, 2015; Naraghi *et al.*, 2015]. The second category consists of studies in which scattering theory is extended to incident fields that are not deterministic, but rather partially coherent [Jannson *et al.*, 1988; Gori *et al.*, 1990; Carney *et al.*, 1997; Greffet *et al.*, 2003; van Dijk *et al.*, 2010; Fischer *et al.*, 2012; Ding *et al.*, 2012; Liu *et al.*, 2014]. These researches are motivated by the fact that light that travels through atmospheric turbulence suffers a loss of coherence.

In this Chapter we bridge both categories by reporting a novel coherence technique that allows one to steer most of the scattered intensity away from the forward direction. In contrast to previous works, this is done by manipulating the incident beam rather than the scatterer. We show that changing the spatial coherence of the beam allows one to dynamically control the scattering distribution. In this tuning of the scattering process, the total power that is scattered remains unchanged.

A special class of partially coherent beams is formed by those with a J_0-Bessel correlation. Such beams are easily produced with the help of uncorrelated, annular sources. Unlike, for example, Gaussian correlation functions, Bessel functions can take on negative values, which leads to qualitatively different physical effects. For example, when a Gaussian-correlated field is focused, the diffraction pattern gets washed out, with the maximum remaining at the focal point. In contrast, a Bessel-correlated

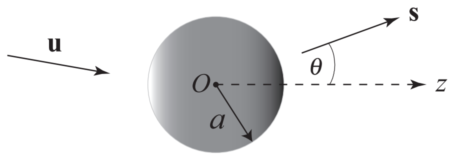

Figure 3.1: A sphere with radius a is illuminated by a plane wave propagating in the direction $\mathbf{u}$. The scattering angle θ is the angle between the positive z axis and a far-zone observation point $r\mathbf{s}$.

field creates an minimum at focus [Gbur and Visser, 2003; van Dijk *et al.*, 2008; Raghunathan *et al.*, 2010]. Likewise, when a Gaussian-correlated beam is scattered, the scattering remains predominantly in the forward direction [van Dijk *et al.*, 2010]. Here we show that scalar Mie scattering with J_0-correlated fields leads to a radically different profile in which the maximum occurs in a cone centered around the forward direction. We examine the influence of the transverse coherence length of the incident field, and find that by reducing this length the angle of maximum scattering can be gradually moved from 0° to 29°. We show that the extinguished power is independent of the coherence length. That means that changing this length results in a redistribution of the total scattered field.

3.2 Mie scattering with partially coherent fields

Let us first consider a plane, monochromatic scalar wave, propagating in a direction specified by a real unit vector $\mathbf{u}$, which is incident on a spherical scatterer. If the wave has an amplitude $a(\mathbf{u}, \omega)$, it can be represented as

$$V^{(\mathrm{inc})}(\mathbf{r}, t) = U^{(\mathrm{inc})}(\mathbf{r}, \omega) \exp(-i\omega t), \tag{3.1}$$

where

$$U^{(\mathrm{inc})}(\mathbf{r}, \omega) = a(\mathbf{u}, \omega) \exp(ik\mathbf{u} \cdot \mathbf{r}). \tag{3.2}$$

Here $\mathbf{r}$ denotes a position in space, t a moment in time, and ω the angular frequency. Also, $k = \omega/c = 2\pi/\lambda$ represents the wave number, c being the speed of light in vacuum and λ the wavelength. The time-independent part of the total field that results from the scattering process is written as the sum of the incident field and the scattered field, viz.,

$$U(\mathbf{r},\omega) = U^{(\mathrm{inc})}(\mathbf{r},\omega) + U^{(\mathrm{sca})}(\mathbf{r},\omega). \tag{3.3}$$

The scattered field in the far-zone of the scatterer, at an observation point $\mathbf{r} = r\mathbf{s}$, where $\mathbf{s}$ is a unit vector, has the asymptotic form [Born and Wolf, 1995, Ch. 13.1]

$$U^{(\mathrm{sca})}(r\mathbf{s},\omega) \sim a(\mathbf{u}_\perp,\omega)\, f(\mathbf{s},\mathbf{u},\omega)\frac{e^{ikr}}{r} \quad (kr \to \infty), \tag{3.4}$$

with $f(\mathbf{s},\mathbf{u},\omega)$ the scattering amplitude. To facilitate future notation, the amplitude now has argument $\mathbf{u}_\perp$ rather than $\mathbf{u}$. Here $\mathbf{u}_\perp$ is the projection, considered as a two-dimensional vector, of $\mathbf{u}$ onto the xy plane. This is allowed because $\mathbf{u}$, being a real unit vector, has a z component that is completely specified by its transverse components.

Next consider the situation where the incident field is not a plane wave but is of a more general form. Its time-independent part of an incident wave field at position $\mathbf{r}$ and frequency ω, can be represented in terms of an angular spectrum of plane-waves propagating in directions $\mathbf{u} = (\mathbf{u}_\perp, u_z)$ into the half-space $z > 0$, viz. [Mandel and Wolf, 1995, Sec. 3.2]

$$U^{(\mathrm{inc})}(\mathbf{r},\omega) = \int_{|\mathbf{u}_\perp|^2\leq 1} a(\mathbf{u}_\perp,\omega)\exp(ik\mathbf{u}\cdot\mathbf{r})\,\mathrm{d}^2u_\perp. \tag{3.5}$$

Limiting the integration to directional vectors $|\mathbf{u}_\perp|^2 \leq 1$ implies that we neglect evanescent waves. According to Eq. (3.4) the scattered field now takes on the form

$$U^{(\mathrm{sca})}(r\mathbf{s},\omega) = \frac{e^{ikr}}{r}\int_{|\mathbf{u}_\perp|^2\leq 1} a(\mathbf{u}_\perp,\omega) f(\mathbf{s},\mathbf{u},\omega)\,\mathrm{d}^2u_\perp. \tag{3.6}$$

In the space-frequency domain the coherence properties of a stochastic field is characterized by its cross-spectral density function [Mandel and Wolf, 1995, Sec. 4.3.2]

$$W(\mathbf{r}_1,\mathbf{r}_2,\omega) = \langle U^*(\mathbf{r}_1,\omega)U(\mathbf{r}_2,\omega)\rangle, \tag{3.7}$$

where the angled brackets indicate the average taken over an ensemble of field realizations. It follows from Eqs. (3.6) and Eq. (3.7) that the cross-spectral density of the scattered field is given by the expression

$$W^{(\mathrm{sca})}(r_1\mathbf{s}_1, r_2\mathbf{s}_2, \omega) = \frac{e^{\mathrm{i}k(r_2-r_1)}}{r_1 r_2} \int_{|\mathbf{u}_{1\perp}|^2 \leq 1} \int_{|\mathbf{u}_{2\perp}|^2 \leq 1} \mathcal{A}(\mathbf{u}_{1\perp}, \mathbf{u}_{2\perp}, \omega) \times f^*(\mathbf{s}_1, \mathbf{u}_1, \omega) f(\mathbf{s}_2, \mathbf{u}_2, \omega)\, \mathrm{d}^2 u_{1\perp} \mathrm{d}^2 u_{2\perp}, \tag{3.8}$$

where

$$\mathcal{A}(\mathbf{u}_{1\perp}, \mathbf{u}_{2\perp}, \omega) = \langle a^*(\mathbf{u}_{1\perp}, \omega) a(\mathbf{u}_{2\perp}, \omega) \rangle \tag{3.9}$$

is the angular correlation function of the incident field [Mandel and Wolf, 1995, Sec. 5.6.3]. The spectral density of the far-zone scattered field is obtained by setting the spatial arguments in Eq. (3.8) equal, i.e.,

$$S^{(\mathrm{sca})}(r\mathbf{s}, \omega) = W^{(\mathrm{sca})}(r\mathbf{s}, r\mathbf{s}, \omega). \tag{3.10}$$

This gives

$$S^{(\mathrm{sca})}(r\mathbf{s}, \omega) = \frac{1}{r^2} \int_{|\mathbf{u}_{1\perp}|^2 \leq 1} \int_{|\mathbf{u}_{2\perp}|^2 \leq 1} \mathcal{A}(\mathbf{u}_{1\perp}, \mathbf{u}_{2\perp}, \omega) \times f^*(\mathbf{s}, \mathbf{u}_1) f(\mathbf{s}, \mathbf{u}_2)\, \mathrm{d}^2 u_{1\perp} \mathrm{d}^2 u_{2\perp}. \tag{3.11}$$

For the case of a homogeneous spherical scatterer, the scattering amplitude depends on the cosine of the angle θ between the direction of incidence, indicated by the vector $\mathbf{u}$, and the direction of scattering $\mathbf{s}$ (see Fig. 4.1). Thus we can write

$$f(\mathbf{s}, \mathbf{u}, \omega) = f(\mathbf{s} \cdot \mathbf{u}, \omega). \tag{3.12}$$

For a sphere of radius a and with refractive index n the scattering amplitude can be expressed as (see [Joachain, 1987, Eq. (4.66)], with a trivial change in notation)

$$f(\mathbf{s} \cdot \mathbf{u}, \omega) = \frac{1}{k} \sum_{l=0}^{\infty} (2l+1) \exp[i\delta_l(\omega)] \sin[\delta_l(\omega)] P_l(\mathbf{s} \cdot \mathbf{u}), \tag{3.13}$$

where P_l denotes a Legendre polynomial of order l, and the phase shifts $\delta_l(\omega)$ are given by the expressions [JOACHAIN, 1987, Sec. 4.3.2 and 4.4.1]

$$\tan[\delta_l(\omega)] = \frac{\bar{k} j_l(ka) j_l'(\bar{k}a) - k j_l(\bar{k}a) j_l'(ka)}{\bar{k} j_l'(\bar{k}a) n_l(ka) - k j_l(\bar{k}a) n_l'(ka)}. \tag{3.14}$$

Here j_l and n_l are spherical Bessel functions and spherical Neumann functions, respectively, of order l. Furthermore,

$$\bar{k} = nk \tag{3.15}$$

is the wavenumber associated with the reduced wavelength within the scatterer, and the primes denote differentiation with respect to the spatial variable.

3.3 J_0-correlated fields

Consider an incident field with a uniform spectral density $S^{(0)}(\omega)$, that is J_0-correlated. This means that its cross-spectral density function in the plane $z = 0$ (the plane which passes through the center of the sphere) is of the form

$$W^{(\mathrm{inc})}(\boldsymbol{\rho}_1, \boldsymbol{\rho}_2, \omega) = S^{(0)}(\omega) J_0(\beta|\boldsymbol{\rho}_2 - \boldsymbol{\rho}_1|), \tag{3.16}$$

where J_0 denotes the Bessel function of the first kind and zeroth order, and $\boldsymbol{\rho}_1 = (x_1, y_1)$ and $\boldsymbol{\rho}_2 = (x_2, y_2)$ are two dimensional position points in the $z = 0$ plane. The parameter β is, roughly speaking, the inverse of the effective transverse coherence width of the incident field. The generation of such a beam was reported in [RAGHUNATHAN *et al.*, 2010].

In order to evaluate Eq. (3.11) for this case, we need to calculate the angular correlation function $\mathcal{A}(\mathbf{u}_{1\perp}, \mathbf{u}_{2\perp}, \omega)$. This function is related to the cross-spectral density through the expression [MANDEL AND WOLF, 1995, Sec. 5.6.3]

$$\mathcal{A}(\mathbf{u}_{1\perp}, \mathbf{u}_{2\perp}, \omega) = \left(\frac{k}{2\pi}\right)^4 \iint_{-\infty}^{\infty} W^{(\mathrm{inc})}(\boldsymbol{\rho}_1, \boldsymbol{\rho}_2, \omega) \times \exp[-ik(\mathbf{u}_{2\perp} \cdot \boldsymbol{\rho}_2 - \mathbf{u}_{1\perp} \cdot \boldsymbol{\rho}_1)] \, \mathrm{d}^2\rho_1 \mathrm{d}^2\rho_2. \tag{3.17}$$

On substituting from Eq. (3.16) into Eq. (3.17), we find that

$$\mathcal{A}(\mathbf{u}_{1\perp}, \mathbf{u}_{2\perp}, \omega) = \left(\frac{k}{2\pi}\right)^4 S^{(0)}(\omega) \iint_{-\infty}^{\infty} J_0(\beta|\boldsymbol{\rho}_2 - \boldsymbol{\rho}_1|) \times \exp[-ik(\mathbf{u}_{2\perp} \cdot \boldsymbol{\rho}_2 - \mathbf{u}_{1\perp} \cdot \boldsymbol{\rho}_1)]\, \mathrm{d}^2\rho_1 \mathrm{d}^2\rho_2. \tag{3.18}$$

It is useful to change variables to

$$\boldsymbol{\rho}_+ = (\boldsymbol{\rho}_1 + \boldsymbol{\rho}_2)/2, \tag{3.19}$$

$$\boldsymbol{\rho}_- = (\boldsymbol{\rho}_2 - \boldsymbol{\rho}_1). \tag{3.20}$$

The Jacobian of this transformation being unity, this leads to

$$\begin{aligned}\mathcal{A}(\mathbf{u}_{1\perp}, \mathbf{u}_{2\perp}, \omega) &= \left(\frac{k}{2\pi}\right)^4 S^{(0)}(\omega) \\ &\times \int J_0(\beta\rho_-)\, \exp[-\mathrm{i}k\boldsymbol{\rho}_- \cdot (\mathbf{u}_{1\perp} + \mathbf{u}_{2\perp})/2]\, \mathrm{d}^2\rho_- \\ &\times \int \exp[-\mathrm{i}k\boldsymbol{\rho}_+ \cdot (\mathbf{u}_{2\perp} - \mathbf{u}_{1\perp})]\, \mathrm{d}^2\rho_+, \qquad (3.21)\\ &= \left(\frac{k}{2\pi}\right)^4 S^{(0)}(\omega) \int \exp[-\mathrm{i}k\boldsymbol{\rho}_+ \cdot (\mathbf{u}_{2\perp} - \mathbf{u}_{1\perp})]\, \mathrm{d}^2\rho_+ \\ &\times \int_0^{\infty} \int_0^{2\pi} J_0(\beta\rho_-) \exp(-\mathrm{i}k\rho_-|\mathbf{u}_{1\perp} + \mathbf{u}_{2\perp}| \cos\phi/2) \\ &\times \rho_-\, \mathrm{d}\rho_- \mathrm{d}\phi, \qquad (3.22)\\ &= \left(\frac{k}{2\pi}\right)^4 S^{(0)}(\omega) \int \exp[-\mathrm{i}k\boldsymbol{\rho}_+ \cdot (\mathbf{u}_{2\perp} - \mathbf{u}_{1\perp})]\, \mathrm{d}^2\rho_+ \\ &\times 2\pi \int_0^{\infty} J_0(\beta\rho_-) J_0(k\rho_-|\mathbf{u}_{1\perp} + \mathbf{u}_{2\perp}|/2) \rho_-\, \mathrm{d}\rho_-. \qquad (3.23)\end{aligned}$$

Making use of the two Dirac delta function representations [Olver *et al.*, 2010]

$$\delta(x - a) = \frac{1}{2\pi} \int_{-\infty}^{\infty} e^{\mathrm{i}(x-a)t}\, \mathrm{d}t, \tag{3.24}$$

$$\delta(x - a) = x \int_0^{\infty} t J_0(xt) J_0(at)\, \mathrm{d}t, \tag{3.25}$$

we finally obtain the expression

$$\mathcal{A}(\mathbf{u}_{1\perp}, \mathbf{u}_{2\perp}, \omega) = \frac{k^2}{2\pi\beta} S^{(0)}(\omega)\, \delta^2(\mathbf{u}_{2\perp} - \mathbf{u}_{1\perp})\, \delta\left(\beta - k|\mathbf{u}_{1\perp} + \mathbf{u}_{2\perp}|/2\right). \tag{3.26}$$

On substituting from this result into Eq. (3.11), while making use of the two-dimensional delta function of Eq. (3.26) we find for the spectral density of the scattered field the expression

$$S^{(\mathrm{sca})}(r\mathbf{s}, \omega) = \frac{S^{(0)}(\omega)k^2}{2\pi\beta r^2} \int_{|\mathbf{u}_{1\perp}|^2 \leq 1} \delta(\beta - k|\mathbf{u}_{1\perp}|)\, |f(\mathbf{s}\cdot\mathbf{u}_1, \omega)|^2 \, \mathrm{d}^2 u_{1\perp}. \tag{3.27}$$

It is follows from the delta function in Eq. (3.27) that the incident Bessel-correlated beam must satisfy the condition

$$0 < \beta < k \tag{3.28}$$

in order to produce a scattered field. Since $1/\beta$ is a rough measure of the transverse coherence length, this implies that this length must exceed $1/k = \lambda/2\pi$. To illustrate that this condition is not restrictive, consider the idealized case of a J_0-correlated field that is generated by a completely incoherent, infinitely thin ring-shaped source. According to the far-zone form of the van Cittert-Zernike theorem [Mandel and Wolf, 1995, Sec. 4.4.4], the spectral degree of coherence now takes on the form [Wang *et al.*, 2015b], (Chapter 2 of this thesis)

$$\mu^{(\infty)}(\boldsymbol{\rho}_2 - \boldsymbol{\rho}_1, \omega) = J_0\left(\frac{kc|\boldsymbol{\rho}_2 - \boldsymbol{\rho}_1|}{\Delta z}\right), \tag{3.29}$$

where c denotes the ring radius, and Δz is the approximate distance from the center of the ring to the two observation points $(\boldsymbol{\rho}_1, z)$ and $(\boldsymbol{\rho}_2, z)$. Since these points are in the far zone, we can safely estimate that $\Delta z \geq 2c$. Comparing this with Eq. (3.16) gives $\beta \leq 0.5k$, in agreement with Eq. (3.28). This translates into a transverse coherence length $1/\beta \geq \lambda/\pi$. A shorter coherence length can be obtained by positioning the scatterer in the near-zone of either a Lambertian source, for which the spectral degree of coherence in the source plane equals [Mandel and Wolf, 1995, Eq. (5.3-53)]

$$\mu^{(0)}(\boldsymbol{\rho}_2 - \boldsymbol{\rho}_1, \omega) = \frac{\sin(k|\boldsymbol{\rho}_2 - \boldsymbol{\rho}_1|)}{k|\boldsymbol{\rho}_2 - \boldsymbol{\rho}_1|}, \tag{3.30}$$

or a source of blackbody radiation [Carter and Wolf, 1975]. However, we will not consider such sources here.

Having thus established that we may, without loss of generality, set $|\mathbf{u}_{1\perp}| = \beta/k$, we next write the vector $\mathbf{u}_1$, indicating a direction of incidence, and the vector $\mathbf{s}$, indicating the direction of scattering, as

$$\mathbf{u}_1 = (\beta k^{-1}\cos\alpha, \beta k^{-1}\sin\alpha, \sqrt{1-\beta^2/k^2}), \tag{3.31}$$

$$\mathbf{s} = (\sin\theta\cos\gamma, \sin\theta\sin\gamma, \cos\theta). \tag{3.32}$$

Their vector product equals

$$\mathbf{s}\cdot\mathbf{u}_1 = \beta k^{-1}\cos(\alpha-\gamma)\sin\theta + \cos\theta\sqrt{1-\beta^2/k^2}. \tag{3.33}$$

Expressing $\mathbf{u}_{1\perp}$ in polar coordinates gives

$$\begin{aligned} S^{(\mathrm{sca})}(r\mathbf{s},\omega) &= \frac{S^{(0)}(\omega)k^2}{2\pi\beta r^2}\int_0^1\int_0^{2\pi}\delta(\beta - k|\mathbf{u}_{1\perp}|) \\ &\quad\times |f(\mathbf{s}\cdot\mathbf{u}_1,\omega)|^2\,|\mathbf{u}_{1\perp}|\,\mathrm{d}\alpha\,\mathrm{d}u_{1\perp}, \qquad (3.34)\\ &= \frac{S^{(0)}(\omega)}{2\pi r^2k^2}\int_0^{2\pi}\sum_l\sum_m(2l+1)(2m+1)\exp[\mathrm{i}(\delta_l-\delta_m)] \\ &\quad\times \sin\delta_l\sin\delta_m P_l\left[\beta k^{-1}\cos(\alpha-\gamma)\sin\theta + \cos\theta\sqrt{1-\beta^2/k^2}\right] \\ &\quad\times P_m\left[\beta k^{-1}\cos(\alpha-\gamma)\sin\theta + \cos\theta\sqrt{1-\beta^2/k^2}\right]\,\mathrm{d}\alpha, \qquad (3.35)\end{aligned}$$

where we have used that $\delta(\beta - k|\mathbf{u}_\perp|) = k^{-1}\delta(\beta/k - |\mathbf{u}_\perp|)$. On integration over α the γ dependence drops out, so we can write

$$\begin{aligned} S^{(\mathrm{sca})}(r\mathbf{s},\omega) &= \frac{S^{(0)}(\omega)}{2\pi r^2k^2}\int_0^{2\pi}\sum_l\sum_m(2l+1)(2m+1)\exp[\mathrm{i}(\delta_l-\delta_m)] \\ &\quad\times \sin\delta_l\sin\delta_m P_l\left[\beta k^{-1}\cos\alpha\sin\theta + \cos\theta\sqrt{1-\beta^2/k^2}\right] \\ &\quad\times P_m\left[\beta k^{-1}\cos\alpha\sin\theta + \cos\theta\sqrt{1-\beta^2/k^2}\right]\,\mathrm{d}\alpha. \qquad (3.36)\end{aligned}$$

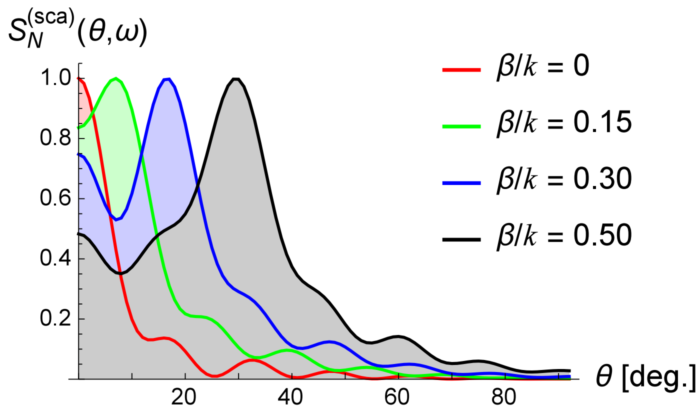

Figure 3.2: Angular distribution of the normalized intensity of the scattered field for selected values of the normalized coherence parameter β/k, namely: 0 (red), 0.15 (green), 0.30 (blue) and 0.50 (black). In this example the wavelength $\lambda = 632.8$ nm, the refractive index $n = 1.33$, and the sphere radius $a = 2\lambda$.

This expression shows how the angular distribution of the scattered field arises from an intricate interplay of the sphere radius a, its refractive index n, and the inverse coherence length β. Formidable as Eq. (3.36) may look, it can easily be solved numerically.

3.4 Changing the coherence length

The dependence of the scattered radiant intensity on the normalized coherence parameter β/k is shown in Fig. 3.2 for scattering angles up to 90°. The left most curve (red) is for $\beta/k = 0$, which corresponds to the case of a fully coherent incident field. We indeed retrieve the classical Mie result with strong forward scattering. However, when the coherence length is decreased to $\beta/k = 0.15$ (green curve), the forward scattering is somewhat suppressed and the maximum scattering occurs at an angle of $\theta = 7°$. For the cases $\beta/k = 0.30$ (blue) and $\beta/k = 0.50$ (black) the angle of maximum scattering moves to 17° and 29°, respectively. Also, the minima are raised from their near-zero value. We note that as long as

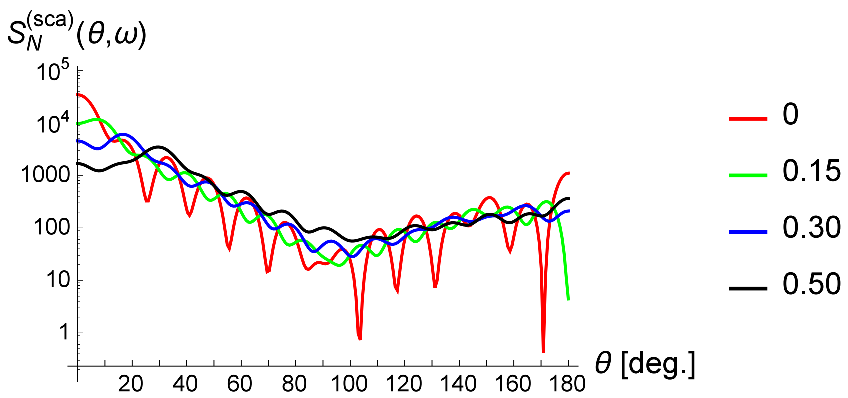

Figure 3.3: Angular distribution of the logarithmic intensity of the scattered field for selected values of the normalized coherence parameter β/k: 0 (red), 0.15 (green), 0.30 (blue) and 0.50 (black). The parameters are the same as in Fig. 3.2.

$\beta/k < 0.12$ the maximum occurs in the forward direction. This maximum only shifts to larger angles when the correlation function Eq. (4.7) takes on negative values for pairs of points in the sphere, i.e. when $J_0(\beta 2a) < 0$.

The unnormalized scattered field for all scattering angles is shown on a logarithmic scale in Fig. 3.3. For the fully coherent case we obtain the well-known Mie resonances (red curve). These become much less pronounced for the partially coherent cases (green, blue and black curves). In these last three cases the backscattering is strongly decreased compared with the fully coherent case.

3.5 Total scattered power

The optical theorem in its classical form [Born and Wolf, 1995; van de Hulst, 1981] relates the total extinguished power (due to scattering and absorption) to the scattering amplitude in the forward direction. Since this theorem assumes the incident field to be a monochromatic plane wave, rather than a partially coherent field, it does not apply to the present case. However, the theorem has been generalized to deal with stochastic fields by Carney et al. [Carney *et al.*, 1997]. They derived that the ensembleaveraged extinguished power $\langle P_e(\omega)\rangle$ is then given by the expression

$$\langle P_e(\omega)\rangle = \frac{4\pi}{k}\,\mathrm{Im}\left[\int_{|\mathbf{u}_{1\perp}|\leq 1}\int_{|\mathbf{u}_{2\perp}|\leq 1} \mathcal{A}(\mathbf{u}_1,\mathbf{u}_2,\omega) \right.$$
$$\left. \times\, f(\mathbf{u}_1\cdot\mathbf{u}_2)\,\mathrm{d}^2u_{1\perp}\mathrm{d}^2u_{2\perp}\right]. \tag{3.37}$$

Since we are assuming a non-absorbing scatterer, the extinction is entirely due to scattering, i.e., the extinguished power is equal to the radiant intensity of the scattered field integrated over a 4π solid angle:

$$\langle P_e(\omega)\rangle = \int_0^{2\pi}\int_0^{\pi} J^{(\mathrm{sca})}(\mathbf{s},\omega)\sin\theta\,\mathrm{d}\theta\mathrm{d}\phi. \tag{3.38}$$

On substituting from Eq. (3.26) for the angular correlation function into Eq. (3.37), we obtain the formula

$$\langle P_e(\omega)\rangle = \frac{2kS^{(0)}(\omega)}{\beta}$$
$$\times\,\mathrm{Im}\left[\int_{|\mathbf{u}_{1\perp}|\leq 1} \delta(\beta - k|\mathbf{u}_{1\perp}|)f(\mathbf{u}_1\cdot\mathbf{u}_1)\,\mathrm{d}^2u_{1\perp}\right]. \tag{3.39}$$

Evaluating this in polar coordinates gives

$$\langle P_e(\omega)\rangle = \frac{4\pi S^{(0)}(\omega)}{k}\,\mathrm{Im}\left[f(\mathbf{u}\cdot\mathbf{u})\right]. \tag{3.40}$$

In Eq. (3.40) the two arguments of the scattering amplitude f are equal, i.e., $f(\mathbf{u}\cdot\mathbf{u})$ represents the forward scattering amplitude. It is seen from this expression that the total scattered power does *not* depend on the coherence parameter β. This implies that varying β, as was illustrated in Figs. 3.2 and 3.3, results in a redistribution of the scattered intensity with the total scattered power being unaffected. Also, it was verified numerically that Eqs. (3.40) and (3.38) yield the same result.

Some related results were reported in [Wang *et al.*, 2015b] (Chapter 2 of this thesis) where it was suggested that Bessel-correlated fields can give rise to strongly suppressed scattering in the forward direction. In contrast to the present study, this result was obtained for a random spherical scatterer while making use of the first-order Born approximation. However, it is well known that this approximation is incompatible with the optical theorem [Gottfried and Yan, 2003], i.e., it violates energy conservation. In contrast, using Mie theory allows us to to make use of the optical theorem. We thus find that the extinguished power is independent of the coherence length. That means that changing the coherence length of the incident field results in a redistribution of the total scattered field. Also, our analysis pertains to the important class of scatterers that are deterministic, rather than random. Furthermore the angular shifts of the direction of maximum scattering that we find while using Mie theory, are significantly larger than those obtained using the Born approximation.

3.6 Conclusions

In summary, we have demonstrated that the angular distribution of a field that is scattered by a homogeneous sphere can be controlled. In contrast to previous works, this is done by manipulating the incident beam rather than the scatterer. In particular, an incident beam with a J_0 Bessel-correlation gives rise to an unusual scattering profile. This profile can be changed by varying the spatial coherence length. The total power of the scattered field remains constant when the transverse coherence length is varied. This provides a new tool to steer the scattered field dynamically without losing energy. This method may be used to selectively address detectors that are not (or cannot be) located along the line of sight connecting the source and the scatterer. Such detectors have the advantage that they are not saturated by the illuminating beam.

Chapter 4

Strong suppression of forward or backward Mie scattering by using spatial coherence

This Chapter is based on

- Yangyundou Wang, Hugo F. Schouten, and Taco D. Visser, "Strong suppression of forward or backward Mie scattering by using spatial coherence," Journal of the Optical Society of America A, vol. 33, pp. 513–518 (2016).

Abstract
We derive analytic expressions relating Mie scattering with partially coherent fields to scattering with fully coherent fields. These equations are then used to demonstrate how the intensity of the forward- or the backward-scattered field can be suppressed several orders of magnitude by tuning the spatial coherence properties of the incident field. This method allows the creation of cone-like scattered fields, with the angle of maximum intensity given by a simple formula.

4.1 Introduction

In 1908 Gustav Mie obtained, on the basis of Maxwell's equations, a rigorous solution for the diffraction of a plane monochromatic wave by a homogeneous sphere [Mie, 1908]. His seminal work has since been applied in a wide range of fields such as astronomy, climate studies, atomic physics, optical trapping etc. Extending and generalizing the theory of Mie scattering remains an important activity to this day [Mishchenko *et al.*, 2000; Hergert and Wriedt (eds.), 2012].

In recent years, a large number of studies have been devoted to the question of how the angular distribution of scattered fields may be controlled. This line of research was initiated by Kerker *et al.* in 1983 [Kerker *et al.*, 1983]. They derived conditions under which the forward or backward scattering by magnetic spheres is strongly suppressed. Since then both the influence of the particle's composition [Nieto-Vesperina *et al.*, 2011; Garcia-Camara *et al.*, 2011; Geffrin *et al.*, 2012; Person *et al.*, 2013; Xie *et al.*, 2015; Korotkova, 2015; Naraghi *et al.*, 2015], and that of the coherence properties of the incident field on the scattering process have been examined [Jannson *et al.*, 1988; Gori *et al.*, 1990; Greffet *et al.*, 2003; Lindberg *et al.*, 2006; van Dijk *et al.*, 2010; Fischer *et al.*, 2012; Wang *et al.*, 2015b].

We recently demonstrated that a J_0 Bessel-correlated beam that is incident on a homogeneous sphere, produces a highly unusual distribution of the scattered field [Wang *et al.*, 2015a], (Chapter 3 of this thesis). In the present study we derive expressions that relate the scattered field for this particular case to that of an incident field that is spatially fully coherent. These expressions allow us to tailor the transverse coherence length of the field to obtain strongly suppressed forward or backward scattering. We also derive an approximate formula for the angle at which the scattered intensity reaches its maximum value. This expression is found to work surprisingly well.

In Section 4.2 we briefly review scalar Mie theory. Bessel-correlated fields are discussed in Section 4.3. In Section 4.4 we derive an equation for the intensity of the forward-scattered field. We show by example how this expression can be used to reduce the forward scattering signal by several orders of magnitude. An expression for the backward-scattered field is derived in Section 4.5. This is then applied to design a partially coherent incident field that causes strongly suppressed backscattering. In the last section we discuss possible ways to realize J_0 Bessel-correlated fields, and offer some conclusions.

4.2 Scalar Mie scattering

Let us begin by considering a plane, monochromatic scalar wave of frequency ω and with unit amplitude, that is propagating in a direction specified by a real unit vector $\mathbf{u}$. If this wave is incident on a deterministic, spherical scatterer with radius a and refractive index n (see Fig. 4.1), then the scattering amplitude in an observation direction $\mathbf{s}$ in the far-zone can be expressed as (See [Joachain, 1987, Eq. (4.66)], with a trivial change in notation)

$$f(\mathbf{s}\cdot\mathbf{u},\omega) = \frac{1}{k}\sum_{l=0}^{\infty}(2l+1)\exp[i\delta_l(\omega)]\sin[\delta_l(\omega)]P_l(\mathbf{s}\cdot\mathbf{u}), \tag{4.1}$$

where k is the free-space wavenumber, P_l denotes a Legendre polynomial of order l, and the phase shifts $\delta_l(\omega)$ are given by the expressions [Joachain, 1987, Sec. 4.3.2 and 4.4.1]

$$\tan[\delta_l(\omega)] = \frac{\bar{k}j_l(ka)j_l'(\bar{k}a) - kj_l(\bar{k}a)j_l'(ka)}{\bar{k}j_l'(\bar{k}a)n_l(ka) - kj_l(\bar{k}a)n_l'(ka)}. \tag{4.2}$$

Here j_l and n_l are spherical Bessel functions and spherical Neumann functions, respectively, of order l. Furthermore,

$$\bar{k} = nk \tag{4.3}$$

is the wavenumber associated with the reduced wavelength within the scatterer, and the primes denote differentiation. The intensity of the scattered field equals

$$S_{\text{fc}}^{(\text{sca})}(\theta,\omega) = \frac{1}{r^2}|f(\cos\theta,\omega)|^2, \tag{4.4}$$

where r is the distance between the scattering sphere and the point of observation, and the subscript "fc" indicates an incident field that is fully coherent.

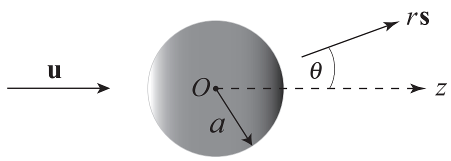

Figure 4.1: A sphere with radius a is illuminated by a plane wave propagating in the direction $\mathbf{u}$, which is taken to be the z axis. The scattering angle θ is the angle between the direction of the incident field and a far-zone observation point $r\mathbf{s}$.

An example of the angular distribution of the field for fully coherent Mie scattering is shown in Fig. 4.2. Many deep minima can be seen, with the first one occuring at $\theta = 0.69°$, where $S_{\text{fc}}^{(\text{sca})} = 3.15 \times 10^{-6}$. We will show that such a minimum can be "moved" to the forward direction ($\theta = 0°$) by using an incident field that is not fully coherent, but rather is J_0-correlated. This then results in a strongly suppressed forward-scattered field.

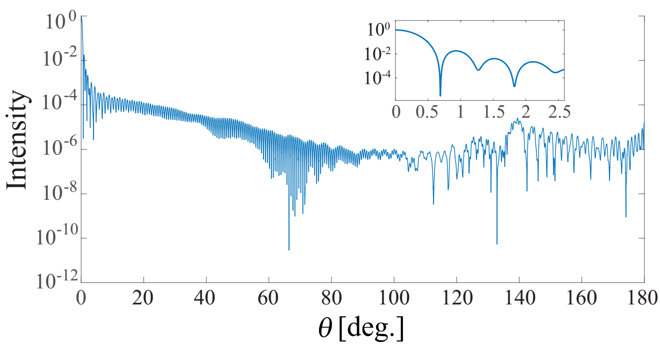

Figure 4.2: Angular distribution, on a logarithmic scale, of the normalized intensity of the scattered field $S_{\text{fc}}^{(\text{sca})}(\theta, \omega)$ for a fully coherent incident field. In this example the sphere radius $a = 50\lambda$, the refractive index $n = 1.33$, and the wavelength $\lambda = 632.8$ nm. The inset shows the first few scattering minima up to $\theta = 2.5°$.

Note that, just like the vast majority of previous studies that deal with scattering of partially coherent fields, we use a scalar theory rather than a vector approach. The partial wave expansion (4.1) is quite similar to what is obtained in an electromagnetic theory. In the latter the scattered field is written as the sum of two infinite series, one electric the other magnetic. However, when the field is either unpolarized or linearly polarized, it is to be expected that a scalar approach will give an accurate description.

4.3 Mie scattering with J_0 Bessel-correlated fields

In the space-frequency domain the second-order coherence properties of a stochastic field $U(\mathbf{r},\omega)$ are characterized by its cross-spectral density function at two positions $\mathbf{r}_1$ and $\mathbf{r}_2$ [Mandel and Wolf, 1995, Sec. 4.3.2], namely

$$W(\mathbf{r}_1,\mathbf{r}_2,\omega) = \langle U^*(\mathbf{r}_1,\omega)U(\mathbf{r}_2,\omega)\rangle, \tag{4.5}$$

where the angular brackets denote an average taken over an ensemble of field realizations. The spectral density (the intensity at frequency ω) at a point $\mathbf{r}$ is defined as

$$S(\mathbf{r},\omega) = \langle U^*(\mathbf{r},\omega)U(\mathbf{r},\omega)\rangle = W(\mathbf{r},\mathbf{r},\omega). \tag{4.6}$$

We will consider an incident field with a uniform spectral density $S^{(0)}(\omega)$, that is J_0-correlated. This means that its cross-spectral density function in the plane $z=0$ (the plane that passes through the center of the sphere) is of the form

$$W^{(\mathrm{inc})}(\boldsymbol{\rho}_1,\boldsymbol{\rho}_2,\omega) = S^{(0)}(\omega)J_0(\beta|\boldsymbol{\rho}_2-\boldsymbol{\rho}_1|). \tag{4.7}$$

Here J_0 denotes the Bessel function of the first kind and zeroth order, and $\boldsymbol{\rho}_1=(x_1,y_1)$ and $\boldsymbol{\rho}_2=(x_2,y_2)$ are two-dimensional position vectors in the $z=0$ plane. The inverse of the parameter β is a rough measure of the effective transverse coherence length of the incident field. The generation of such a beam was reported in [Raghunathan *et al.*, 2010].

In a previous publication [Wang *et al.*, 2015a] (Chapter 3 of this thesis) we derived that in the case of a J_0-correlated field, the angular distribution of the intensity of the scattered field is given by the expression

$$
\begin{aligned}
S_{\rm pc}^{(\rm sca)}(\theta,\omega) = \frac{S^{(0)}(\omega)}{2\pi r^2 k^2} \int_0^{2\pi} & \sum_l \sum_m (2l+1)(2m+1) \\
& \times \exp[\mathrm{i}(\delta_l - \delta_m)] \sin\delta_l \sin\delta_m \\
& \times P_l\left[\beta k^{-1}\cos\alpha\sin\theta + \cos\theta\sqrt{1-\beta^2/k^2}\right] \\
& \times P_m\left[\beta k^{-1}\cos\alpha\sin\theta + \cos\theta\sqrt{1-\beta^2/k^2}\right] \,\mathrm{d}\alpha,
\end{aligned} \tag{4.8}
$$

where the subscript "pc" indicates partial coherence. We note that β/k cannot exceed 1. On comparing Eq. (4.8), which pertains to a partially coherent field, with Eq. (4.1), which is for a fully coherent field, we see that this result can be written in the form

$$
\begin{aligned}
& S_{\rm pc}^{(\rm sca)}(\theta,\omega) = \frac{S^{(0)}(\omega)}{2\pi r^2} \\
& \times \int_0^{2\pi} \left| f(\beta k^{-1}\cos\alpha\sin\theta + \cos\theta\sqrt{1-\beta^2/k^2})\right|^2 \mathrm{d}\alpha.
\end{aligned} \tag{4.9}
$$

This expression, which relates the scattering of a J_0-correlated field with that by a plane wave, will be used in the next sections. To simplify the notation we will set the spectral density of the incident field equal to unity ($S^{(0)}(\omega) = 1$), and from now on we no longer display the ω dependence.

4.4 Suppression of forward scattering

The intensity of the scattered field, as given by Eq. (4.9), greatly simplifies when we consider the forward direction ($\theta = 0^\circ$). We then have that

$$
S_{\rm pc}^{(\rm sca)}(\theta = 0^\circ) = \frac{1}{r^2}\left| f\left(\sqrt{1-\beta^2/k^2}\right)\right|^2. \tag{4.10}
$$

This expression has a clear physical meaning. Since both $\mathbf{s}$ and $\mathbf{u}$ are unit vectors, the argument $\mathbf{s}\cdot\mathbf{u}$ of the scattering amplitude $f(\mathbf{s}\cdot\mathbf{u})$ in Eq. (4.1) can be interpreted as the cosine of an angle, ϕ say, such that $\cos\phi = \mathbf{s}\cdot\mathbf{u}$. It follows from Eq. (4.10) that for the case of a J_0-correlated field this angle is such that

$$
\cos\phi = \sqrt{1-\beta^2/k^2}, \tag{4.11}
$$

as is illustrated in Fig. 4.3. This result implies that, *for an incident J_0-correlated field with coherence parameter β/k, the forward scattered intensity ($\theta = 0°$) is equal to the intensity that is scattered in the fully coherent case in the direction ϕ, which is given by Eq. (4.11).* This observation can be expressed as

$$S_{\rm pc}^{(\rm sca)}(\theta = 0°) = S_{\rm fc}^{(\rm sca)}(\phi). \tag{4.12}$$

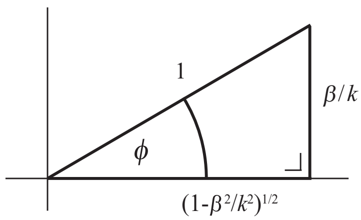

Figure 4.3: Illustrating the connection between the scattering angle ϕ and the coherence parameter β/k.

The connection between fully coherent scattering and scattering with a J_0-correlated fields that is expressed by Eq. (4.12) allows us to suppress the forward scattered intensity by "moving" a minimum of the scattering distribution to $\theta = 0°$ by altering the coherence parameter β/k. To illustrate this, we return to the example of a sphere with radius $a = 50\lambda$ and refractive index $n = 1.33$ illuminated by a fully coherent field with wavelength $\lambda = 632.8$ nm, which was presented in Fig. 4.2. The first scattering minimum occurs at $\theta = 0.69°$, where the normalized scattered intensity is 3.15×10^{-6}. Using Eq. (4.11) with $\cos\phi = \cos(0.69°) = 0.999$, gives $\beta/k = 0.0121$. This implies that a J_0 Bessel-correlated field with this particular value of β/k will have a forward scattered intensity that is almost six orders of magnitude less than its fully coherent counterpart. The intensity of the forward scattered field as a function of the coherence parameter β/k is plotted in Fig. 4.4. We notice that the value $\beta/k = 0$ corresponds to the fully coherent case. It is seen that near $\beta/k = 0.0121$ the forward scattered field is indeed strongly suppressed. In fact, the forward scattered intensity is reduced by more than five orders of magnitude compared with the case of an incident field that is spatially fully coherent.

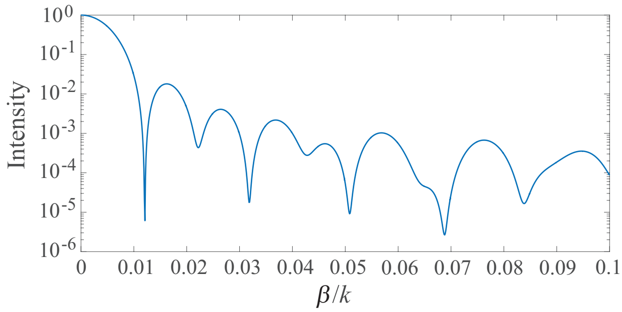

Figure 4.4: Logarithmic plot of the forward scattered intensity as function of the coherence parameter β/k. In this example the wavelength $\lambda = 632.8$ nm, the sphere radius $a = 50\lambda$ and the refractive index $n = 1.33$.

It was shown in [Wang *et al.*, 2015a] (Chapter 2 of this thesis) that the total scattered power remains constant when the coherence parameter β/k is varied. This means that the scattered intensity is merely redistributed. The precise form of the scattered field for the case $\beta/k = 0.0121$ is shown in Fig. 4.5 (blue curve). The intensity of the forward scattered field $S_{\text{pc}}^{(\text{sca})}(\theta = 0°)$ is about 5×10^{-5} times smaller than the maximum that occurs at $\theta \approx 0.65°$ (see inset). Notice that the deep minima of Fig. 4.2 are no longer present.

If we plot the scattered intensity for another value of the refractive index, namely $n = 1.50$, we see that the angular distribution becomes quite different (red curve), but the maximum occurs at precisely the same position, in fact the two curves in the region shown in the inset are indistinguishable. Apparently, the angle θ_{max} at which the scattered intensity reaches its highest value, is quite insensitive to the precise value of the refractive index. It is possible to explain this behavior by analyzing the relation between the coherence parameter β/k and θ_{max} in a simpler but related situation, namely the scattering of J_0-correlated light by a Gaussian random scatterer while using the first-order Born approximation. As explained in Appendix A, one then finds that

$$\sin\theta_{\text{max}} \approx \beta/k. \tag{4.13}$$

This equation implies that, to first order, the angle θ_{max} at which the

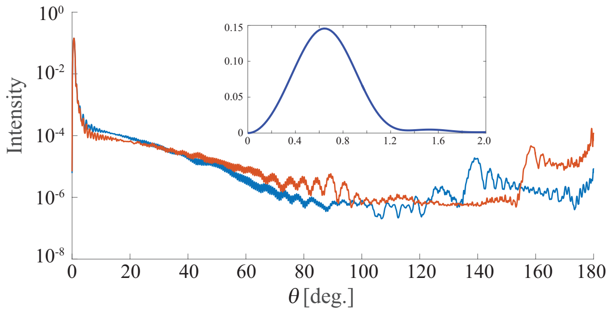

Figure 4.5: Logarithmic plot of the angular distribution of the scattered intensity for a J_0 Bessel-correlated field with coherence parameter $\beta/k = 0.0121$, for two values of the refractive index: $n = 1.33$ (blue curve) and $n = 1.50$ (red curve). The inset shows the same, but for scattering angles up to $2°$ (non-logarithmic, with both curves normalized by their respective values for the fully coherent case). The other parameters in this example are the same as for Fig. 4.2.

scattered intensity reaches its peak, does not depend on the refractive index n, or on the sphere radius a, but only on the coherence parameter. In Fig. 4.6 the value of θ_{max} is plotted as a function of β/k for several values of the sphere radius a. It is seen that the agreement between the result of the Born approximation given by Eq. (4.13) (red curve) and a numerical evaluation of Eq. (4.8) for $a = 50\lambda$ (blue curve) is surprisingly good. It is only for small values of β/k that a discrepancy is seen. This is can be understood as follows. Because the first zero of $J_0(x)$ is at $x = 2.4$, Eq. (4.7) implies that as long as $\beta 2a < 2.4$ the function J_0 will be positive, and the cross-spectral density function between all possible pairs of points within the scatterer will be qualitatively similar to a Gaussian. It is known from earlier studies [van Dijk *et al.*, 2010] that for such a correlation function the scattering remains predominantly in the forward direction, i.e., $\theta_{\text{max}} = 0°$. Only when $\beta 2a > 2.4$ will there be pairs of points that are negatively correlated, which gives rise to a qualitatively different scattering profile. For a sphere radius of 50λ this means that β/k must exceed 0.004 in order for any significant suppression of the forward-scattered intensity to occur. It is indeed seen that only for values somewhat larger than this threshold, the angle $\theta_{\max}$ is very well approximated by Eq. (4.13). For the three smaller spheres (corresponding to the orange, green and purple curves) a similar result holds.

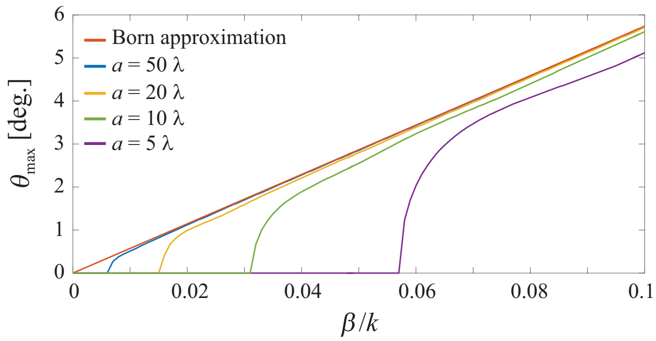

Figure 4.6: The angle $\theta_{\max}$, the angle at which the scattered field has its maximum intensity, as a function of the coherence parameter β/k for selected values of the sphere radius a. The result of the first-order Born approximation, Eq. (4.13), is given by the straight red curve. The other curves are obtained by numerical evaluation of Eq. (4.8). In all cases the refractive index $n = 1.33$.

4.5 Suppression of backward scattering

Just as for the forward scattered field, we find that the expression for the back-scattered intensity ($\theta = 180°$), as given by Eq. (4.9), takes on a simpler form, namely

$$S_{\mathrm{pc}}^{(\mathrm{sca})}(\theta = 180°) = \frac{1}{r^2}\left|f\left(-\sqrt{1-\beta^2/k^2}\right)\right|^2. \tag{4.14}$$

This formula implies that, *for an incident J_0-correlated field with coherence parameter β/k, the backward-scattered intensity is equal to the intensity that is scattered in the fully coherent case in a direction $180° - \phi$, with the angle ϕ defined by Eq. (4.11).* Thus we find that

$$S_{\mathrm{pc}}^{(\mathrm{sca})}(\theta = 180°) = S_{\mathrm{fc}}^{(\mathrm{sca})}(180° - \phi). \tag{4.15}$$

Let us again return to the example of a sphere with radius $a = 50\lambda$ and refractive index $n = 1.33$, as shown in Fig. 4.2. From this plot we find that the scattered field for the fully coherent case has an intensity minimum near $\theta = 179.62°$ with a normalized value of 9.4×10^{-7}, whereas the backward-scattered intensity equals 1.7×10^{-5}. According to Eqs. (4.15) and (4.11) this minimum can be "moved" 0.38° to $\theta = 180°$ by making the field partially coherent with $\beta/k = 6.5 \times 10^{-3}$. A plot of the backscattered intensity as a function of β/k is given in Fig. 4.7. It is indeed seen that $S_{\rm pc}^{(\rm sca)}(\theta = 180°)$ is strongly suppressed when β/k reaches this prescribed value. The back-scattered intensity is now reduced to a mere 5.5% of that of the fully coherent case. This result is in exact agreement with the two intensities that were mentioned above.

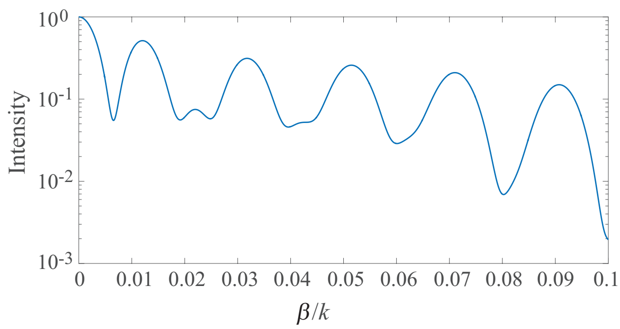

Figure 4.7: The backward scattered intensity as a function of the normalized coherence parameter β/k. Notice that $\beta/k = 0$ corresponds to an incident field that is fully coherent. In this example the wavelength $\lambda = 632.8$ nm, the sphere radius $a = 50\lambda$ and the refractive index $n = 1.33$.

4.6 Conclusions

The practical generation of a J_0 Bessel-correlated beam has been reported in [Raghunathan *et al.*, 2010]. In that study an optical diffuser was used to first obtain a spatially incoherent field that was passed through a thin annular aperture. Imaging this aperture with a lens then produces (according to the van Cittert-Zernike theorem [Mandel and Wolf, 1995]) a field with the desired correlation function. An alternative approach would be to use a spatial light modulator (SLM) to dynamically impart a J_0 Bessel correlation on the field.

In [Raghunathan *et al.*, 2010] the focusing of a J_0-correlated beam was found to produce, instead of a maximum, an intensity minumum at the geometrical focus. Because of the similarity between focusing and scattering by a dielectric sphere, one can say with hindsight that suppression of the forward-scattered field is to be expected.

It is to be noted that a change in the scattering pattern implies a change in the force that is exerted on the sphere [Nieto-Vesperina *et al.*, 2011]. That means that control of the scattering direction can be used to dynamically vary the properties of an optical trap as reported in [Raghunathan *et al.*, 2010].

We also remark that the near-zero scattering in the forward direction that we obtain does not violate the optical theorem. This issue was addressed in [Wang *et al.*, 2015a] (Chapter 3 of this thesis).

In summary, we have investigated the scattering of a J_0 Bessel-correlated field by a dielectric sphere. Equations were derived that connect this situation with the scattering of a fully coherent field. These formulas were applied to design fields for which the forward- or the backward-scattered intensity is significantly reduced. Examples were presented that show a forward scattering suppression of five orders of magnitude, and a suppression of the back-scattered intensity by almost two orders of magnitude. An approximate expression for the angle at which the scattered field reaches its hightest intensity was derived.

In contrast to earlier researches that aim at modifying Mie scattering, our approach is not based on changing the properties of the scattering object, but rather those of the illuminating beam. Our results show that the use of spatial coherence offers a new tool to actively steer the scattered field.

Appendix A - Derivation of Eq. (4.13)

In [Wang *et al.*, 2015b] (Chapter 2 of this thesis) the scattering of a J_0 Bessel-correlated field by a random sphere was examined within the accuracy of the first-order Born approximation. The correlation of the scattering potential is taken to be Gaussian, i.e.,

$$C_F(\mathbf{r}_1', \mathbf{r}_2', \omega) = C_0 \exp\left[-(\mathbf{r}_2' - \mathbf{r}_1')^2/2\sigma_F^2\right], \tag{A-1}$$

where C_0 is a positive constant, and σ_F denotes the coherence length of the scattering potential. It was then derived that

$$\begin{aligned} S^{(\mathrm{sca})}(r\mathbf{s}, \omega) = \frac{C_0}{r^2} \iint_V & W^{(\mathrm{inc})}(\mathbf{r}_1', \mathbf{r}_2', \omega) \\ & \times \exp\left[-(\mathbf{r}_2' - \mathbf{r}_1')^2/2\sigma_F^2\right] \\ & \times \exp[-ik\mathbf{s} \cdot (\mathbf{r}_2' - \mathbf{r}_1')]\, \mathrm{d}^3r_1'\mathrm{d}^3r_2', \end{aligned} \tag{A-2}$$

where V is the volume of the scatterer, and $\mathbf{r}_i' = (\boldsymbol{\rho}_i', z_i')$ with $i = 1, 2$. If we assume the the field to be longitudinally coherent [Mandel and Wolf, 1995, Sec. 5.2.1], then

$$W^{(\mathrm{inc})}(\mathbf{r}_1', \mathbf{r}_2', \omega) = e^{\mathrm{i}k(z_2' - z_1')} J_0(\beta|\boldsymbol{\rho}_2' - \boldsymbol{\rho}_1'|), \tag{A-3}$$

where the transverse part of the cross-spectral density of the incident field is taken from Eq. (4.7) with $S^{(0)}(\omega) = 1$. We next change to the sum and difference variables

$$\boldsymbol{\rho}_+ = (\boldsymbol{\rho}_1' + \boldsymbol{\rho}_2')/2, \tag{A-4}$$

$$\boldsymbol{\rho}_- = \boldsymbol{\rho}_2' - \boldsymbol{\rho}_1', \tag{A-5}$$

$$z_+ = (z_1' + z_2')/2, \tag{A-6}$$

$$z_- = z_2' - z_1'. \tag{A-7}$$

The Jacobian of this transformation is unity, and we find that

$$\begin{aligned} S^{(\mathrm{sca})}(r\mathbf{s}, \omega) = \frac{C_0}{r^2} & \int \mathrm{d}z_+ \iint \mathrm{d}^2\rho_+ \\ & \times \int e^{\mathrm{i}kz_-(1-s_z)} e^{-z_-^2/2\sigma_F^2}\, \mathrm{d}z_- \\ & \times \iint J_0(\beta\rho_-) e^{-\rho_-^2/2\sigma_F^2} e^{\mathrm{i}k\mathbf{s}_\perp \cdot \boldsymbol{\rho}_-}\, \mathrm{d}^2\rho_-. \end{aligned} \tag{A-8}$$

The product of the first two integrals yields the scattering volume V. If we assume that σ_F is small compared to the size of the scatterer, then the integration over z_- can be extended to the entire real axis, and we obtain the result

$$\int_{-\infty}^{\infty} e^{\mathrm{i}kz_-(1-s_z)} e^{-z_-^2/2\sigma_F^2}\, \mathrm{d}z_- \\ = \sqrt{2\pi}\sigma_F e^{-k^2\sigma_F^2(1-s_z)^2/2}. \tag{A-9}$$

The remaining integral over $\boldsymbol{\rho}_-$ is seen to be a Fourier-Bessel transform, i.e.,

$$\iint J_0(\beta\rho_-) e^{-\rho_-^2/2\sigma_F^2} e^{\mathrm{i}k\mathbf{s}_\perp\cdot\boldsymbol{\rho}_-}\, \mathrm{d}^2\rho_- \tag{A-10}$$

$$= 2\pi \int_0^{\infty} J_0(\beta\rho_-) J_0(k|\mathbf{s}_\perp|\rho_-) e^{-\rho_-^2/2\sigma_F^2} \rho_-\, \mathrm{d}\rho_-. \tag{A-11}$$

The right-hand side of Eq. (A-11) contains the product of two oscillating Bessel functions that in general will tend to cancel each other on integration. Therefore we expect the integral, and hence the total scattered field, to reach its maximum value when the arguments of the two Bessel functions are identical, i.e., when

$$\beta = k|\mathbf{s}_\perp|, \tag{A-12}$$

and such a cancellation does not occur. On using that $|\mathbf{s}_\perp| = \sin\theta$, we thus find for θ_{max}, the angle at which the scattered intensity is maximal, that

$$\sin\theta_{\mathrm{max}} = \beta/k, \tag{A-13}$$

which is Eq. (4.13).

Chapter 5

Creating von Laue patterns in crystal scattering with partially coherent sources

This Chapter is based on

- Yangyundou Wang, David Kuebel, Taco D. Visser and Emil Wolf, "Creating new von Laue patterns in crystal scattering with partially coherent sources," Physical Review A, vol. 94, 033812 (2016).

Abstract
When spatially coherent radiation is diffracted by a crystalline object, the field is scattered in specific directions, giving rise to so-called von Laue patterns. We examine the role of spatial coherence in this process. Using the first-order Born approximation, a general analytic expression for the far-zone spectral density of the scattered field is obtained. This equation relates the coherence properties of the source to the angular distribution of the scattered intensity. We apply this result to two types of sources. Quasihomogeneous Gaussian Schell-model sources are found to produce von Laue spots whose size is governed by the effective source width. Delta-correlated ring sources produce von Laue rings and ellipses instead of point-like spots. In forward scattering polychromatic ellipses are created, whereas in backscattering striking, overlapping ring patterns are formed. We show that both the directionality and the wavelength-selectivity of

the scattering process can be controlled by the state of coherence of the illuminating source.

5.1 Introduction

The diffraction of radiation by a three-dimensional, periodic potential, i.e., from a crystalline object, is a subject whose origins were developed a century ago by von Laue, Friedrich, Knipping and the Bragg father-son team [James, 1950]. Specifically, in the von Laue method, broad spectrum radiation, which is assumed to be spatially coherent, is diffracted by a monocrystal with a fixed orientation [Ashcroft and Mermin, 1976, Ch. 6]. The resulting diffraction peaks are separated both spatially and spectrally. The location of these von Laue spots is determined by the crystal's structure [Born and Wolf, 1995, Sec. 13.1.3]. Here we report how the state of spatial coherence of the incident field can drastically affect their size, shape and spectral composition.

The influence of the state of coherence of the incident field on the scattering process has been investigated in several publications, see, for example, [Jannson *et al.*, 1988; Gori *et al.*, 1990; Greffet *et al.*, 2003; Lindberg *et al.*, 2006; Mie, 1908; Fischer *et al.*, 2012; Wang *et al.*, 2015b; Wang *et al.*, 2015a; Hyde IV, 2015]. These studies were all concerned with either spherical particles, cylinders, or planar scatterers. In contrast, scattering of partially coherent fields by a medium with a periodic potential has remained largely unexplored. Notable exceptions are a study by Dušek [Dušek, 1995], who described dispersion effects in crystal scattering with completely incoherent radiation, and a paper by Hoenders and Bertolotti [Hoenders and Bertolotti, 2005] in which the van Cittert-Zernike theorem was generalized to two-dimensional periodic media. Recently, a more general approach to this problem was suggested in [Wolf, 2013], although there the analysis was limited to one-dimensional scatterers.

In the present paper we study the scattering properties of media with a periodic, three-dimensional scattering potential. We begin by analyzing the scattering of an incident field, generated by a source with an arbitrary state of spatial coherence, by a general mono-crystalline structure of identical point scatterers. We then examine the special case of large, three-dimensional arrays of scatterers whose unit cells are rectangular parallelepipeds. Such cells form *orthorhombic crystals* [Kittel, 1986]. The incident field is taken to be generated by a planar, partially coherent source that is located far away from the crystal. The use of the first-order Born approximation allows us to derive an analytic expression for the spectral density of the far-zone scattered field in terms of a correlation function of the source, namely its *cross-spectral density* [MANDEL AND WOLF, 1995, Sec. 4.3.2]. We then apply this result to two types of sources. Gaussian Schell-model (GSM) sources [MANDEL AND WOLF, 1995, Sec. 5.2.2] generate an incident field that is Gaussian correlated. Such fields are found to give rise to larger von Laue diffraction spots than those produced by their spatially fully coherent counterparts. When the GSM source is also quasihomogeneous [MANDEL AND WOLF, 1995, Sec. 5.2.2], the spot size is directly related to the source width. For the case of a δ-correlated annular source, the incident field is J_0-correlated. This can produce multicolored, elliptical von Laue patterns in the forward direction and an overlapping, multiple ring pattern in the backward direction. Our results show that both the directionality and the wavelength-selectivity of the scattering process can be controlled by altering the state of coherence of the illuminating source or the distance between the annular source and the crystal.

5.2 Scattering from crystalline structures

The incident field at position $\mathbf{r}$ and at frequency ω, $U^{(\mathrm{in})}(\mathbf{r},\omega)$, is taken to be partially coherent. In the space-frequency domain formulation of coherence theory, its correlation properties are characterized by the *cross-spectral density function* [WOLF, 2007]

$$W^{(\mathrm{in})}(\mathbf{r}_1,\mathbf{r}_2,\omega) = \langle U^{(\mathrm{in})*}(\mathbf{r}_1,\omega)U^{(\mathrm{in})}(\mathbf{r}_2,\omega)\rangle, \tag{5.1}$$

where the angular brackets denote an average taken over an ensemble of realizations of the field, and the asterisk indicates complex conjugation. The normalized version of this correlation function is the *spectral degree of coherence*

$$\mu^{(\mathrm{in})}(\mathbf{r}_1,\mathbf{r}_2,\omega) = \frac{\langle U^{(\mathrm{in})*}(\mathbf{r}_1,\omega)U^{(\mathrm{in})}(\mathbf{r}_2,\omega)\rangle}{[S^{(\mathrm{in})}(\mathbf{r}_1,\omega)S^{(\mathrm{in})}(\mathbf{r}_2,\omega)]^{1/2}}, \tag{5.2}$$

where the incident *spectral density* is defined as

$$S^{(\mathrm{in})}(\mathbf{r},\omega) \equiv W^{(\mathrm{in})}(\mathbf{r},\mathbf{r},\omega). \tag{5.3}$$

We consider a general, three-dimensional crystalline array of identical point scatterers. In that case the *scattering potential* $F(\mathbf{r}, \omega)$ can be written as

$$F(\mathbf{r}, \omega) = F_0(\omega) \sum_{\mathbf{R}} \delta^3(\mathbf{r} - \mathbf{R}), \tag{5.4}$$

with $F_0(\omega) \in \mathbb{R}$, δ^3 denoting the three-dimensional Dirac delta function, and with the position vectors of the scatterers given by

$$\mathbf{R} = N_1 \mathbf{a}_1 + N_2 \mathbf{a}_2 + N_3 \mathbf{a}_3. \tag{5.5}$$

Here $\mathbf{a}_1$, $\mathbf{a}_2$, and $\mathbf{a}_3$ denote the *direct lattice vectors* that span the crystal, with N_i any integer, and $i = 1, 2, 3$. The periodicity of $F(\mathbf{r}, \omega)$ allows us to express it as a Fourier series, i.e.,

$$F(\mathbf{r}, \omega) = \sum_{\mathbf{G}} f(\mathbf{G}, \omega)\, e^{\mathrm{i}\mathbf{G}\cdot\mathbf{r}}, \tag{5.6}$$

with $f(\mathbf{G}, \omega)$ the *structure factor*, and $\mathbf{G}$ a *reciprocal lattice vector* [Kittel, 1986]. The structure factor is given by the expression

$$f(\mathbf{G}, \omega) = V^{-1} \int_V F(\mathbf{r}, \omega)\, e^{-\mathrm{i}\mathbf{G}\cdot\mathbf{r}}\, \mathrm{d}^3 r, \tag{5.7}$$

where V denotes the volume of a unit cell, over which the integration extends. From this it follows that in our case

$$f(\mathbf{G}, \omega) = F_0(\omega), \tag{5.8}$$

for all vectors $\mathbf{G}$.

Within the validity of the first-order Born approximation [Born and Wolf, 1995, Sec. 13.1], the scattered field in a direction indicated by the unit vector $\mathbf{s} = (s_x, s_y, s_z)$, is given by the formula

$$U^{(\mathrm{sca})}(r\mathbf{s}, \omega) = \int_{\mathbb{R}^3} U^{(\mathrm{in})}(\mathbf{r}', \omega) G(r\mathbf{s}, \mathbf{r}', \omega) F(\mathbf{r}', \omega)\, \mathrm{d}^3 r', \tag{5.9}$$

where $\mathbf{r} = r\mathbf{s}$ is a point of observation, and $G(r\mathbf{s}, \mathbf{r}', \omega)$ is the outgoing free-space Green's function pertaining to the Helmholtz equation. Because the scattering potential is identically zero outside the domain of the scatterer, we have extended the integration in Eq. (5.9) to the entire three-dimensional space, i.e., to $\mathbb{R}^3$. Far away from the scatterer the Green's function takes on the asymptotic form

$$G(r\mathbf{s}, \mathbf{r}', \omega) = \frac{e^{\mathrm{i}k|\mathbf{r}-\mathbf{r}'|}}{|\mathbf{r}-\mathbf{r}'|} \sim \frac{e^{\mathrm{i}kr}}{r}\, e^{-\mathrm{i}k\mathbf{s}\cdot\mathbf{r}'}, \tag{5.10}$$

where k denotes the wavenumber associated with frequency ω. The spectral density of the scattered field is, in strict analogy with Eq. (5.3), given by the expression

$$S^{(\mathrm{sca})}(r\mathbf{s}, \omega) = \langle U^{(\mathrm{sca})*}(r\mathbf{s}, \omega) U^{(\mathrm{sca})}(r\mathbf{s}, \omega)\rangle. \tag{5.11}$$

On substituting from Eqs. (5.6), (5.8), (5.9), and (5.10) into Eq. (5.11), and interchanging the order of ensemble averaging and integration, we obtain

$$\begin{aligned} S^{(\mathrm{sca})}(r\mathbf{s}, \omega) = \frac{F_0^2(\omega)}{r^2} \int_{\mathbb{R}^6} & W^{(\mathrm{in})}(\mathbf{r}', \mathbf{r}'', \omega) e^{-\mathrm{i}k\mathbf{s}\cdot(\mathbf{r}''-\mathbf{r}')} \\ & \times \sum_{\mathbf{G}} e^{-\mathrm{i}\mathbf{G}\cdot\mathbf{r}'} \sum_{\mathbf{H}} e^{\mathrm{i}\mathbf{H}\cdot\mathbf{r}''}\, \mathrm{d}^3 r' \mathrm{d}^3 r'', \end{aligned} \tag{5.12}$$

with the cross-spectral density function $W^{(\mathrm{in})}(\mathbf{r}', \mathbf{r}'', \omega)$ of the incident field given by Eq. (5.1), and $\mathbf{G}$ and $\mathbf{H}$ denoting a reciprocal lattice vectors. Interchanging integration and summation, and re-arranging terms yields

$$\begin{aligned} S^{(\mathrm{sca})}(r\mathbf{s}, \omega) = \frac{F_0^2(\omega)}{r^2} \sum_{\mathbf{G}} \sum_{\mathbf{H}} \int_{\mathbb{R}^6} & W^{(\mathrm{in})}(\mathbf{r}', \mathbf{r}'', \omega) \\ & \times e^{\mathrm{i}\mathbf{r}'\cdot(k\mathbf{s}-\mathbf{G})} e^{\mathrm{i}\mathbf{r}''\cdot(\mathbf{H}-k\mathbf{s})}\, \mathrm{d}^3 r' \mathrm{d}^3 r''. \end{aligned} \tag{5.13}$$

We note that this expression relates the scattered field to the six-dimensional spatial Fourier transform of the cross-spectral density of the incident field. To simplify the notation we omit the ω-dependence from now on.

Next we make use of the fact that, far away from the source, the cross-spectral density function itself is also a Fourier transform, namely

$$\begin{aligned} W^{(\mathrm{in})}(\mathbf{r}', \mathbf{r}'') = \left(\frac{k}{2\pi\Delta z}\right)^2 e^{\mathrm{i}k(z''-z')} \iint_{z=0} & W^{(0)}(\boldsymbol{\rho}_1, \boldsymbol{\rho}_2) \\ & \times e^{-\mathrm{i}k(\boldsymbol{\rho}''\cdot\boldsymbol{\rho}_2 - \boldsymbol{\rho}'\cdot\boldsymbol{\rho}_1)/\Delta z}\, \mathrm{d}^2\rho_1 \mathrm{d}^2\rho_2, \end{aligned} \tag{5.14}$$

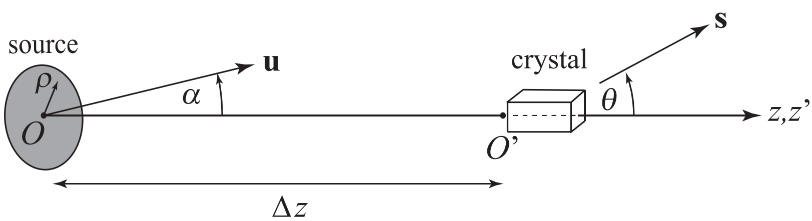

Figure 5.1: Illustrating the notation. The origin O of the first coordinate system is taken in the source plane $z = 0$. The origin O' of the primed coordinates is taken at $(x, y, z) = (0, 0, \Delta z)$.

where the superscript (0) indicates the source plane $z = 0$, and with $\mathbf{r}' = (\boldsymbol{\rho}', z')$ and $\mathbf{r}'' = (\boldsymbol{\rho}'', z'')$. The distance Δz between the source and the scatterer is illustrated in Fig. 5.1. On making use of this expression in Eq. (5.13) we get the formula

$$S^{(\mathrm{sca})}(r\mathbf{s}) = \left(\frac{F_0 k}{2\pi r \Delta z}\right)^2 \sum_{\mathbf{G}} \sum_{\mathbf{H}} \int_{\mathbb{R}^6} \iint_{z=0} e^{\mathrm{i}k(z''-z')} W^{(0)}(\boldsymbol{\rho}_1, \boldsymbol{\rho}_2) \\ \times e^{-\mathrm{i}k(\boldsymbol{\rho}''\cdot\boldsymbol{\rho}_2 - \boldsymbol{\rho}'\cdot\boldsymbol{\rho}_1)/\Delta z} e^{\mathrm{i}\mathbf{r}'\cdot(k\mathbf{s}-\mathbf{G})} e^{\mathrm{i}\mathbf{r}''\cdot(\mathbf{H}-k\mathbf{s})}\, \mathrm{d}^2\rho_1 \mathrm{d}^2\rho_2 \mathrm{d}^3 r' \mathrm{d}^3 r''. \tag{5.15}$$

Writing this out in Cartesian components gives

$$S^{(\mathrm{sca})}(r\mathbf{s}) = \left(\frac{F_0 k}{2\pi r \Delta z}\right)^2 \sum_{\mathbf{G}} \sum_{\mathbf{H}} \int_{\mathbb{R}} e^{-\mathrm{i}kz'} e^{\mathrm{i}z'(ks_z - G_z)}\, \mathrm{d}z' \\ \times \int_{\mathbb{R}} e^{\mathrm{i}kz''} e^{\mathrm{i}z''(H_z - ks_z)}\, \mathrm{d}z'' \int_{\mathbb{R}^8} W^{(0)}(x_1, y_1, x_2, y_2) \\ \times e^{-\mathrm{i}k(x''x_2 + y''y_2 - x'x_1 - y'y_1)/\Delta z} e^{\mathrm{i}x'(ks_x - G_x)} e^{\mathrm{i}y'(ks_y - G_y)} \\ \times e^{\mathrm{i}x''(H_x - ks_x)} e^{\mathrm{i}y''(H_y - ks_y)}\, \mathrm{d}x_1 \mathrm{d}y_1 \mathrm{d}x_2 \mathrm{d}y_2 \mathrm{d}x' \mathrm{d}y' \mathrm{d}x'' \mathrm{d}y''. \tag{5.16}$$

The integrals over z' and z'' are readily evaluated to give

$$\int_{\mathbb{R}} e^{\mathrm{i}z'(ks_z - G_z - k)}\, \mathrm{d}z' = 2\pi\delta(ks_z - G_z - k), \tag{5.17}$$

and

$$\int_{\mathbb{R}} e^{\mathrm{i}z''(H_z - ks_z + k)}\, \mathrm{d}z'' = 2\pi\delta(H_z - ks_z + k), \tag{5.18}$$

respectively. In order to have a scattered field that is non-zero, Eqs. (5.17) and (5.18) have to be satisfied simultaneously. This implies that

$$G_z = H_z = k(s_z - 1). \tag{5.19}$$

Similarly, the integrals over the remaining four primed variables also yield δ-functions, for example

$$\int_{\mathbb{R}} e^{\mathrm{i}x'(kx_1/\Delta z + ks_x - G_x)}\,\mathrm{d}x' = 2\pi\delta(kx_1/\Delta z + ks_x - G_x). \tag{5.20}$$

Thus we find the four relations

$$x_1 = \Delta z(G_x/k - s_x), \tag{5.21}$$
$$y_1 = \Delta z(G_y/k - s_y), \tag{5.22}$$
$$x_2 = \Delta z(H_x/k - s_x), \tag{5.23}$$
$$y_2 = \Delta z(H_y/k - s_y). \tag{5.24}$$

Substitution in Eq. (5.16) gives the final result

$$S^{(\mathrm{sca})}(r\mathbf{s}) = \left(\frac{F_0 4\pi^2 \Delta z}{kr}\right)^2 \sum_{\mathbf{G},\mathbf{H}} W^{(0)}(x_1, y_1, x_2, y_2), \tag{5.25}$$

with the arguments (x_1, y_1, x_2, y_2) of the cross-spectral density function $W^{(0)}$ given by Eqs. (5.21)–(5.24), and the double summation over the reciprical lattice vectors such that $G_z = H_z$. Eq. (5.25) is a general expression for the far-zone scattered field in terms of the cross-spectral density function of the source and the reciprocal lattice of the crystal.

5.3 Orthorhombic crystals

From here on we assume the scattering structure to be an orthorhombic crystal [Kittel, 1986], consisting of unit cells with sides a, b, c, as sketched in Fig. 5.2. We note that this choice of coordinate axes means that we consider a field that is normally incident along the z direction.

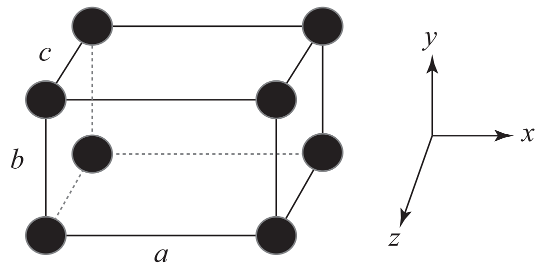

Figure 5.2: A rectangular parallelepiped unit cell of eight identical point scatterers. The direct lattice vectors are $\mathbf{a}_1 = a\hat{\mathbf{x}}$, $\mathbf{a}_2 = b\hat{\mathbf{y}}$ and $\mathbf{a}_3 = c\hat{\mathbf{z}}$. The orthorhombic scatterer is assumed to consist of many of these unit cells.

For an orthorhombic crystal the Cartesian components of its reciprocal lattice vectors are given by the formulas

$$G_x = 2\pi\frac{n_1}{a}, \tag{5.26}$$

$$G_y = 2\pi\frac{n_2}{b}, \tag{5.27}$$

$$G_z = 2\pi\frac{n_3}{c}, \tag{5.28}$$

and

$$H_x = 2\pi\frac{m_1}{a}, \tag{5.29}$$

$$H_y = 2\pi\frac{m_2}{b}, \tag{5.30}$$

$$H_z = 2\pi\frac{m_3}{c}, \tag{5.31}$$

with the indices n_i and m_i any integer, and $i = 1, 2, 3$. Eq. (5.19) yields the restriction $n_3 = m_3$. The above expressions will be used in Eqs. (5.21)–(5.24).

5.4 Gaussian Schell-model sources

For a planar source of the Gaussian Schell model type [Mandel and Wolf, 1995], the cross-spectral density function in the source plane reads

$$W^{(0)}(\boldsymbol{\rho}_1, \boldsymbol{\rho}_2) = \sqrt{S^{(0)}(\boldsymbol{\rho}_1) S^{(0)}(\boldsymbol{\rho}_2)}\mu^{(0)}(\boldsymbol{\rho}_2 - \boldsymbol{\rho}_1), \tag{5.32}$$

with the spectral density and the spectral degree of coherence both having a Gaussian form, i.e.,

$$S^{(0)}(\boldsymbol{\rho}) = A^2 e^{-\rho^2/2\sigma_S^2}, \tag{5.33}$$

$$\mu^{(0)}(\boldsymbol{\rho}_2 - \boldsymbol{\rho}_1) = e^{-(\boldsymbol{\rho}_2 - \boldsymbol{\rho}_1)^2/2\sigma_\mu^2}. \tag{5.34}$$

Here A^2 denotes the maximum spectral density, σ_S the effective source width, and σ_μ the effective transverse coherence length.

Let us next make the additional assumption that the source is quasi-homogeneous. For such sources the spectral density $S^{(0)}(\boldsymbol{\rho})$ changes much more slowly with $\boldsymbol{\rho}$ than the spectral degree of coherence $\mu^{(0)}(\boldsymbol{\rho}_2 - \boldsymbol{\rho}_1)$ changes with $|\boldsymbol{\rho}_2 - \boldsymbol{\rho}_1|$. That implies that $\sigma_\mu^2 \ll \sigma_S^2$. The far-zone spectral degree of coherence of the field that is generated by such a source satisfies the reciprocity relation [Mandel and Wolf, 1995, Sec. 5.3.2],

$$\mu^{(\infty)}(r_1\mathbf{s}_1, r_2\mathbf{s}_2) = \frac{\tilde{S}^{(0)}[k(\mathbf{s}_{2\perp} - \mathbf{s}_{1\perp})]}{\tilde{S}^{(0)}(0)} e^{\mathrm{i}k(r_2 - r_1)}, \tag{5.35}$$

where the superscript (∞) indicates points in the far zone, and $\mathbf{s}_{i\perp} = (s_{ix}, s_{iy})$, with $i = 1, 2$, are the transverse parts of the directional unit vector $\mathbf{s}_i$. If we apply the spectral density distribution (5.33) to this expression, we find for the spectral degree of coherence of the field that is incident on the crystal the equation

$$\mu^{(\mathrm{in})}(r_1\mathbf{s}_1, r_2\mathbf{s}_2) = e^{-k^2\sigma_S^2(\mathbf{s}_{2\perp} - \mathbf{s}_{1\perp})^2/2} e^{\mathrm{i}k(r_2 - r_1)}. \tag{5.36}$$

Eq. (5.36) shows that we can change the state of coherence of the incident field, or more precisely, its effective transverse coherence length, by changing the width σ_S of the source.

If we substitute from Eq. (5.32) into Eq. (5.25) for the case of an orthorhombic crystal, as was described in the previous section, we obtain the formula

$$
\begin{aligned}
S^{(\mathrm{sca})}(r\mathbf{s}) = \beta \sum_{\substack{n_i, m_j \\ n_3 = m_3}} \exp &\left\{ -\frac{(\Delta z)^2}{4\sigma_S^2} \left[\left(\frac{2\pi n_1}{ka} - s_x \right)^2 + \left(\frac{2\pi n_2}{kb} - s_y \right)^2 \right.\right. \\
&\left.\left. + \left(\frac{2\pi m_1}{ka} - s_x \right)^2 + \left(\frac{2\pi m_2}{kb} - s_y \right)^2 \right] \right\} \\
&\times \exp\left(-\frac{(\Delta z)^2}{2\sigma_\mu^2} \left\{ \left[\frac{2\pi}{ka}(m_1 - n_1) \right]^2 + \left[\frac{2\pi}{kb}(m_2 - n_2) \right]^2 \right\} \right),
\end{aligned}
\tag{5.37}
$$

with $i, j = 1, 2, 3$, and where for brevity we have introduced the parameter β, where

$$
\beta = \left(\frac{AF_0 4\pi^2 \Delta z}{kr} \right)^2. \tag{5.38}
$$

The maximum term in the summation occurs when the arguments of both exponentials are zero, i.e., when $m_1 = n_1$ and $m_2 = n_2$, and for a scattering direction $\mathbf{s}$ such that

$$
s_x = \frac{\lambda n_1}{a}, \tag{5.39}
$$

$$
s_y = \frac{\lambda n_2}{b}, \tag{5.40}
$$

with the wavelength $\lambda = 2\pi/k$. For the longitudinal component of $\mathbf{s}$ we have from Eqs. (5.19) and (5.28) that

$$
s_z = 1 + \frac{\lambda n_3}{c}. \tag{5.41}
$$

These three formulas are the well-known von Laue equations [Born and Wolf, 1995, Sec. 13.1.3]. They indicate the directions $\mathbf{s}$ of maximum scattering for an incident field that is spatially fully coherent.

On making use in Eq. (5.37) of the assumption that $\sigma_\mu^2 \ll \sigma_S^2$, it follows that we may safely neglect all terms for which $m_1 \neq n_1$ and $m_2 \neq n_2$. This then gives

$$S^{(\mathrm{sca})}(r\mathbf{s}) = \beta \sum_{n_i} \exp\left\{ -\frac{(\Delta z)^2}{2\sigma_S^2} \left[\left(\frac{2\pi n_1}{ka} - s_x \right)^2 + \left(\frac{2\pi n_2}{kb} - s_y \right)^2 \right] \right\}. \tag{5.42}$$

Eq. (5.42) describes the scattered field as a sum of terms. Each term is characterized by the integer triplet (n_1, n_2, n_3). The value of these integers determines a specific wavelength λ and a direction $\mathbf{s}$ at which the scattering reaches a maximum, a so-called von Laue spot. It is worth noting that Eq. (5.42) does *not* depend on the coherence length σ_μ of the source, however it *does* depend on the state of coherence of the incident field. This is because for a distant quasi-homogeneous Gaussian Schell-model source, the reciprocity relation Eq. (5.36) implies that the coherence of the incident field is governed by the effective source size σ_S, rather than σ_μ. When this source size is decreased, the spectral degree of coherence of the field that is incident on the crystal, is increased.

We illustrate our results by considering the example of an orthorhombic crystal with unit cells with sides

$$a = 1.0 \times 10^{-9}\ \mathrm{m}, \tag{5.43}$$

$$b = 1.2 \times 10^{-9}\ \mathrm{m}, \tag{5.44}$$

$$c = 1.5 \times 10^{-9}\ \mathrm{m}. \tag{5.45}$$

We study a single scattering direction by choosing a triplet (n_1, n_2, n_3). The three von Laue equations, together with the requirement that $\mathbf{s}$ is a unit vector, i.e.,

$$s_x^2 + s_y^2 + s_z^2 = 1, \tag{5.46}$$

form an overdetermined system that will only be satisfied for a specific wavelength. For example, for the choice

$$n_1 = 1, \tag{5.47}$$

$$n_2 = 3, \tag{5.48}$$

$$n_3 = -2, \tag{5.49}$$

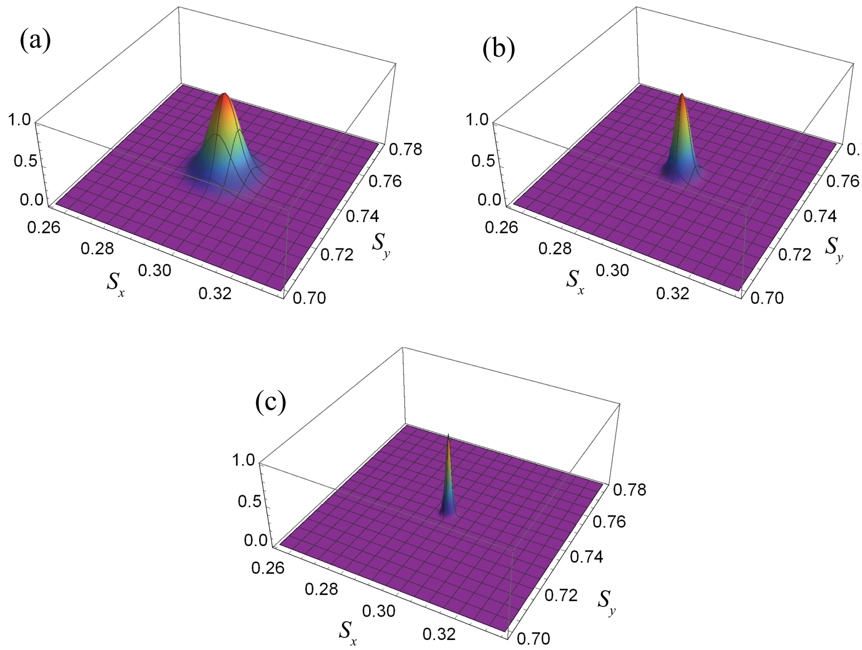

Figure 5.3: Distribution of the normalized scattered intensity around the direction indicated by the von Laue equations for different values of the effective source width, and hence a different transverse coherence length of the incident field. Panel a): $\sigma_S = 5.0 \times 10^{-3}$ m; panel b): $\sigma_S = 2.5 \times 10^{-3}$ m; panel c): $\sigma_S = 1.0 \times 10^{-3}$ m. In these examples $n_1 = 1$, $n_2 = 3$, $n_3 = -2$, and $\Delta z = 1$ m.

it is found that $\lambda = 2.95 \times 10^{-10}$ m, and hence that $s_x = 0.29$, $s_y = 0.73$, and $s_z = 0.60$.

We note that, apart from this particular value of the wavelength, there exists, for every choice of (n_1, n_2, n_3), the trivial solution $\lambda = 0$, and hence $s_z = 1$. This corresponds to a forward propagating field with an infinite frequency. Since this is non-physical, we exclude this solution. We will return to the issue of spurious solutions in the next section.

The influence of the state of coherence of the incident field on the distribution of the scattered field around the direction specified by the von Laue equations, is evaluated by calculating a single term of the summation in Eq. (5.42):

$$S^{(\mathrm{sca})}(n_1, n_2, n_3) = \beta \exp\left\{-\frac{(\Delta z)^2}{2\sigma_S^2}\left[\left(\frac{2\pi n_1}{ka} - s_x\right)^2 + \left(\frac{2\pi n_2}{kb} - s_y\right)^2\right]\right\}, \tag{5.50}$$

where we have changed the arguments of $S^{(\mathrm{sca})}$ from $(r\mathbf{s})$ to the triplet (n_1, n_2, n_3).

An example is presented in Fig. 5.3. The source width σ_S decreases in going from panel a) to panel c). This means that the spectral degree of coherence of the incident field increases. It is seen that the circular, Gaussian intensity distribution, which is centered around the von Laue direction, gets narrower when the spatial coherence of the incident field increases, and becomes more and more point-like.

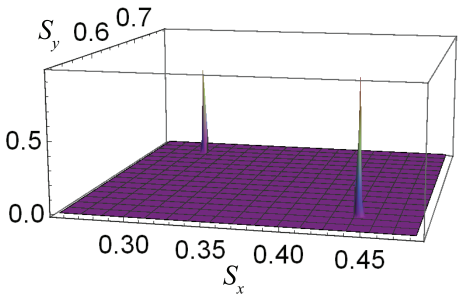

Figure 5.4: Distribution of the normalized scattered intensity around two von Laue spots. The left-hand peak corresponds to $(n_1, n_2, n_3) = (1, 3, -2)$ and hence $\lambda = 2.95 \times 10^{-10}$ m. The right-hand peak is for $(n_1, n_2, n_3) = (2, 3, -2)$, and thus $\lambda = 2.21 \times 10^{-10}$ m. In these two examples $\sigma_S = 1.0 \times 10^{-3}$ m, and $\Delta z = 1$ m.

Let us next choose a second scattering direction by setting

$$n_1 = 2, \tag{5.51}$$

$$n_2 = 3, \tag{5.52}$$

$$n_3 = -2. \tag{5.53}$$

We now find that $\lambda = 2.21 \times 10^{-10}$ m, and hence that $s_x = 0.44$, $s_y = 0.55$, and $s_z = 0.70$. It is clear from Fig. 5.4 that these two diffraction peaks are well separated, both directionally and spectrally.

5.5 Uncorrelated, infinitely thin annular sources

We next consider the idealized case of a completely incoherent, infinitely thin "delta-ring" source. If this ring has a uniform spectral density A^2, and is of radius R, then the cross-spectral density of the field in the source plane is given by the expression

$$W^{(0)}(\boldsymbol{\rho}_1, \boldsymbol{\rho}_2) = A^2 \delta(\rho_1 - R)\delta^2(\boldsymbol{\rho}_2 - \boldsymbol{\rho}_1), \tag{5.54}$$

where δ and δ^2 represent the one- and two-dimensional Dirac δ function, respectively. Such a source produces a J_0 Bessel-correlated field in its far zone. The approximate experimental realization of such a field was reported in [RAGHUNATHAN *et al.*, 2010].

If we substitute from Eq. (5.54) into Eq. (5.25) for the case of an orthorhombic crystal as described in Sec. 5.3, we get the expression

$$\begin{aligned} S^{(\mathrm{sca})}(r\mathbf{s}) &= \beta \sum_{\substack{n_i, m_j \\ n_3 = m_3}} \delta \left\{ \Delta z \left[\left(\frac{2\pi n_1}{ka} - s_x \right)^2 + \left(\frac{2\pi n_2}{kb} - s_y \right)^2 \right]^{1/2} - R \right\} \\ &\quad \times \delta \left[\frac{2\pi}{ka}(n_1 - m_1) \right] \delta \left[\frac{2\pi}{kb}(n_2 - m_2) \right], \qquad (5.55) \\ &= \beta \sum_{n_i} \delta \left\{ \Delta z \left[\left(\frac{2\pi n_1}{ka} - s_x \right)^2 + \left(\frac{2\pi n_2}{kb} - s_y \right)^2 \right]^{1/2} - R \right\}. \qquad (5.56) \end{aligned}$$

In order to determine the components of the directional vector $\mathbf{s}$ and the wavelength λ, we recall Eq. (5.41):

$$s_z = 1 + u, \tag{5.57}$$

where we defined the scaled wavelength u as

$$u \equiv \frac{\lambda n_3}{c}. \tag{5.58}$$

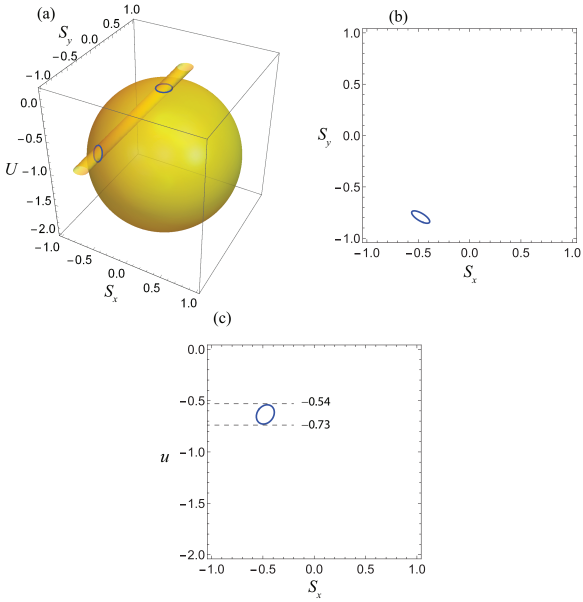

Figure 5.5: (a) An oblique, elliptic cylinder and a unit sphere in (s_x, s_y, u)-space. The sphere is centered on $(0, 0, -1)$, and the cylinder has a radius $R/\Delta z$ in the horizontal plane. The intersections of the cylinder and the sphere are indicated by the two blue curves. (b) The projection of the lower intersection onto the s_x, s_y-plane. (c) The projection of the lower intersection onto the s_x, u-plane. In these examples $a = 1 \times 10^{-9}$ m, $b = 1.2 \times 10^{-9}$ m, $c = 1.5 \times 10^{-9}$ m, $n_1 = -1$, $n_2 = -2$, $n_3 = -2$, $R = 0.1$ m and $\Delta z = 1$ m.

The first requirement, that $|\mathbf{s}| = 1$, defines a unit sphere in (s_x, s_y, u)-space that is centered around the point $(0, 0, -1)$, as is shown in Fig. 5.5. The second condition, which is derived from Eqs. (6.11) and (5.58), reads

$$\left(u\frac{cn_1}{n_3 a} - s_x\right)^2 + \left(u\frac{cn_2}{n_3 b} - s_y\right)^2 = \frac{R^2}{(\Delta z)^2}. \tag{5.59}$$

This defines an oblique, elliptic cylinder, whose intersection with any horizontal plane $u =$ constant, is a circle with center $(s_x, s_y) = (ucn_1/n_3 a, ucn_2/n_3 b)$, and with radius $R/\Delta z$. From this expression it follows readily that the central axis of the cylinder is the line given by the formula

$$(s_x, s_y, u) = (ucn_1/n_3a, ucn_2/n_3b, u). \tag{5.60}$$

For any choice of the triplet (n_1, n_2, n_3), the directions of non-zero scattering and the wavelength are given by the intersections of the cylinder and the unit sphere. These will be two closed curves, as indicated in blue in the example shown in Fig. 5.5(a). The upper curve, near $u = 0$, is the partially coherent analog of the spurious solution that we discussed below Eq. (5.49), and we will therefore not consider it.

The assumption that the scatterer is in the far zone of the source means that R is much smaller than Δz. This implies that the cylinder is quite narrow. According to Eq. (5.57), an intersection of the cylinder in the upper half of the sphere ($u > -1$), corresponds to forward scattering ($s_z > 0$), whereas an intersection in the lower portion of the sphere represents backscattering ($s_z < 0$). Instead of a single von Laue direction, we now have a range of scattering directions, each represented by a point on the intersectional curve. Since these points each have a distinct u coordinate, Eq. (5.58) implies that they all represent scattering at a distinct wavelength, i.e., the von Laue curves show dispersion. It is worth remarking that this spread in u values, and hence the dispersion, will be more pronounced for oblique scattering than for scattering in the forward direction.

The projection of the sphere-cylinder intersection onto the the s_x, s_y-plane is obtained by substituting $u = -1 \pm (1 - s_x^2 - s_y^2)^{1/2}$ into Eq. (5.59), with the plus (minus) sign taken for intersections in the upper (lower) half of the sphere. This gives the formula

$$\begin{aligned} \frac{R^2}{(\Delta z)^2} = &\left[\left(-1 \pm \sqrt{1 - s_x^2 - s_y^2}\right) \frac{cn_1}{n_3a} - s_x\right]^2 \\ &+ \left[\left(-1 \pm \sqrt{1 - s_x^2 - s_y^2}\right) \frac{cn_2}{n_3b} - s_y\right]^2. \end{aligned} \tag{5.61}$$

The projection of the lower curve of Fig. 5.5(a) is plotted in panel (b). This curve represents scattering along a range of directions $\mathbf{s}$, each with a specific value of u, and hence with a different wavelength. The variation of the wavelength with the direction $\mathbf{s}$ can be studied by projecting the intersection onto the s_x, u-plane. This is done by substituting $s_y = \pm[1 - s_x^2 - (1+u)^2]^{1/2}$ into Eq. (5.59), with the plus (minus) sign taken when s_y is positive (negative). The result is

$$\frac{R^2}{(\Delta z)^2} = \left[u\frac{cn_1}{n_3 a} - s_x\right]^2 + \left[u\frac{cn_2}{n_3 b} \mp \sqrt{1 - s_x^2 - (1+u)^2}\right]^2. \tag{5.62}$$

The projection of the lower curve is shown in Fig. 5.5(c). It is seen that the value of u varies between -0.54 and -0.73. According to Eq. (5.58), this corresponds to a wavelength range of $4.05 \times 10^{-10}\,\mathrm{m} \leq \lambda \leq 5.47 \times 10^{-10}\,\mathrm{m}$.

The distinction between forward and backward scattering can be made by considering the angle, γ say, between the axis of the cylinder and the positive u axis. It follows from Eq. (5.60) that

$$\tan\gamma = \sqrt{\left(\frac{cn_1}{n_3 a}\right)^2 + \left(\frac{cn_2}{n_3 b}\right)^2}. \tag{5.63}$$

Ignoring the finite radius of the cylinder for simplicity, the lowest intersection of the cylinder with the sphere will be above the equator ($u = -1$) when this angle exceeds 45°. Hence, we conclude that forward scattering occurs when

$$\left(\frac{cn_1}{n_3 a}\right)^2 + \left(\frac{cn_2}{n_3 b}\right)^2 > 1. \tag{5.64}$$

When this quantity is less than unity, the scattering is in the backward direction.

Colorful von Laue patterns in the visible spectrum can be produced by crystals with sides on the order of microns. Examples of three symmetrically located, forward-scattered patterns ($s_z > 0$), are plotted in Fig. 5.6(a). Their projection onto the s_x, u plane is shown in panel (b). Using Eq. (5.58), it is found that the wavelengths for these three ellipses range from 405 to 660 nm, as is indicated in the color rendering. By increasing the distance Δz between the source and the crystal (see Fig. 5.1), one gradually approaches the case of spatially coherent illumination. This should lead to a decrease in dispersion. Indeed it found for example, that when Δz is increased from 1 to 5 m, the wavelength range is reduced to 465 to 600 nm.

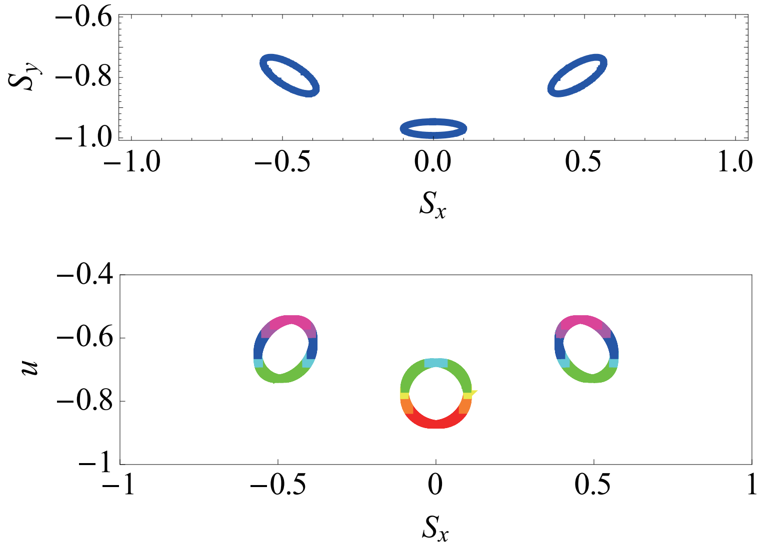

Figure 5.6: (a): Three different von Laue patterns scattered in the forward direction ($s_z > 0$) for, from left to right, $n_1 = -1, 0, 1$, and $n_2 = n_3 = -2$. (b): The projection of these curves onto the s_x, u-plane, showing their colors in the visible spectrum. In this example $a = 1 \times 10^{-6}$ m, $b = 1.2 \times 10^{-6}$ m, $c = 1.5 \times 10^{-6}$ m, $R = 0.1$ m and $z = 1$ m.

Examples of scattering in the backward direction ($s_z < 0$), are presented in Fig. 5.7. Near-circular, overlapping intensity patterns are produced with a wavelength interval from 444 to 480 nm. The directional radius of these patterns, i.e., their spread in the s_x, s_y plane, can easily be tailored by changing either the source radius R or the source-crystal distance Δz. Decreasing the ratio $R/\Delta z$ decreases the directional radius.

5.6 Conclusions

We have analyzed the role of spatial coherence in scattering from a periodic potential. This was done within the context of the so-called von Laue method, in which a polychromatic field is diffracted by a crystal with a fixed orientation. A general expression, Eq. (5.25), that relates the

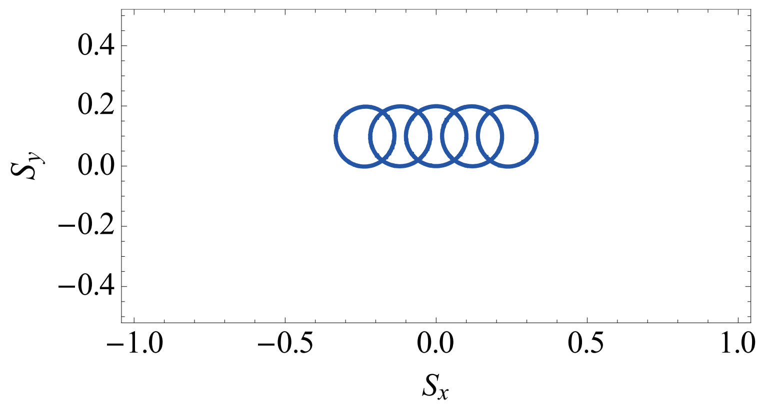

Figure 5.7: Showing five different backscattered von Laue rings for, from left to right, $n_1 = -2, -1, 0, 1, 2$, and $n_2 = 1$ and $n_3 = -25$. In this example $a = 4 \times 10^{-6}$ m, $b = 4.8 \times 10^{-6}$ m, $c = 6.0 \times 10^{-6}$ m, $R = 0.1$ m, and $\Delta z = 1$ m.

scattered field to the cross-spectral density of the source, was derived. This result was applied to two different types of partially coherent sources namely quasihomogeneous Gaussian Schell model sources (GSM) and δ-correlated, thin annular sources. The sphere-cylinder construction that we used for the latter type, can, at least in principle, also be applied to the GSM source. However, we chose, for that case at least, to stay closer to the traditional treatment. The GSM sources were seen to produce von Laue spots whose size is directly related to the size of the source. The annular sources were found to generate elliptical von Laue patterns rather than spots. Both the dispersion and the angular spread of these patterns can be tuned by changing the source radius or the distance between the source and the crystal. In summary, we have shown how spatial coherence can be used to tailor scattering by an object with a periodic potential. Our work may be extended to sources with different shapes and correlation functions, other crystals, and crystals with a different orientation.

Acknowledgments

This material is based upon work supported by the Air Force Office of Scientific Research under award number FA9550-16-1-0119, the Natural Science Basic Research Plan in Shaanxi Province of China (No. 2016JQ1011) and the National Natural Science Foundations of China (NSFC) (No. 11504296).

Chapter 6

The electromagnetic field produced by a refractive axicon

This Chapter is based on

- Yangyundou Wang, Shenggang Yan, Ari T. Friberg, David Kuebel and Taco D. Visser, "The electromagnetic field produced by a refractive axicon," to be submitted.

Abstract
We study the field that is produced by a refractive axicon. The results from geometrical optics, scalar wave optics and electromagnetic diffraction theory are compared. In particular, the axial intensity, the on-axis effective wavelength, the transverse intensity, and the far-zone field are examined. The state of polarization of the incident beam is found to strongly affect the transverse intensity distribution, but not the intensity distribution in the far zone.

6.1 Introduction

Axicons [McLeod, 1954], sometimes called conical prisms, are optical elements that have rotational symmetry. Whereas ordinary lenses produce a focal spot, axicons produce a focal line, known as the *axicon line image*, which, with increasing distance from the axicon, gradually evolves into a ring-shaped pattern. This makes them useful for applications as diverse as imaging with an extended depth of focus [Sochacki *et al.*, 1992], surface inspection [Brinkmann *et al.*, 1996], stimulated Brillouin scattering [Velchev and Ubachs, 2001], optical pumping [Schafer, 1986], laser drilling [Rioux *et al.*, 1978], optical trapping [Shao *et al.*, 2006], frequency doubling [Wulle and Herminghaus, 1993], triangulation [Bickel *et al.*, 1985], optical coherence tomography [Ding *et al.*, 2002], and corneal surgery [Ren and Birngruber, 1990]. Moreover, they can be used to create so-called non-diffracting Bessel beams [Hernandez-Figueroa *et al.*, 2014]. Useful reviews of axicon lenses are presented in [Soroko, 1989] and [Jaroszewicz, 1997].

Three types of axicons can be distinguished: diffractive axicons [Edmonds, 1974; Durnin *et al.*, 1987; Tervo and Turunen, 2001], reflective axicons [Fujiwara, 1962; Turunen and Friberg, 1993a; Dutta *et al.*, 2014; Radwell *et al.*, 2016] and refractive axicons [McLeod, 1960; Zapata-Rodriguez and Sanchez-Losa, 2005]. In this study we consider the latter variety. A vector analyisis for lenses that produce a converging spherical wavefront has been presented in a well-known study by Richards and Wolf [Richards and Wolf, 1959]. However, an electromagnetic study of refractive axicons, as presented here, has to the best of our knowledge not been undertaken yet.

We begin by briefly reviewing several axicon properties. In section 6.2 a geometrical optics approach is used. This is followed by a scalar wave analysis in section 6.3, in which also the transition of the line image into a ring-shaped intensity profile is examined. In section 6.4 we derive expressions for the electromagnetic field that is produced by incident beams whose polarization state is either uniform, e.g., beams that are linearly polarized, or whose polarization state is non-uniform [Brown, 2011], namely beams with radial or azimuthal polarization. We apply these formulas in Section 6.5 to study the on-axis intensity, the effective on-axis wavelength, the tranverse field intensity, the state of polarization, and the far-zone field. Throughout our analysis we make use of the paraxial approximation. This justifies neglecting the longitudinal field components.

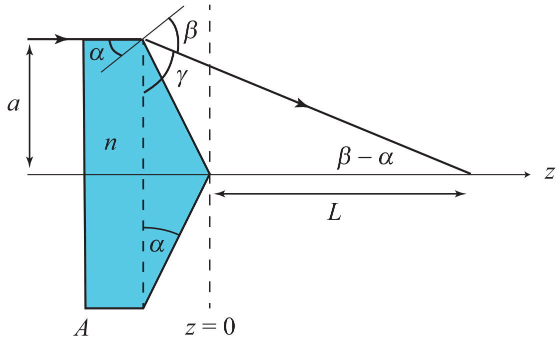

Figure 6.1: A refractive axicon with radius a, base angle α and refractive index n. Rays are normally incident on the front face A. A marginal ray crosses the z-axis at a distance L from the apex which is taken to be in the plane $z = 0$.

6.2 Geometrical rays

A linear, plano-convex refractive axicon, as sketched in Fig. 6.1, is rotationally symmetric about the z axis and has a cone-shaped form. For holding the cone during manufacturing and use, a cylindrical section is necessary. The axicon is characterized by three parameters: the refractive index n, the base angle α, and the radius a. We consider an axicon that is illuminated by a collection of rays that are all parallel to the z axis. At the conical surface of the axicon these rays are refracted toward the axis, all under the same angle $\beta - \alpha$. It is seen that they are focussed along a line which extends over a distance L from the apex of the cone, as shown in Fig. 6.1. From Snell's law we have that $\sin\beta = n \sin\alpha$. Hence the length of the focal line equals

$$L = a \tan\gamma - a \tan\alpha, \tag{6.1}$$

with the angle γ given by the expression

$$\gamma = 90^\circ - \beta + \alpha. \tag{6.2}$$

The length of the focal line versus the base angle α is shown in Fig. 6.2. It is seen that for applications in which a long focal line is needed, the base angle must be quite small. We will from here on restrict ourselves to this paraxial regime.

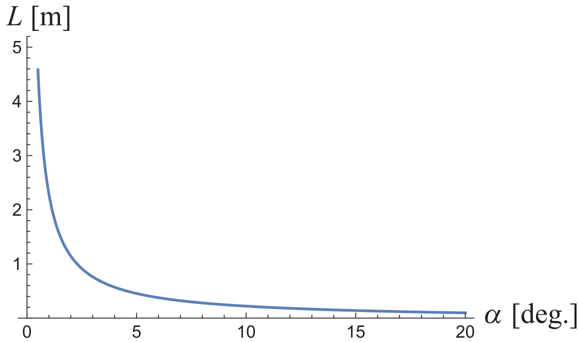

Figure 6.2: The length L of the focal line as a function of the base angle α. In this example the refractive index $n = 1.5$, and the axicon radius $a = 2$ cm.

We assume that the incident field has a Gaussian intensity profile, i.e.,

$$I^{(\mathrm{in})}(\boldsymbol{\rho}) = I_0 \exp(-2\rho^2/w_0^2), \tag{6.3}$$

with I_0 and w_0 positive constants, and $\rho = |(x, y)|$ being the radial distance from the z-axis. In order to calculate the axial intensity distribution, we consider a thin ring on the front face A with inner radius ρ and outer radius $\rho + \delta\rho$. The power flow through the ring is

$$P(\rho) = I_0 \exp(-2\rho^2/w_0^2) 2\pi\rho\, \delta\rho. \tag{6.4}$$

The transmitted portion of this power is projected onto the z axis between the two positions

$$L_1 = \rho(\tan\gamma - \tan\alpha), \tag{6.5}$$

$$L_2 = (\rho + \delta\rho)(\tan\gamma - \tan\alpha), \tag{6.6}$$

where we have used Eq. (6.1) with the variable a replaced by the radial distances ρ and $\rho + \delta\rho$, respectively. The rays carrying this power make an angle $\beta-\alpha$ with the z axis. If we define the length $\delta L = L_2 - L_1$, then the axial intensity or "power per unit length" equals

$$\frac{P(\rho)}{\delta L} T_1^2(\omega) T_2^2(\omega) \cos(\beta-\alpha) = \\ \frac{2\pi I_0 T_1^2(\omega) T_2^2(\omega) \cos(\beta-\alpha)}{\tan\gamma - \tan\alpha} \rho \exp\left(-2\rho^2/w_0^2\right). \tag{6.7}$$

Here $T_1(\omega)$ and $T_2(\omega)$ are the amplitude transmission coefficients at frequency ω of the air-glass interface for normal incidence, and of the glass-air interface for incidence at an angle α, respectively. From Eq. (6.1) we find that $z = \rho(\tan\gamma - \tan\alpha)$, and thus the axial intensity is given by the formula

$$I(z) = D_1 z \exp[-2z^2/w_0^2(\tan\gamma - \tan\alpha)^2], \tag{6.8}$$

where we have introduced the abbreviation

$$D_1 = \frac{2\pi I_0 T_1^2(\omega) T_2^2(\omega) \cos(\beta-\alpha)}{(\tan\gamma - \tan\alpha)^2}. \tag{6.9}$$

This factor is independent of the position z. Note that this geometrical model predicts a non-zero field on axis only when $0 \leq z \leq L$. In the next section we will compare the prediction of Eq. (6.8) with the result of a scalar analysis.

6.3 Scalar fields

Let us next consider a plane, monochromatic scalar wave of frequency ω with a Gaussian amplitude distribution, that is propagating in the positive z direction. The wave is normally incident on the front face A of the axicon. In the space-frequency domain this wave can be represented as

$$U^{(\mathrm{in})}(\boldsymbol{\rho}, \omega) = U_0(\omega) \exp(-\rho^2/w_0^2), \tag{6.10}$$

where $U_0(\omega)$ denotes the spectral amplitude, which we take to be unity, and w_0 is the beam width in the plane A (see Fig. 6.3) . The base angle α is taken to be quite small, which justifies using the paraxial approximation.

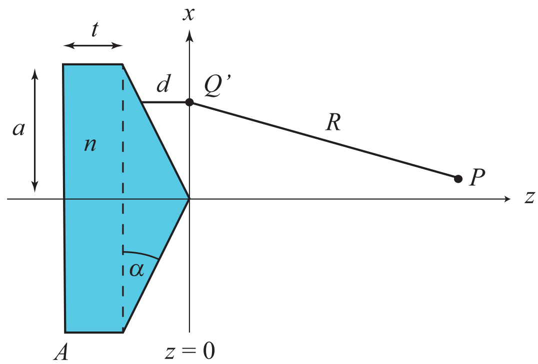

Figure 6.3: A paraxial refractive axicon with radius a, base angle α and refractive index n. A plane wave with a Gaussian amplitude distribution is normally incident on the front face A. The thickness of the cylindrical base is denoted by t, and $z = 0$ indicates the output plane.

In order to calculate the field in the output plane $z = 0$, we notice that at position $Q'(\boldsymbol{\rho}, 0)$ the field has travelled a length d through air, namely

$$d \approx \rho \tan \alpha \approx \rho\alpha. \tag{6.11}$$

The phase difference Δ between the field at Q' and that on the z axis is therefore

$$\Delta = (1 - n)kd = (1 - n)k\rho\alpha, \tag{6.12}$$

where k denotes the free-space wavenumber associated with frequency ω. We thus find that the output field in the plane $z = 0$ is related to the incident field in the entrance plane A by the formula

$$U^{(\text{out})}(\boldsymbol{\rho}, \omega) = T(\rho, \omega)U^{(\text{in})}(\boldsymbol{\rho}, \omega), \tag{6.13}$$

with $T(\rho, \omega)$ given by the expression

$$T(\rho, \omega) = C(\omega) \exp[ik(1 - n)\rho\alpha], \tag{6.14}$$

and with the factor $C(\omega)$ being independent of ρ, namely

$$C(\omega) = T_1(\omega)T_2(\omega) \exp(iknt). \tag{6.15}$$

Here $T_1(\omega)$ and $T_2(\omega)$ are the transmission coefficients defined below Eq. (6.7), and t is the thickness of the cylindrical axicon base.

The field at a position $P(\mathbf{r})$ behind the lens is, according to the Huygens-Fresnel principle [Born and Wolf, 1995, Chap. 8], given by the expression

$$U(\mathbf{r},\omega) = -\frac{\mathrm{i}}{\lambda}\iint_{z=0} U^{(\mathrm{out})}(\boldsymbol{\rho}',\omega)\frac{e^{\mathrm{i}kR}}{R}\mathrm{d}^2\rho', \tag{6.16}$$

where $R = [z^2 + (x-\xi)^2 + (y-\eta)^2]^{1/2}$ is the distance between $P(x,y,z)$ and $Q'(\xi,\eta,0)$, and λ is the free-space wavelength. Using the Fresnel approximation, together with Eq. (6.13), this diffraction integral can be expressed as

$$\begin{aligned} U(x,y,z) = {} & -\frac{\mathrm{i}C}{\lambda z}\exp(\mathrm{i}kz) \\ & \times \iint_{z=0} \exp\left[\mathrm{i}k(1-n)\sqrt{\xi^2+\eta^2}\alpha\right] \\ & \times \exp[-(\xi^2+\eta^2)/w_0^2] \\ & \times \exp\left\{\mathrm{i}\frac{k}{2z}[(x-\xi)^2+(y-\eta)^2]\right\}\mathrm{d}\xi\mathrm{d}\eta, \end{aligned} \tag{6.17}$$

where for brevity the ω-dependence has been omitted. In cylindrical coordinates

$$\boldsymbol{\rho}' = (\xi,\eta) = \rho'(\cos\mu, \sin\mu), \tag{6.18}$$

$$\boldsymbol{\rho} = (x,y) = \rho(\cos\delta,\sin\delta), \tag{6.19}$$

the field at P can be written as

$$\begin{aligned} U(\boldsymbol{\rho},z) = {} & -\frac{\mathrm{i}C}{\lambda z}\exp(\mathrm{i}kz)\exp\left(\mathrm{i}\frac{k}{2z}\rho^2\right) \\ & \times \int_0^{2\pi}\int_0^a \exp\left[\mathrm{i}k(1-n)\rho'\alpha\right]\exp(-\rho'^2/w_0^2) \\ & \times \exp\left(\mathrm{i}\frac{k}{2z}\rho'^2\right) \\ & \times \exp\left[-\mathrm{i}\frac{k\rho\rho'}{z}\cos(\mu-\delta)\right]\rho'\mathrm{d}\rho'\mathrm{d}\mu. \end{aligned} \tag{6.20}$$

The integral over the angle μ is independent of δ, and hence we obtain the formula

$$\begin{aligned} U(\boldsymbol{\rho}, z) = & -\frac{\mathrm{i}2\pi C}{\lambda z} \exp(\mathrm{i}kz) \exp\left(\mathrm{i}\frac{k}{2z}\rho^2\right) \\ & \times \int_0^a \exp\left[\mathrm{i}k(1-n)\rho'\alpha\right] \exp\left(\mathrm{i}\frac{k}{2z}\rho'^2\right) \\ & \times \exp(-\rho'^2/w_0^2) J_0\left(\frac{k\rho\rho'}{z}\right) \rho' \mathrm{d}\rho', \end{aligned} \tag{6.21}$$

with J_0 a Bessel function of the first kind of order zero. The intensity then follows from the definition

$$I(\boldsymbol{\rho}, z) = |U(\boldsymbol{\rho}, z)|^2. \tag{6.22}$$

The oscillatory integral in Eq. (6.21) can be evaluated numerically, but it is instructive to find an approximate solution by using the method of stationary phase [Mandel and Wolf, 1995, Sec. 3.3]. If we consider only the contribution of the interior stationary point, which means that the edge contribution is ignored, the result is (see Appendix A for details)

$$\begin{aligned} U(\boldsymbol{\rho}, z) = & -\mathrm{i}C(2\pi kz)^{1/2}(n-1)\alpha \exp(\mathrm{i}\pi/4) \exp(\mathrm{i}kz) \\ & \times \exp\left(\mathrm{i}k\rho^2/2z\right) \exp\left[-\mathrm{i}kz(n-1)^2\alpha^2/2\right] \\ & \times \exp[-z^2(1-n)^2\alpha^2/w_0^2] J_0[(n-1)k\rho\alpha], \\ & (\text{for } 0 < z < L). \end{aligned} \tag{6.23}$$

For the intensity we hence find that

$$\begin{aligned} I(\boldsymbol{\rho}, z) = & D_2\, z \exp[-2z^2(1-n)^2\alpha^2/w_0^2] \\ & \times \left\{J_0[(n-1)k\rho\alpha]\right\}^2, \quad (\text{for } 0 < z < L), \end{aligned} \tag{6.24}$$

where the constant D_2 is independent of position and given by the expression

$$D_2 = C^2 2\pi k(n-1)^2\alpha^2. \tag{6.25}$$

Before discussing the implications of the these diffraction integrals, it is important to note that Eq. (6.21) is valid for all axial positions z, but that Eq. (6.23) applies only for the interval $0 \leq z \leq L$. When z is beyond the focal line the method of stationary phase, just like the geometrical model, predicts an axial field that is identically zero.

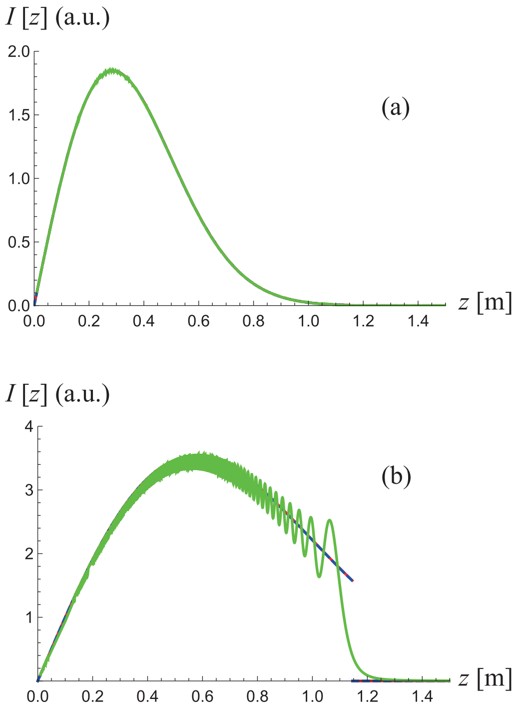

Figure 6.4: The normalized intensity distribution along the z axis as given by geometrical optics [Eq. (6.8)] (blue), wave optics using the full diffraction integral [Eq. (6.21)] (green), and wave optics using the method of stationary phase [Eq. (6.24)] (red). In panel (a) the beam waist $w_0 = 0.5$ cm, in panel (b) $w_0 = 1$ cm. In both these examples the refractive index $n = 1.5$, the base angle $\alpha = 1^\circ$, the axicon radius $a = 1$ cm, and the wavelength $\lambda = 632.8$ nm.

6.3.1 The axial intensity

The axial intensity distribution produced by an axicon is shown in Fig. 6.4(a) based on the three different models we have discussed so far: geometrical optics [Eq. (6.8)], scalar wave optics using the full diffraction integral [Eq. (6.21)], and scalar wave optics using the method of stationary phase [Eq. (6.24)]. For our first choice of parameters the three curves are virtualy indistinguishable. The intensity is seen to first rise, after which an exponential decay sets in. The length of the focal line as calculated from Eq. (6.1), $L = 1.15$ m in this case. The beam waist w_0 was taken to be less than the axicon radius. Neglecting the boundary contribution, as is done in the stationary phase expression Eq. (6.24), is then justified. However, when the waist size and the radius are set equal, as illustrated in panel (b), the edge contribution becomes significant. The diffaction integral Eq. (6.21), in which the edge contribution is *not* neglected, now predicts an intensity with a modulation with increasing size and decreasing periodicity, followed by a steep decline to zero. That the boundary contribution leads to an oscillatory intensity has been discussed previously, e.g., in [Durnin *et al.*, 1987] and [Horvath and Bor, 2001]. This behavior is in stark contrast with Eqs. (6.8) and Eq. (6.24). These two formulas both still predict a smooth intensity distribution, but now with a discontinuous drop to zero at the end of the focal line ($z = L$).

6.3.2 The transverse intensity

The normalized transverse intensity distribution, as given by Eq. (6.24), is seen to be

$$I(\boldsymbol{\rho}) = \{J_0[(n-1)k\rho\alpha]\}^2\,, \quad (z < L), \tag{6.26}$$

which is independent of z. It is this ability of axicons to produce "diffraction-free," or "propagation-invariant" Bessel beams that has attracted much attention [Turunen *et al.*, 1988; Vasara *et al.*, 1989; Turunen and Friberg, 1993b; Turunen and Friberg, 2009; Levy *et al.*, 2016]. Because Eq. (6.26) is only valid when $z < L$, it cannot be used to investigate the transition of the axicon line image to a ring-shaped profile. We therefore use Eq. (6.21), which, in contrast to Eq. (6.26), does *not* rely on the stationary phase approximation. In Fig. 6.5 the transverse intensity is

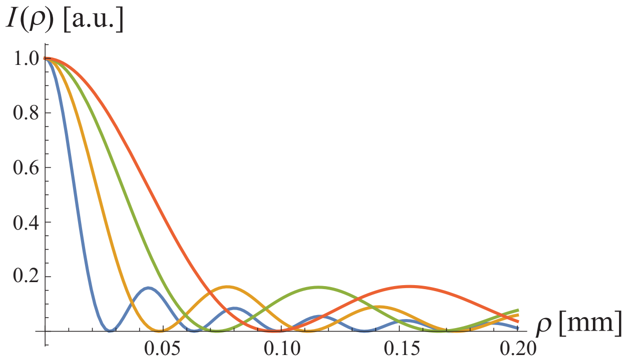

Figure 6.5: The normalized transverse intensity distribution according to Eq. (6.21) in different planes. From left to right, $z = 1$ m, 2 m, 3 m and 4 m. In these examples $\lambda = 632.8$ nm; $\alpha = 1°$, $w_0 = 1$ cm, $a = 1$ cm and $n = 1.5$.

shown in different cross-sections. The left-most curve ($z = 1$ m), is practically identical with the J_0^2 prediction of Eq. (6.26). For values larger than the focal line length $L = 1.14$ m [see Eq. (6.1)], the distribution gets progressively broader. We note that, for clarity, all curves in Fig. 6.5 are normalized to 1 at $\rho = 0$. In reality, obviously, the axial intensity will decrease when z gets larger.

The gradual broadening of the central peak is accompanied by the onset of side lobes, which eventually leads to a ring-like intensity profile. This is shown in Fig. 6.6 where the horizontal axis indicates the polar angle θ, rather than the radial distance ρ. The side lobes, positioned between $\theta = 0.002$ and $\theta = 0.008$, have a maximum intensity that increases with increasing z. Gradually, this maximum begins to exceed the unit intensity on the axis ($\theta = 0$).

The influence of the beam waist parameter w_0 can be examined by increasing its value from 1 cm to 1 m. The result is shown in Figure 6.7, in which it can be seen that the position of the maxima remains the same, but the secondary sidelobes are now more suppressed.

For even larger distances, as plotted in Fig. 6.8, these side lobes get narrower, and a ring-like field develops around the angle $\theta = \beta - \alpha = 0.0087$, which is precisely the geometrical angle of refraction shown in

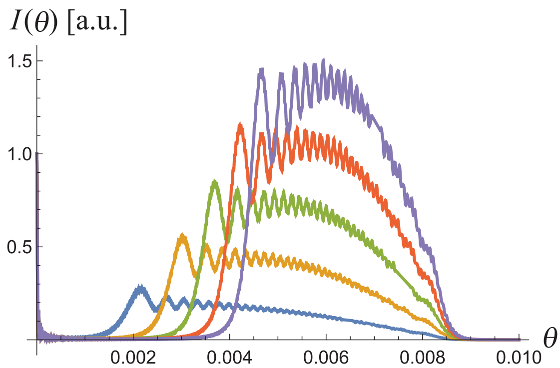

Figure 6.6: The transverse intensity distribution according to Eq. (6.21), normalized to unity at $\theta = 0$, as a function of the polar angle, in different cross-sections. From left to right, z = 1.4 m, 1.6 m, 1.8 m, 2.0 m and 2.2 m. All parameters are the same as in Fig. 6.5.

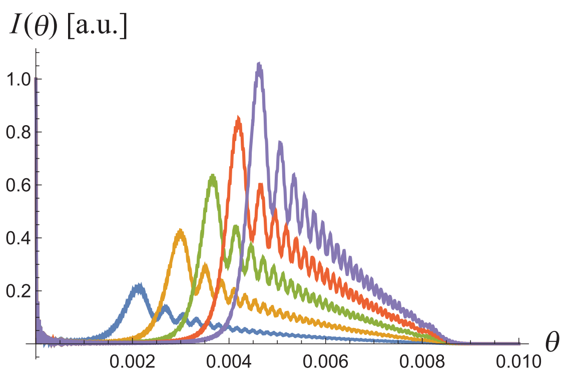

Figure 6.7: The transverse intensity distribution according to Eq. (6.21), normalized to unity at $\theta = 0$, as a function of the polar angle, in different cross-sections. From left to right, z = 1.4 m, 1.6 m, 1.8 m, 2.0 m and 2.2 m. The beam waist w_0 is now increased to 1 m, from 1 cm in Figs. 6.5 and 6.6. All the other parameters are the same as in Fig. 6.5.

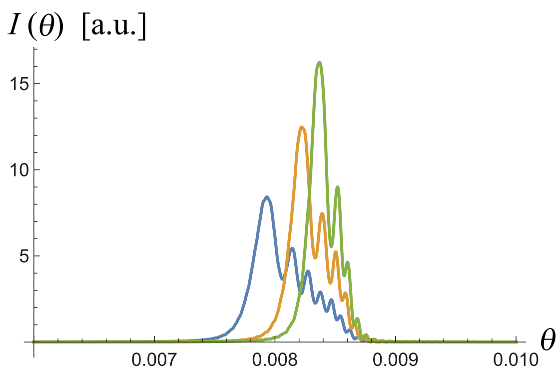

Figure 6.8: The transverse intensity distribution according to Eq. (6.21), normalized to unity at $\theta = 0$, as a function of the polar angle, in different cross-sections. From left to right, $z = 10$ m, 15 m, and 20 m. The beam waist $w_0 = 1$ m. All other parameters are the same as in Fig. 6.5.

Fig. 6.1. Notice that in Figs. 6.5 to 6.8 the same normalization is used. This means, for example, that for the right-most curve in Fig. 6.8, ($z =$ 20 m), the intensity of the ring-like side lobe is about 16 times higher than that of the field on axis.

6.4 Electromagnetic fields

In this section we analyze two types of incident electromagnetic beams, namely beams with a uniform polarization, i.e., beams whose state of polarization is the same at all points in a cross-section, and radially and azimuthally polarized beams, which are non-uniformly polarized.

6.4.1 Linear polarization

We begin by assuming a monochromatic, normally incident field that is linearly polarized along the x-direction, i.e.,

$$\mathbf{E}^{(\mathrm{in})}(\mathbf{r}) = E_0\,\hat{\mathbf{x}}\,e^{\mathrm{i}kz} = E_0(1,0,0)e^{\mathrm{i}kz}, \tag{6.27}$$

with $E_0 > 0$. We note that this incident field has a constant amplitude, in contrast to the Gaussian fields that were discussed in earlier sections. The

Fresnel transmission coefficient T_1 for normal incidence at the front face A gives rise to an overall amplitude factor that is independent of position, i.e. [Jackson, 1998, Sec. 7.3]

$$T_1 = \frac{2}{n+1}. \tag{6.28}$$

As can be seen from Fig. 6.3, the field travels a distance $t + \alpha(a - \rho)$ from the entrance plane A to the inside of the conical surface. Hence the field there, indicated by the superscript $(-)$, equals

$$\mathbf{E}^{(-)}(\mathbf{r}) = E_0 T_1 e^{\mathrm{i}kz} e^{\mathrm{i}kn[t+\alpha(a-\rho)]}(1, 0, 0). \tag{6.29}$$

The inward normal vector of the cone is given by the expression

$$\hat{\mathbf{n}} = -(\sin\alpha\cos\phi, \sin\alpha\sin\phi, \cos\alpha), \tag{6.30}$$

where the caret symbol denotes a unit vector. We define the vector $\mathbf{s}$, which is normal to the plane of incidence at the conical surface, as

$$\begin{align} \mathbf{s} &= \hat{\mathbf{z}} \times \hat{\mathbf{n}}, \tag{6.31}\\ &= (\sin\alpha\sin\phi, -\sin\alpha\cos\phi, 0). \tag{6.32} \end{align}$$

The vector $\hat{\mathbf{p}}$, which lies in the plane of incidence and is also perpendicular to the wave vector within the axicon, is defined as

$$\begin{align} \hat{\mathbf{p}} &= \hat{\mathbf{z}} \times \hat{\mathbf{s}}, \tag{6.33}\\ &= (\cos\phi, \sin\phi, 0). \tag{6.34} \end{align}$$

The electric field vector can now be decomposed into an s and a p polarized part by writing

$$\mathbf{E}^{(-)}(\rho, \phi) = \mathbf{E}_s^{(-)}(\rho, \phi) + \mathbf{E}_p^{(-)}(\rho, \phi), \tag{6.35}$$

with

$$\begin{align} \mathbf{E}_s^{(-)}(\rho, \phi) &= [\mathbf{E}^{(-)}(\rho, \phi) \cdot \hat{\mathbf{s}}]\, \hat{\mathbf{s}}, \tag{6.36}\\ &= \Lambda(\rho)(\sin^2\phi, -\cos\phi\sin\phi, 0). \tag{6.37}\\ \mathbf{E}_p^{(-)}(\rho, \phi) &= [\mathbf{E}^{(-)}(\rho, \phi) \cdot \hat{\mathbf{p}}]\, \hat{\mathbf{p}}, \tag{6.38}\\ &= \Lambda(\rho)(\cos^2\phi, \cos\phi\sin\phi, 0), \tag{6.39} \end{align}$$

and where we introduced the abbreviation

$$\Lambda(\rho) = E_0 T_1 e^{\mathrm{i}kz} e^{\mathrm{i}kn[t+\alpha(a-\rho)]}. \tag{6.40}$$

These two field components are transmitted with their respective Fresnel coefficients, T_s and T_p, for which we have [Born and Wolf, 1995, Sec. 1.5.2]

$$T_s = \frac{2n\cos\alpha}{n\cos\alpha + \sqrt{1-n^2\sin^2\alpha}}, \tag{6.41}$$

$$T_p = \frac{2n\cos\alpha}{\cos\alpha + n\sqrt{1-n^2\sin^2\alpha}}. \tag{6.42}$$

Whereas the s polarized part remains otherwise unchanged, the p polarized part of the electric field is, according to Snell's law, also rotated over an angle $\beta - \alpha$ around the vector $\mathbf{s}$ (see Fig. 6.1), with

$$\sin\beta = n\sin\alpha. \tag{6.43}$$

If we now introduce a vector $\hat{\mathbf{q}}$ by defining

$$\hat{\mathbf{q}} = (\cos(\beta-\alpha)\cos\phi, \cos(\beta-\alpha)\sin\phi, \sin(\beta-\alpha)), \tag{6.44}$$

it is readily verified that

$$\hat{\mathbf{q}} \cdot \hat{\mathbf{s}} = 0, \tag{6.45}$$

and that

$$\hat{\mathbf{q}} \cdot \hat{\mathbf{p}} = \cos(\beta-\alpha). \tag{6.46}$$

This demonstrates that this rotation indeed transforms the vector $\hat{\mathbf{p}}$ into $\hat{\mathbf{q}}$. Hence the field a the right-hand side of the conical surface, indicated by the superscript (+), equals

$$\mathbf{E}^{(+)}(\rho,\phi) = T_s[\mathbf{E}^{(-)}(\rho,\phi)\cdot\hat{\mathbf{s}}]\hat{\mathbf{s}} + T_p[\mathbf{E}^{(-)}(\rho,\phi)\cdot\hat{\mathbf{p}}]\hat{\mathbf{q}}, \tag{6.47}$$

$$= T_s\Lambda(\rho)\begin{pmatrix}\sin^2\phi \\ -\cos\phi\sin\phi \\ 0\end{pmatrix} + T_p\Lambda(\rho)\begin{pmatrix}\cos(\beta-\alpha)\cos^2\phi \\ \cos(\beta-\alpha)\cos\phi\sin\phi \\ \sin(\beta-\alpha)\cos\phi\end{pmatrix}. \tag{6.48}$$

The assumption of paraxiality allows us to neglect the relatively small z component of the electric field in Eq. (6.48) that is introduced by refraction of the p-polarized part. In addition, we note that the Fresnel coefficients are related by the expression [Born and Wolf, 1995, Sec. 1.5.2]

$$T_p\cos(\beta-\alpha) = T_s. \tag{6.49}$$

On making use of this in Eq. (6.48), it follows that the expression for the x component simplifies, and that the y component vanishes, and hence we find that

$$\mathbf{E}^{(+)}(\rho,\phi) = T_s\Lambda(\rho)(1,0,0). \tag{6.50}$$

The field on the right-hand side of the axicon surface propagates to the output plane $z=0$. As indicated by Eq. (6.11), this involves a distance $d=\rho\alpha$ in air, giving rise to a phase factor of $\exp(\mathrm{i}k\rho\alpha)$. Hence the field $\mathbf{E}^{(\mathrm{out})}(\rho,\phi)$ in the output plane is given by the expression

$$\mathbf{E}^{(\mathrm{out})}(\rho,\phi) = \exp(\mathrm{i}k\rho\alpha)\,\mathbf{E}^{(+)}(\rho,\phi), \tag{6.51}$$

$$= \exp(\mathrm{i}k\rho\alpha)T_s\Lambda(\rho)(1,0,0). \qquad (x\text{-polarization}) \tag{6.52}$$

We note that this output field has no ϕ-dependence.

Having established the field in the output plane, the field in the half-space $z>0$ can be calculated by using the diffraction formula

$$\mathbf{E}(\mathbf{r}) = \frac{1}{2\pi}\nabla\times\int_{z'=0}\left[\hat{\mathbf{z}}\times\mathbf{E}^{(\mathrm{out})}(\mathbf{r}')\right]\frac{e^{\mathrm{i}kR}}{R}\,\mathrm{d}^2r', \tag{6.53}$$

where $R = |\mathbf{r} - \mathbf{r}'|$. We note that Eq. (6.53) is derived in [Jackson, 1998, Sec. 10.7] for apertures in a plane conducting screen. However, it is valid for any planar surface, as is shown in [Toraldo di Francia, 1955, pp. 218–221]. On substituting from Eq. (6.52) into Eq. (6.53) we find that

$$\mathbf{E}(\mathbf{r}) = \frac{1}{2\pi} \int_{z'=0} \begin{pmatrix} -E_x^{(\mathrm{out})}(\mathbf{r}')\partial_z \\ 0 \\ E_x^{(\mathrm{out})}(\mathbf{r}')\partial_x \end{pmatrix} \frac{e^{\mathrm{i}kR}}{R} \, \mathrm{d}^2 r'. \tag{6.54}$$

Whereas in Eq. (6.48) the z component was introduced by refraction, in Eq. (6.54) it arises as a result from diffraction. Differentiation with respect to z of the factor $\exp(\mathrm{i}kR)/R$ introduces a prefactor z, whereas differentiation with respect to x leads to a factor $x - x'$. Therefore the z component of the diffracted field drops off quickly with increasing z, and may therefore be neglected. Hence we find that

$$\mathbf{E}(\mathbf{r}) = \frac{-T_s}{2\pi} \hat{\mathbf{x}} \int_{z'=0} e^{\mathrm{i}k\rho'\alpha} \Lambda(\rho') \partial_z \frac{e^{\mathrm{i}kR}}{R} \, \mathrm{d}^2 r'. \qquad (x\text{-polarization}) \tag{6.55}$$

We will make use of this expression in Sec. 6.5.

We have thus far considered an incident beam that is linearly polarized along the x direction. Let us now generalize this to beams with an arbitrary, but uniform state of polarization, namely

$$\mathbf{E}^{(\mathrm{in})}(\mathbf{r}) = E_0 \, \hat{\mathbf{u}} \, e^{\mathrm{i}kz}, \tag{6.56}$$

where

$$\hat{\mathbf{u}} = A_x \hat{\mathbf{x}} + A_y \hat{\mathbf{y}}, \tag{6.57}$$

and with A_x and A_y complex-valued constants such that $|A_x|^2 + |A_y|^2 = 1$. For example, $A_y = \mathrm{i}A_x$ represents a circularly polarized beam. Because the axicon is a linear system with rotational symmetry, the resulting field in the half-space $z > 0$ can be found by simply adding the contributions of both field components of Eq. (6.57), i.e.,

$$\begin{aligned}\mathbf{E}(\mathbf{r}) = &-\frac{1}{2\pi}A_xT_s\hat{\mathbf{x}}\int_{z'=0} e^{\mathrm{i}k\rho'\alpha}\Lambda(\rho')\partial_z\frac{e^{\mathrm{i}kR}}{R}\,\mathrm{d}^2r' \\ &-\frac{1}{2\pi}A_yT_s\hat{\mathbf{y}}\int_{z'=0} e^{\mathrm{i}k\rho'\alpha}\Lambda(\rho')\partial_z\frac{e^{\mathrm{i}kR}}{R}\,\mathrm{d}^2r'. \\ &\text{(uniform polarization)}\end{aligned} \tag{6.58}$$

This expression demonstrates that the x and y field components everywhere in the half-space $z > 0$ have the same amplitude and phase relation as the two components of the incident field. We therefore conclude that the state of polarization of the diffracted field is the same as that of the uniformly polarized incident beam.

We next turn our attention to two types of beams with a non-uniform state of polarization.

6.4.2 Radial Polarization

Consider a monochromatic, normally incident beam that is radially polarized, i.e.,

$$\mathbf{E}^{(\mathrm{in})}(\mathbf{r}) = E_0\,\hat{\boldsymbol{\rho}}\,e^{\mathrm{i}kz}, \tag{6.59}$$

$$= E_0\,(\cos\phi, \sin\phi, 0)\,e^{\mathrm{i}kz}. \tag{6.60}$$

The field at the left-hand side of the axicon surface is

$$\mathbf{E}^{(-)}(\mathbf{r}) = E_0T_1e^{\mathrm{i}kz}e^{\mathrm{i}kn[t+\alpha(a-\rho)]}\hat{\boldsymbol{\rho}}, \tag{6.61}$$

$$= \Lambda(\rho)\,(\cos\phi, \sin\phi, 0), \tag{6.62}$$

with $\Lambda(\rho)$ defined by Eq. (6.40). The s-polarized part is zero, i.e.,

$$\mathbf{E}^{(-)}(\rho,\phi)\cdot\hat{\mathbf{s}} = 0, \tag{6.63}$$

whereas the p-polarized part equals

$$\mathbf{E}^{(-)}(\rho,\phi)\cdot\hat{\mathbf{p}} = \Lambda(\rho). \tag{6.64}$$

The field at the right-hand side of the axicon surface is then

$$\mathbf{E}^{(+)}(\rho,\phi) = T_p[\mathbf{E}^{(-)}(\rho,\phi)\cdot\hat{\mathbf{p}}]\,\hat{\mathbf{q}}, \tag{6.65}$$

$$= T_p\,\Lambda(\rho)\begin{pmatrix}\cos(\beta-\alpha)\cos\phi\\ \cos(\beta-\alpha)\sin\phi\\ \sin(\beta-\alpha)\end{pmatrix}. \tag{6.66}$$

If we again neglect the weak z component and make use of Eq. (6.49) we find that the output field in the plane $z = 0$ is given by the formula

$$\mathbf{E}^{(\text{out})}(\rho,\phi) = \exp(\mathrm{i}k\rho\alpha)\,\mathbf{E}^{(+)}(\rho,\phi), \tag{6.67}$$

$$= T_s\,\Lambda(\rho)\exp(\mathrm{i}k\rho\alpha)(\cos\phi,\sin\phi,0).$$
$$\text{(radial polarization)} \tag{6.68}$$

We will momentarily analyze the diffracted field produced by a radially polarized beam by substituting from Eq. (6.68) into Eq. (6.53).

6.4.3 Azimuthal Polarization

Consider a monochromatic, normally incident beam that is azimuthally polarized, i.e.,

$$\mathbf{E}^{(\text{in})}(\mathbf{r}) = E_0\,\hat{\boldsymbol{\phi}}\,e^{\mathrm{i}kz}, \tag{6.69}$$

$$= E_0\,(-\sin\phi,\cos\phi,0)\,e^{\mathrm{i}kz}. \tag{6.70}$$

The field at the left-hand side of the axicon surface is

$$\mathbf{E}^{(-)}(\mathbf{r}) = E_0 T_1 e^{\mathrm{i}kz}e^{\mathrm{i}kn[t+\alpha(a-\rho)]}\hat{\boldsymbol{\phi}},$$
$$= \Lambda(\rho)\,(-\sin\phi,\cos\phi,0), \tag{6.71}$$

with $\Lambda(\rho)$ defined by Eq. (6.40). The s-polarized part is

$$\mathbf{E}^{(-)}(\rho,\phi)\cdot\hat{\mathbf{s}} = -\Lambda(\rho), \tag{6.72}$$

whereas the p-polarized part now equals zero, i.e..

$$\mathbf{E}^{(-)}(\rho,\phi)\cdot\hat{\mathbf{p}} = 0. \tag{6.73}$$

The field at the right-hand side of the axicon surface is therefore

$$\mathbf{E}^{(+)}(\rho, \phi) = T_s[\mathbf{E}^{(-)}(\rho, \phi) \cdot \hat{\mathbf{s}}]\, \hat{\mathbf{s}}, \tag{6.74}$$

$$= -T_s\, \Lambda(\rho)(\sin\phi, -\cos\phi, 0), \tag{6.75}$$

and hence the output field in the plane $z = 0$ is given by the formula

$$\mathbf{E}^{(\text{out})}(\rho, \phi) = \exp(\mathrm{i}k\rho\alpha)\, \mathbf{E}^{(+)}(\rho, \phi), \tag{6.76}$$

$$= -T_s\, \Lambda(\rho) \exp(\mathrm{i}k\rho\alpha)(\sin\phi, -\cos\phi, 0). \quad \text{(azimuthal polarization)} \tag{6.77}$$

We will analyze the field produced by an azimuthally polarized beam by substituting from Eq. (6.77) into Eq. (6.53).

6.5 The electromagnetic field of an axicon

We are now in a position to compare the field on-axis, the transverse intensity, and the intensity in the far zone for each of the three types of polarization that we discussed in the previous section.

6.5.1 The axial intensity

For linear polarization we find, by applying Eq. (6.55) to points on the z axis and using polar coordinates, for the only non-zero component of the electric field the expression

$$\begin{aligned} E_x(0,0,z) &= \frac{z}{2\pi} T_s \int_0^a \int_0^{2\pi} \exp[\mathrm{i}k\rho'\alpha]\Lambda(\rho') \\ &\quad \times \frac{e^{\mathrm{i}kR}}{R^2}\left[\frac{1}{R} - \mathrm{i}k\right] \rho'\, \mathrm{d}\phi' \mathrm{d}\rho', \qquad (6.78) \\ &= zT_s E_0 T_1 e^{\mathrm{i}kn(t+\alpha a)} \int_0^a e^{\mathrm{i}k(1-n)\rho'\alpha} \\ &\quad \times \frac{e^{\mathrm{i}kR}}{R^2}\left[\frac{1}{R} - \mathrm{i}k\right] \rho'\, \mathrm{d}\rho', \qquad (6.79) \end{aligned}$$

where $R = (\rho'^2 + z^2)^{1/2}$.

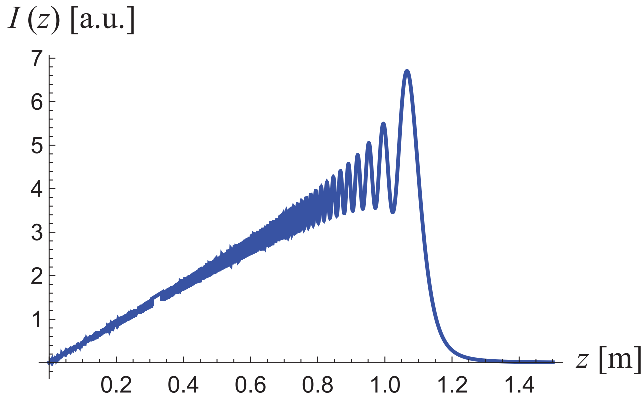

Figure 6.9: The axial intensity distribution $I(z) = |E_x(0,0,z)|^2$ for an incident beam that x-polarized, as given by Eq. (6.79). In this example $n = 1.5$, $a = 1$ cm, $\alpha = 1°$, and $\lambda = 632.8$ nm.

The axial intensity $I(z) = |E_x(0,0,z)|^2$ is plotted in Fig. 6.9. It is seen that for increasing z the intensity oscillates more strongly and then drops suddenly to zero. If we compare this with the scalar result [Eq. (6.21)], for the case of an incident plane wave, i.e., for a beam waist $w_0 \gg a$, the two results are virtually indistinguishable. This should not come as a surprise; in the paraxial regime that we are dealing with, with a base angle $\alpha = 1°$, we expect the scalar case to give results that are similar to that for a linearly polarized field.

For an incident beam that is radially polarized, we find that applying the diffraction integral of Eq. (6.53) to the output field given by Eq. (6.68), yields that both E_x and E_y are zero. As before, we neglect the z component of the electric field.

For an incident beam that is azimuthally polarized, substitution from Eq. (6.77) into Eq. (6.53) yields that all three components of the electric are zero for points along the central axis. Hence we conclude that the axial intensity is non-zero when the incident beam is uniformly polarized, whereas it is zero for an incident beam with radial or azimuthal polarization.

6.5.2 The effective wavelength on axis

The rays that are refracted by the axicon all propagate under an angle $\beta-\alpha$ with the central axis (see Fig. 6.1). We therefore expect the effective axial wavelength λ_{eff} to be given by the expression

$$\lambda_{\text{eff}} = \frac{\lambda}{\cos(\beta-\alpha)}, \tag{6.80}$$

with λ the free-space wavelength of the incident field. We can verify this prediction by numerically determining the succesive zeros of the argument (or phase) of $E_x(0,0,z)$, using Eq. (6.79). This was done for three different values of the axicon base angle α, at a position halfway along the focal line, i.e., at $z = L/2$, [see Eq. (6.1)]. The results are shown in Table 6.3.2, and indicate an excellent agreement within the paraxial regime. This is in contrast with findings reported earlier for systems with a much higher angular aperture [Foley and Wolf, 2005; Visser and Foley, 2005].

base angle α	Eq. (6.80) [nm]	Eq. (6.79) [nm]
1.0°	632.82	632.83
2.5°	632.95	632.95
5.0°	633.41	633.37

Table 6.1: The effective wavelength on axis for an incident beam with $\lambda = 632.8$ nm.

6.5.3 The transverse intensity

Scalar theory, using the method of stationary phase, predicts a normalized transverse intensity profile that is given by Eq. (6.26)

$$I(\rho) = \{J_0[(n-1)k\rho\alpha]\}^2, \quad (z < L), \tag{6.81}$$

which is independent of z. If one does not make use of the stationary phase approximation, scalar theory predicts a more complex behavior, as illustrated by Figs. 6.5–6.8. On the other hand, the electromagnetic analysis for a linearly polarized beam leads to Eq. (6.55), from which we find for the only non-zero field component that

$$
\begin{aligned}
E_x(\mathbf{r}) &= \frac{-1}{2\pi}\int_{z'=0} E_x^{(\mathrm{out})}(\mathbf{r}')\partial_z \frac{e^{\mathrm{i}kR}}{R}\,\mathrm{d}^2r', && (6.82)\\
&= -z\frac{T_sE_0T_1}{2\pi}e^{\mathrm{i}kn(t+\alpha a)}\\
&\quad\times\int_0^a\int_0^{2\pi} e^{\mathrm{i}k\rho'\alpha(1-n)}\frac{e^{\mathrm{i}kR}}{R^2}\left[\mathrm{i}k-1/R\right]\rho'\,\mathrm{d}\phi'\mathrm{d}\rho',\\
&\qquad\text{(linear polarization)} && (6.83)
\end{aligned}
$$

with

$$
R = \sqrt{(x-\rho'\cos\phi')^2+(y-\rho'\sin\phi')^2+z^2}. \tag{6.84}
$$

The results of a numerical evaluation of Eq. (6.83) are, just as for the axial intensity, practically indistinguishable from the scalar results for a large beam waist that were presented in Section 6.3.

The transverse field for the radially polarized case is obtained by substituting from Eq. (6.68) into Eq. (6.53). The resulting expressions are

$$
\begin{aligned}
E_x(\mathbf{r}) &= \frac{-zT_s}{2\pi}\int_0^a\int_0^{2\pi}\Lambda(\rho')\cos\phi'\,e^{\mathrm{i}k\rho'\alpha}(\mathrm{i}k-1/R)\\
&\quad\times\frac{e^{\mathrm{i}kR}}{R^2}\rho'\,\mathrm{d}\phi'\mathrm{d}\rho', && (6.85)\\
E_y(\mathbf{r}) &= \frac{-zT_s}{2\pi}\int_0^a\int_0^{2\pi}\Lambda(\rho')\sin\phi'\,e^{\mathrm{i}k\rho'\alpha}(\mathrm{i}k-1/R)\\
&\quad\times\frac{e^{\mathrm{i}kR}}{R^2}\rho'\,\mathrm{d}\phi'\mathrm{d}\rho'.\\
&\qquad\text{(radial polarization)} && (6.86)
\end{aligned}
$$

The transverse field for the azimuthally polarized case is obtained by

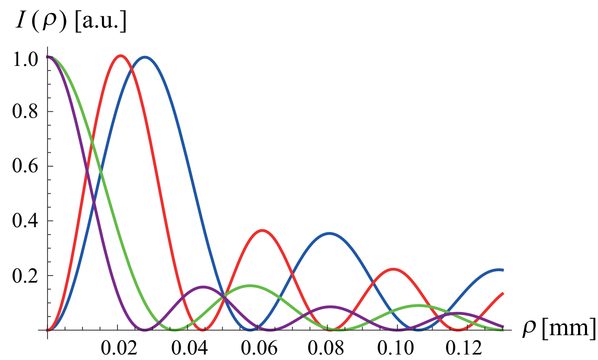

Figure 6.10: Comparison of the transverse intensity distribution for an incident beam that x-polarized ([Eq. (6.83)] (purple and green curves), and for a radially polarized [Eqs. (6.85) and (6.86)] or azimuthally polarized beam [Eqs. (6.87) and (6.88)] (red and blue curves), for $z = 0.5$ m and $z = 1.5$ m. The other parameters are $n = 1.5$, $a = 1$ cm, $\alpha = 1°$, and $\lambda = 632.8$ nm.

substituting from Eq. (6.77) into Eq. (6.53). The resulting expressions are

$$E_x(\mathbf{r}) = \frac{zT_s}{2\pi} \int_0^a \int_0^{2\pi} \Lambda(\rho') \sin\phi' \, e^{\mathrm{i}k\rho'\alpha} (\mathrm{i}k - 1/R) \times \frac{e^{\mathrm{i}kR}}{R^2} \rho' \, \mathrm{d}\phi' \mathrm{d}\rho', \tag{6.87}$$

$$E_y(\mathbf{r}) = \frac{-zT_s}{2\pi} \int_0^a \int_0^{2\pi} \Lambda(\rho') \cos\phi' \, e^{\mathrm{i}k\rho'\alpha} (\mathrm{i}k - 1/R) \times \frac{e^{\mathrm{i}kR}}{R^2} \rho' \, \mathrm{d}\phi' \mathrm{d}\rho'. \quad \text{(azimuthal polarization)} \tag{6.88}$$

On comparing Eqs. (6.87) and (6.88) with Eqs. (6.85) and (6.86), it is seen that an azimuthally polarized beam and a radially polarized beam produce exactly the same transverse intensity distribution. The transverse intensity distributions for a radially or azimuthally polarized beam and a linearly polarized beam are compared in Fig. 6.10. The radially and azimuthally polarized beams produce identical fields with a dark core that is surrounded by rings of decreasing intensity. When the plane of observation is changed from $z = 0.5$ m to $z = 1.5$ m, the central peak of the linearly polarized field broadens (purple and green curves), whereas the first peak of the radially or azimuthally polarized field is seen to move outward (red and blue curves).

6.5.4 The far-zone intensity

Far away from the output plane ($z = 0$), Eq. (6.53) for the diffracted field takes the asymptotic form [Jackson, 1998, Eq. 10.109]

$$\mathbf{E}(r\hat{\mathbf{r}}) = \mathrm{i}k\frac{e^{\mathrm{i}kr}}{2\pi r}\hat{\mathbf{r}} \times \int_{z'=0} \hat{\mathbf{z}} \times \mathbf{E}^{(\mathrm{out})}(\mathbf{r}')e^{-\mathrm{i}k\hat{\mathbf{r}}\cdot\mathbf{r}'}\,\mathrm{d}^2r'. \tag{6.89}$$

A derivation of Eq. (6.89) can be found in Appendix B. On defining the integrals

$$\mathcal{E}_i(r\hat{\mathbf{r}}) = \mathrm{i}k\frac{e^{\mathrm{i}kr}}{2\pi r}\int_{z'=0} E_i^{(\mathrm{out})}(\mathbf{r}')e^{-\mathrm{i}k\hat{\mathbf{r}}\cdot\mathbf{r}'}\,\mathrm{d}^2r' \quad (i = x, y, z), \tag{6.90}$$

where the unit vector corresponding to the directon of observation is given by

$$\hat{\mathbf{r}} = (\sin\theta\cos\phi, \sin\theta\sin\phi, \cos\theta), \tag{6.91}$$

we can derive that, with $\mathbf{E}^{(\mathrm{out})}(\mathbf{r}')$ given by Eq. (6.52),

$$\mathbf{E}(r\hat{\mathbf{r}}) = \begin{pmatrix} -\cos\theta\,\mathcal{E}_x(r\hat{\mathbf{r}}) \\ 0 \\ \sin\theta\cos\phi\,\mathcal{E}_x(r\hat{\mathbf{r}}) \end{pmatrix}. \qquad (x\text{-polarization}) \tag{6.92}$$

Because of the assumption of paraxiality, we have that $\sin\theta \ll \cos\theta$, and the z component of the field may again be neglected. On substituting from Eq. (6.52) into the definition (6.90), we obtain the expression

$$\begin{aligned}\mathcal{E}_x(r\hat{\mathbf{r}}) &= \mathrm{i}k\frac{e^{\mathrm{i}kr}}{2\pi r}T_s\int_0^a e^{\mathrm{i}k\rho'\alpha}\Lambda(\rho')\rho' \\ &\quad\times\left\{\int_0^{2\pi} e^{-\mathrm{i}k\rho'\sin\theta\cos(\phi'-\phi)}\,\mathrm{d}\phi'\right\}\,\mathrm{d}\rho'. \qquad (6.93)\\ &= \mathrm{i}k\frac{e^{\mathrm{i}kr}}{r}T_sT_1E_0e^{\mathrm{i}kn(t+\alpha a)} \\ &\quad\times\int_0^a e^{\mathrm{i}k\rho'\alpha(1-n)}\rho' J_0(k\rho'\sin\theta)\,\mathrm{d}\rho'. \\ &\quad (x\text{-polarization}) \qquad (6.94)\end{aligned}$$

The far-zone intensity

$$I(\theta) = |E_x(r\hat{\mathbf{r}})|^2 = \cos^2\theta|\mathcal{E}_x(r\hat{\mathbf{r}})|^2, \tag{6.95}$$

is plotted in Fig. 6.11 as a function of the angle θ. The intensity is seen to be sharply-peaked, corresponding to a thin, ring-like distribution. In this case the ring subtends an angle $\theta = 0.0087$ at the origin. We note that this is in exact agreement with the geometrical angle of refraction $\beta - \alpha$, as depicted in Fig. 6.1.

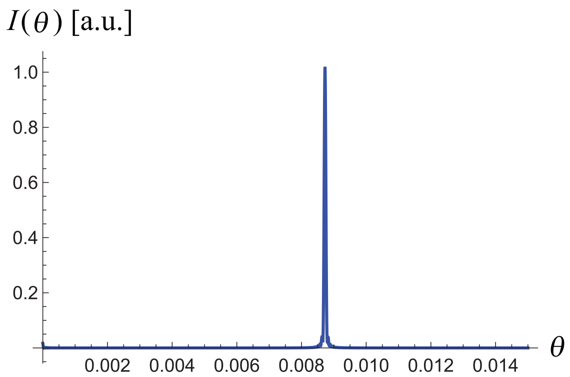

Figure 6.11: The far-zone intensity distribution $I(\theta)$ as given by Eq. (6.95) for an incident beam that is x-polarized. In this example $n = 1.5$, $a = 1$ cm, $\alpha = 1°$, and $\lambda = 632.8$ nm.

When the incident beam is radially polarized, substitution from Eq. (6.68) into Eq. (6.89) yields

$$\mathbf{E}(r\hat{\mathbf{r}}) = \begin{pmatrix} -\cos\theta\,\mathcal{E}_x(r\hat{\mathbf{r}}) \\ -\cos\theta\,\mathcal{E}_y(r\hat{\mathbf{r}}) \\ 0 \end{pmatrix}, \tag{6.96}$$

where

$$\begin{aligned}\mathcal{E}_x(r\hat{\mathbf{r}}) &= k\frac{e^{\mathrm{i}kr}}{r}T_sT_1E_0e^{\mathrm{i}kn(t+\alpha a)}\cos\phi \\ &\quad\times\int_0^a e^{\mathrm{i}k\rho'\alpha(1-n)}\rho' J_1(k\rho'\sin\theta)\,\mathrm{d}\rho',\end{aligned} \tag{6.97}$$

$$\begin{aligned}\mathcal{E}_y(r\hat{\mathbf{r}}) &= k\frac{e^{\mathrm{i}kr}}{r}T_sT_1E_0e^{\mathrm{i}kn(t+\alpha a)}\sin\phi \\ &\quad\times\int_0^a e^{\mathrm{i}k\rho'\alpha(1-n)}\rho' J_1(k\rho'\sin\theta)\,\mathrm{d}\rho'.\\ &\text{(radial polarization)}\end{aligned} \tag{6.98}$$

It is clear from the ϕ dependence in Eqs. (6.97) and (6.98) that the far-zone field is radially polarized, as is to be expected.

In a similar fashion, we find from substituting from Eq. (6.77) into Eq. (6.89) that for an azimuthally polarized beam

$$\mathbf{E}(r\hat{\mathbf{r}}) = \begin{pmatrix} \cos\theta\,\mathcal{E}_x(r\hat{\mathbf{r}}) \\ \cos\theta\,\mathcal{E}_y(r\hat{\mathbf{r}}) \\ 0 \end{pmatrix}, \tag{6.99}$$

with

$$\begin{aligned}\mathcal{E}_x(r\hat{\mathbf{r}}) &= -k\frac{e^{\mathrm{i}kr}}{r}T_sT_1E_0e^{\mathrm{i}kn(t+\alpha a)}\sin\phi \\ &\quad\times\int_0^a e^{\mathrm{i}k\rho'\alpha(1-n)}\rho' J_1(k\rho'\sin\theta)\,\mathrm{d}\rho',\end{aligned} \tag{6.100}$$

$$\begin{aligned}\mathcal{E}_y(r\hat{\mathbf{r}}) &= k\frac{e^{\mathrm{i}kr}}{r}T_sT_1E_0e^{\mathrm{i}kn(t+\alpha a)}\cos\phi \\ &\quad\times\int_0^a e^{\mathrm{i}k\rho'\alpha(1-n)}\rho' J_1(k\rho'\sin\theta)\,\mathrm{d}\rho'.\\ &\text{(azimuthal polarization)}\end{aligned} \tag{6.101}$$

It is seen from Eqs. (6.100) and (6.101) that this field is azimuthally polarized. A comparison of Eqs. (6.96) and (6.99) shows that the far zone intensity produced by radially polarized and azimuthally polarized beams are identical. Moreover, a numerical evaluation shows that the far-zone intensity distribution for these two types of polarization is the same as that for a linearly polarized beam shown in Fig. 6.11. This may seem somewhat counterintuitive because Eq. (6.94) involves a J_0 function, whereas the corresponding expressions for the radial and azimuthal cases contain a J_1 function. However, the respective integrands are all products of two rapidly oscillating functions, namely an exponent and a J_0 or a J_1 Bessel function. Loosely speaking, these oscillations will tend to cancel each other, exept when they occur in unison. This happens when the functional arguments are equal, i.e., when $-k\rho'\alpha(1-n) = k\rho' \sin\theta$, which implies that these integrals will all be approximately zero except when $\sin\theta = \beta - \alpha$. This is precisely the geometrical angle of refraction that was mentioned above in connection with Fig. 6.11.

6.6 Conclusions

We have analyzed the field of a paraxial refractive axicon within the frameworks of geometrical optics, scalar optics and electromagnetic optics. The field along the central axis, and the transition to a ring-like distribution were examined. It was shown that the scalar theory and the electromagnetic theory are in very good agreement for the case of an incident beam that is linearly polarized. However, scalar theory cannot describe the field that is produced when the incident beam is radially polarized or azimuthally polarized. In those two latter cases the axial intensity is zero, and the transverse intensity is a field with a dark core surrounded by rings of decreasing intensity. In the far-zone, the axicon produces a ring-like field whose intensity distribution is independent of the state of polarization of the incident field.

Acknowledgments

This material is based upon work supported by the Air Force Office of Scientific Research under award number FA9550-16-1-0119.

Appendix A - Derivation of Eq. (6.23)

In this appendix the stationary-phase calculation of the axicon field is outlined, c.f. [Friberg, 1996]. We note that this method applies to systems for which the Fresnel number $N = a^2/(\lambda L) \gg 1$, see [Zapata-Rodriguez and Sanchez-Losa, 2005] To this end, let us assume that $f(\rho')$ and $g(\rho')$ are two well-behaved functions in an integral in the form of

$$F(k) = \int_0^a f(\rho') \exp[\mathrm{i}kg(\rho')]\, \mathrm{d}\rho'. \tag{A-1}$$

If k tends to infinity, the general solution of this integral is [Mandel and Wolf, 1995, Sec. 3.3]

$$F(k) \sim \left(\frac{2\pi}{k}\right)^{1/2} \frac{\exp(\pm \mathrm{i}\pi/4)}{|g''(\rho'_c)|^{1/2}} f(\rho'_c) \exp[\mathrm{i}kg(\rho'_c)],$$
$$(k \to \infty), \tag{A-2}$$

where ρ'_c is known as the critical point, which is obtained when the derivative of $g(\rho')$ is zero, i.e., $g'(\rho') = 0$. From comparing Eqs. (6.21) and (A-1), it is clear that

$$f(\rho') = \exp(-\rho'^2/w_0^2) J_0\left(\frac{k\rho\rho'}{z}\right)\rho', \tag{A-3}$$

$$g(\rho') = (1-n)\rho'\alpha + \frac{\rho'^2}{2z}. \tag{A-4}$$

Thus, the derivatives of $g(\rho')$ are

$$g'(\rho') = (1-n)\alpha + \frac{\rho'}{z}, \tag{A-5}$$

$$g''(\rho') = \frac{1}{z}. \tag{A-6}$$

The fact that $g''(\rho') > 0$ implies that the plus sign must be chosen in Wq. (A-2). It follows immediately from Eq. (A-5) that the critical point

$$\rho'_c = z(n-1)\alpha. \tag{A-7}$$

Substitution from Eqs. (A-3), (A-4) and (A-6) into Eq. (A-2) yields Eq. (6.23). Notice that the interior critical point is confined to the range of integration, i.e.

$$0 \leq \rho_c' \leq a. \tag{A-8}$$

This means, according to Eq. (A-7), that the method of stationary phase predicts a field that is identically zero when

$$z > \frac{a}{\alpha(n-1)}. \tag{A-9}$$

As is well known, geometrical optics may be regarded as the asymptotic limit of physical optics as the wavenumber k tends to infinity [Born and Wolf, 1995, Sec. 3.1]. Therefore, Eq. (A-2) reproduces the geometrical optics result that the field is zero when z exceeds the focal line length L. It is easily verified numerically that L, as given by Eq. (6.1), is indeed very well approximated by the right-hand side of Eq. (A-9).

Appendix B - Derivation of Eq. (6.89)

We begin by applying a product rule to Eq. (6.53), namely

$$\begin{aligned}\nabla \times (\mathbf{A} \times \mathbf{B}) = \mathbf{A}(\nabla \cdot \mathbf{B}) - (\mathbf{A} \cdot \nabla)\mathbf{B} \\ + (\mathbf{B} \cdot \nabla)\mathbf{A} - \mathbf{B}(\nabla \cdot \mathbf{A}).\end{aligned} \tag{B-1}$$

Since $\mathbf{A} = \hat{\mathbf{z}}$ is a constant vector, the third and fourth terms are both zero. Furthermore,

$$\nabla \cdot \mathbf{B} = \nabla \cdot \left(\mathbf{E}^{(\text{out})}(\mathbf{r}') \frac{e^{\mathrm{i}kR}}{R} \right), \tag{B-2}$$

$$\begin{aligned} &= E_x^{(\text{out})}(\mathbf{r}') \partial_x \frac{e^{\mathrm{i}kR}}{R} + E_y^{(\text{out})}(\mathbf{r}') \partial_y \frac{e^{\mathrm{i}kR}}{R} \\ &+ E_z^{(\text{out})}(\mathbf{r}') \partial_z \frac{e^{\mathrm{i}kR}}{R}, \end{aligned} \tag{B-3}$$

$$\begin{aligned} &= \frac{E_x^{(\text{out})}(\mathbf{r}') e^{\mathrm{i}kR} \left[\mathrm{i}k(x - x') - (x - x')/R \right]}{R^2} \\ &+ \frac{E_y^{(\text{out})}(\mathbf{r}') e^{\mathrm{i}kR} \left[\mathrm{i}k(y - y') - (y - y')/R \right]}{R^2} \\ &+ \frac{E_z^{(\text{out})}(\mathbf{r}') e^{\mathrm{i}kR} \left[\mathrm{i}kz - z/R \right]}{R^2}. \end{aligned} \tag{B-4}$$

Because in the far zone $R \gg \lambda$, we may write

$$\begin{aligned} \nabla \cdot \mathbf{B} = &\frac{E_x^{(\text{out})}(\mathbf{r}') \mathrm{i}k(x - x') e^{\mathrm{i}kR}}{R^2} \\ &+ \frac{E_y^{(\text{out})}(\mathbf{r}') \mathrm{i}k(y - y') e^{\mathrm{i}kR}}{R^2} \\ &+ \frac{E_z^{(\text{out})}(\mathbf{r}') \mathrm{i}kz e^{\mathrm{i}kR}}{R^2}. \end{aligned} \tag{B-5}$$

Thus, the first term on the right-hand side of Eq. (B-1) becomes

$$\begin{aligned} \mathbf{A}(\nabla \cdot \mathbf{B}) = \hat{\mathbf{z}} \Bigg[&\frac{E_x^{(\text{out})}(\mathbf{r}') \mathrm{i}k(x - x') e^{\mathrm{i}kR}}{R^2} \\ &+ \frac{E_y^{(\text{out})}(\mathbf{r}') \mathrm{i}k(y - y') e^{\mathrm{i}kR}}{R^2} \\ &+ \frac{E_z^{(\text{out})}(\mathbf{r}') \mathrm{i}kz e^{\mathrm{i}kR}}{R^2} \Bigg]. \end{aligned} \tag{B-6}$$

For the second term of Eq. (B-1) we have that

$$-(\mathbf{A} \cdot \nabla)\mathbf{B} = -\mathbf{E}^{(\text{out})}(\mathbf{r}') \partial_z \frac{e^{\mathrm{i}kR}}{R}, \tag{B-7}$$

Making again use of the fact that $R \gg \lambda$, we obtain the result

$$-(\mathbf{A}\cdot\nabla)\mathbf{B} = -\mathbf{E}^{(\mathrm{out})}(\mathbf{r}')\mathrm{i}kz\frac{e^{\mathrm{i}kR}}{R^2}. \tag{B-8}$$

Thus we can re-write Eq. (6.53) as

$$\begin{aligned}\mathbf{E}(r\hat{\mathbf{r}}) = \frac{\mathrm{i}k}{2\pi}\int_{z'=0} &\Big\{\hat{\mathbf{z}}\Big[E_x^{(\mathrm{out})}(\mathbf{r}')(x-x') \\ &+ E_y^{(\mathrm{out})}(\mathbf{r}')(y-y') + E_z^{(\mathrm{out})}(\mathbf{r}')z\Big] \\ &- \mathbf{E}^{(\mathrm{out})}(\mathbf{r}')(\hat{\mathbf{z}}\cdot\mathbf{r})\Big\}\,\frac{e^{\mathrm{i}kR}}{R^2}\,\mathrm{d}^2r'. \end{aligned}\tag{B-9}$$

Because x' and y' are bounded by the size of the axicon radius a, we may neglect the terms in x' and y' as $R\to\infty$. Also, we use that in that limit $kR \approx kr - k\hat{\mathbf{r}}\cdot\mathbf{r}'$, and that $1/R^2 \approx 1/r^2$. This yields

$$\begin{aligned}\mathbf{E}(r\hat{\mathbf{r}}) &= \frac{\mathrm{i}ke^{\mathrm{i}kr}}{2\pi r^2}\int_{z'=0}\Big\{\hat{\mathbf{z}}\Big[E_x^{(\mathrm{out})}(\mathbf{r}')x + E_y^{(\mathrm{out})}(\mathbf{r}')y \\ &\quad + E_z^{(\mathrm{out})}(\mathbf{r}')z\Big] - \mathbf{E}^{(\mathrm{out})}(\mathbf{r}')\,(\hat{\mathbf{z}}\cdot\mathbf{r})\Big\}\,e^{-\mathrm{i}k\hat{\mathbf{r}}\cdot\mathbf{r}'}\mathrm{d}^2r', \qquad \text{(B-10)} \\ &= \frac{\mathrm{i}ke^{\mathrm{i}kr}}{2\pi r}\int_{z'=0}\Big[\hat{\mathbf{z}}\left(\mathbf{E}^{(\mathrm{out})}(\mathbf{r}')\cdot\hat{\mathbf{r}}\right) \\ &\quad - \mathbf{E}^{(\mathrm{out})}(\mathbf{r}')(\hat{\mathbf{z}}\cdot\hat{\mathbf{r}})\Big]\,e^{-\mathrm{i}k\hat{\mathbf{r}}\cdot\mathbf{r}'}\mathrm{d}^2r', \qquad \text{(B-11)}\end{aligned}$$

Using the “BACCAB” rule

$$\mathbf{A}\times(\mathbf{B}\times\mathbf{C}) = \mathbf{B}(\mathbf{A}\cdot\mathbf{C}) - \mathbf{C}(\mathbf{A}\cdot\mathbf{B}), \tag{B-12}$$

we finally obtain the formula

$$\mathbf{E}(r\hat{\mathbf{r}}) = \frac{\mathrm{i}ke^{\mathrm{i}kr}}{2\pi r}\hat{\mathbf{r}}\times\int_{z'=0}\hat{\mathbf{z}}\times\mathbf{E}^{(\mathrm{out})}(\mathbf{r}')e^{-\mathrm{i}k\hat{\mathbf{r}}\cdot\mathbf{r}'}\mathrm{d}^2r', \tag{B-13}$$

which is Eq. (6.89).

Bibliography

A. ALU AND N. ENGHETA, "Cloaking a sensor", *Phys. Rev. Lett.* 102, 233901 (2009).

A. ALU AND N. ENGHETA, "How does zero forward-scattering in magnetodielectric nanoparticles comply with the optical theorem?", *J. Nanophoton* 4, 041590 (2010).

N.W. ASHCROFT AND N.D. MERMIN, *Solid State Physics*, Harcourt, Orlando (1976).

M.J. BERAN AND G.B. JR. PARRENT, *Theory of Partial Coherence*, Prentice Hall, Englewood Cliffs (1964).

M. BERTOLOTTI, A. FERRARI, AND L. SEREDA, "Coherence properties of nonstationary polychromatic light sources", *J. Opt. Soc. Am. B* 12, pp. 341–347 (1995).

M. BERTOLOTTI, L. SEREDA, AND A. FERRARI, "Application of the spectral representation of stochastic processes to the study of nonstationary light: a tutorial", *J. Eur. Opt. Soc. A* 6, pp. 153–171 (1997).

G. BICKEL, G. HAUSLER, AND M. HAUL, "Triangulation with expanded range of depth", *Opt. Eng.* 24, pp. 975–977 (1985).

C.F. BOHREN AND D.R. HUFFMAN, *Absorption and Scattering of Light by Small Particles*, Wiley, New York (2004).

M. Born and E. Wolf, *Principles of Optics: Electromagnetic Theory of Propagation, Interference and Diffraction of Light*, Cambridge University Press, Cambridge (1995).

S. Brinkmann, T. Dresel, R. Schreiner, and J. Schwider, "Axicon-type test interferometer for cylindrical surfaces", Simulation and Experiment in Laser Metrology, pp. 82–87, Akademie Verlag, Berlin (1996).

T.G. Brown, *Unconventional polarization states: beam propagation, focusing, and imaging*, volume 56 of *Progress in Optics*, Elsevier, Amsterdam (2011).

D. Cabaret, S. Rossano, and C. Brouder, "Mie scattering of a partially coherent beam", *Opt. Commun.* 150, pp. 239–250 (1998).

P.S. Carney and E. Wolf, "An energy theorem for scattering of partially coherent beams", *Opt. Commun.* 155, pp. 1–6 (1998).

P.S. Carney, E. Wolf, and G.S. Agarwal, "Statistical generalizations of the optical cross-section theorem with application to inverse scattering", *J. Opt. Soc. Am. A* 14, pp. 3366–3371 (1997).

W. H Carter and E. Wolf, "Coherence properities of Lambertian and non-Lambertian sources", *J. Opt. Soc. Am. A* 65, pp. 1067–1071 (1975).

W.H. Carter and E. Wolf, "Scattering from quasi-homogeneous media", *Opt. Commun.* 67, pp. 85–90 (1988).

T. van Dijk, D.G. Fischer, T.D. Visser, and E. Wolf, "Effects of spatial coherence on the angular distribution of radiant intensity generated by scattering on a sphere", *Phys. Rev. Lett.* 104, 173902 (2010).

T. van Dijk, G. Gbur, and T.D. Visser, "Shaping the focal intensity distribution using spatial coherence", *J. Opt. Soc. Am. A* 25, pp. 575–581 (2008).

C. Ding, Y. Cai, Y. Zhang, and L. Pan, "Scattering of a partially coherent plane-wave pulse on a deterministic sphere", *Phys. Lett. A* 376, pp. 2697–2702 (2012).

Z. Ding, H. Ren, Y. Zhao, J.S. Nelson, and Z. Chen, "High-resolution optical coherence tomography over a large depth range with an axicon lens", *Opt. Lett.* 27, pp. 243–245 (2002).

M. Dušek, "Diffraction of partially coherent beams on three-dimensional periodic structures and the angular shifts of the diffraction maxima", *Phys. Rev. E* 52, pp. 6833–6840 (1995).

J. Durnin, J.J. Miceli Jr., and J.H. Eberly, "Diffraction-free beams", *Phys. Rev. Lett.* 58, pp. 1499–1501 (1987).

R. Dutta, K. Saastamoinen, J. Turunen, and A.T. Friberg, "Broadband spatiotemporal axicon fields", *Opt. Express* 22, pp. 25015–25026 (2014).

W.R. Edmonds, "Imaging properties of a conic axicon", *Appl. Opt.* 13, pp. 1762–1764 (1974).

D.G. Fischer, T. van Dijk, T.D. Visser, and E. Wolf, "Coherence effects in Mie scattering", *J. Opt. Soc. Am. A* 29, pp. 78–84 (2012).

J. T. Foley and E. Wolf, "Wave-front spacing in the focal region of high-numerical-aperture systems", *Opt. Lett.* 30, pp. 1312–1314 (2005).

A.T. Friberg, "Stationary phase analysis of generalized axicons", *J. Opt. Soc. Am. A.* 13, pp. 743–750 (1996).

S. Fujiwara, "Optical properties of conic surfaces. i. reflecting cone", *J. Opt. Soc. Am. A.* 52, 3, pp. 287–292 (1962).

B. Garcia-Camara, R. Alcaraz de la Osa, J. M. Saiz, F. Gonzalez, and F. Moreno, "Directionality in scattering by nanoparticles: Kerker's null-scattering conditions revisited", *Opt. Lett.* 36, pp. 728–730 (2011).

G. Gbur and T.D. Visser, "Can spatial coherence effects produce a local minimum of intensity at focus?", *Opt. Lett.* 28, pp. 1627–1629 (2003).

G. Gbur and T.D. Visser, "The structure of partially coherent fields", volume 55 of *Progress in Optics*, pp. 285–329, Elsevier, Amsterdam (2010).

G. Gbur, T.D. Visser, and E. Wolf, "Anomalous behaviour of spectra near phase singularities of focused waves", *Phys. Rev. Lett.* 88, 013901 (2002).

J.M. Geffrin, B. Garcia-Camara, R. Gomez-Medina, P. Albella, L.S. Froufe-Perez, C. Eyraud, A. Litman, R. Vaillon, F. Gonzalez, M. Nieto-Vesperinas, J.J. Saenz, and F. Moreno, "Magnetic and electric coherence in forward- and back-scattered electromagnetic waves by a single dielectric subwavelength sphere", *Nature Commun.* 3, 1171 (2012).

J.W. Goodman, *Statistical Optics*, Wiley, New York (1985).

F. Gori, C. Palma, and M. Santarsiero, "A scattering experiment with partially coherent light", *Opt. Commun.* 74, pp. 353–356 (1990).

K. Gottfried and Tung-Mow Yan, *Quantum Mechanics: Fundamentals*, Springer, New York (2003).

J.-J. Greffet, M. De La Cruz-Gutierrez, P.V. Ignatovich, and A. Radunsky, "Influence of spatial coherence on scattering by a particle", *J. Opt. Soc. Am. A* 20, pp. 2315–2320 (2003).

A. Haussmann, "Rainbows in nature: recent advances in observation and theory", *Eur. J. Phys.* 37, 063001 (2016).

W. Hergert and T. Wriedt (eds.), *The Mie Theory – Basics and Applications*, Springer, Heidelberg (2012).

H.E. Hernandez-Figueroa, E. Recami, and M. Zamboni-Rached (eds.), *Non-Diffracting Waves*, Wiley, Weinheim (2014).

B.J. Hoenders and M. Bertolotti, "Theory of partial coherence for weakly periodic media", *J. Opt. Soc. Am. A* 22, pp. 2682–2690 (2005).

Z.L. Horvath and Zs. Bor, "Diffraction of short pulses with boundary diffraction wave theory", *Phys. Rev. E* 63, 026601 (2001).

H.C. van de Hulst, *Light Scattering from Small Particles*, Dover, New York (1981).

M.W. Hyde IV, "Physical optics solution for the scattering of a partially coherent wave from a circular cylinder", *Opt. Commun.* 338, pp. 233—239 (2015).

J.D. Jackson, *Classical Electrodynamics (3rd ed.)*, Wiley, New York (1998).

R.W. James, *X-Ray Crystallography (4th ed.)*, Methuen and Co., London (1950).

J. Jannson, T. Jannson, and E. Wolf, "Spatial coherence discrimination in scattering", *Opt. Lett.* 13, pp. 1060–1062 (1988).

Z. Jaroszewicz, *Axicons - Design and Propagation Properties*, SPIE Polish Chapter, Warsaw (1997).

C.J. Joachain, *Quantum Collision Theory (3rd ed.)*, Elsevier, Amsterdam (1987).

M. Kerker, D.-S. Wang, and C. L. Giles, "Electromagnetic scattering by magnetic spheres", *J. Opt. Soc. Am.* 73, pp. 765–767 (1983).

C. Kittel, *Introduction to Solid State Physics (6th ed.)*, Wiley, New York (1986).

O. Korotkova, "Design of weak scattering media for controllable light scattering", *Opt. Lett.* 40, pp. 284–287 (2015).

U. Levy, S. Derevyanko, and Y. Silberberg, "Light propagation in free space", volume 61 of *Progress in Optics*, pp. 237–281, Elsevier, Amsterdam (2016).

J. Lindberg, T. Setälä, M. Kaivola, and A.T. Friberg, "Spatial coherence effects in light scattering from metallic nanocylinders", *J. Opt. Soc. Am. A* 23, pp. 1349–1358 (2006).

J. Liu, L. Bi, P. Yang, and G.W. Kattawar, "Scattering of partially coherent electromagnetic beams by water droplets and ice crystals", *J. Quant. Spectrosc. Radiat. Transf.* 134, pp. 74–84 (2014).

L. Mandel and E. Wolf, *Optical Coherence and Quantum Optics*, Cambridge University Press, Cambridge (1995).

A.S. Marathay, *Elements of Optical Coherence Theory*, Wiley, New York (1982).

J.H. McLeod, "The axicon: a new type of optical element", *J. Opt. Soc. Am.* 44, pp. 592–597 (1954).

J.H. McLeod, "Axicons and their uses", *J. Opt. Soc. Am.* 50, pp. 166–169 (1960).

G. Mie, "Beiträge zur Optik trüber Medien, speziell kolloidaler Metallösungen", *Ann. der Physik* 25, pp. 377–445 (1908).

M.I. Mishchenko, J.W. Hovenier, and L.D. Travis (eds.), *Light Scattering by Nonspherical Particles*, Academic Press, San Diego (2000).

R.R. Naraghi, S. Sukhov, and A. Dogariu, "Directional control of scattering by all-dielectric core-shell spheres", *Opt. Lett.* 40, pp. 585–588 (2015).

M. Nieto-Vesperina, R. Gomez-Medina, and J.J. Saenz, "Angle-suppressed scattering and optical forces on submicrometer dielectric particles", *J. Opt. Soc. Am. A* 28, pp. 54–59 (2011).

F.W.J. Olver, D.W. Lozier, R.F. Boisvert, and C.W. Clark (eds.), *NIST Digital Library of Mathematical Functions*, Cambridge University Press, Cambridge (2010).

A. Papoulis, *Probability, Random Variables and Stochastic Processes (3rd ed.)*, McGraw Hill, New York (1991).

J. Perina, *Coherence of Light (2nd ed.)*, Reidel, Dordrecht (1985).

S. Person, M. Jain, Z. Lapin, JJ. Saenz, G. Wicks, and L. Novotny, "Demonstration of zero optical backscattering from single nanoparticles", *Nano Lett.* 13, pp. 1806–1809 (2013).

N. Radwell, R.D. Hawley, J.B Gotte, and S. Franke-Arnold, "Achromatic vector vortex beams from a glass cone", *Nature Commun.* 7, 10564 (2016).

S.B. Raghunathan, T. van Dijk, E.J.G. Peterman, and T.D. Visser, "Experimental demonstration of an intensity minimum at the focus of a laser beam created by spatial coherence: Application to optical trapping of dielectric particles", *Opt. Lett.* 35, pp. 4166–4168 (2010).

Q. Ren and R. Birngruber, "Axicon: A new laser beam delivery system for corneal surgery", *IEEE J. Quantum Electron.* 26, pp. 2305–2308 (1990).

B. Richards and E. Wolf, "Electromagnetic diffraction in optical systems. ii. structure of the image field in an aplanatic system", *Proc. R. Soc. London, Ser. A* 253, pp. 358–379 (1959).

M. Rioux, R. Tremblay, and P.A. Bélanger, "Linear, annular, and radial focusing with axicons and applications to laser machining", *Appl. Opt.* 17, pp. 1532–1536 (1978).

F.P. Schafer, "On some properties of axicons", *Appl. Phys. B* 39, pp. 1–8 (1986).

H.F. Schouten and T.D. Visser, "The role of correlation functions in the theory of optical wave fields", *Am. J. Phys.* 76, pp. 867–871 (2008).

B. Shao, S.C. Esener, J.M. Nascimento, E.L. Botvinick, and M.W. Berns, "Dynamically adjustable annular laser trapping based on axicons", *Appl. Opt.* 45, pp. 6421–6428 (2006).

J. Sochacki, A. Kolodziejczyk, Z. Jaroszewicz, and S. Bara, "Nonparaxial design of generalized axicons", *Appl. Opt.* 31, pp. 5326–5330 (1992).

L.M. Soroko, "Axicons and meso-optical imaging devices", volume 27 of *Progress in Optics*, pp. 109–160, Elsevier, Amsterdam (1989).

J. Tervo and J. Turunen, "Generation of vectorial propagation-invariant fields by polarization-grating axicons", *Opt. Commun.* 192, pp. 13–18 (2001).

G. Toraldo di Francia, *Electromagnetic Waves*, Interscience, New York (1955).

G.J. Troup, *Optical Coherence Theory-recent Developments*, Methuen, London (1985).

J. Turunen and A.T. Friberg, "Electromagnetic theory of reflaxicon fields", *Pure Appl. Opt.* 2, pp. 539–547 (1993a).

J. Turunen and A.T. Friberg, "Self-imaging and propagation-invariance in electromagnetic fields", *Pure Appl. Opt.* 2, pp. 51–60 (1993b).

J. Turunen and A.T. Friberg, "Propagation-invariant optical fields", volume 54 of *Progress in Optics*, pp. 1–88, Elsevier, Amsterdam (2009).

J. Turunen, A. Vasara, and A.T. Friberg, "Holographic generation of diffraction-free beams", *Appl. Opt.* 27, pp. 3959–3962 (1988).

A. Vasara, J. Turunen, and A.T. Friberg, "Realization of general nondiffracting beams with computer-generated holograms", *J. Opt. Soc. Am. A.* 6, pp. 1748–1754 (1989).

I. Velchev and W. Ubachs, "Higher-order stimulated Brillouin scattering with nondiffracting beams", *Opt. Lett.* 26, pp. 530–532 (2001).

T.D. Visser, D.G. Fischer, and E. Wolf, "Scattering of light from quasi-homogeneous sources by quasi-homogeneous media", *J. Opt. Soc. Am. A* 23, pp. 1631–1638 (2006).

T.D. Visser and J.T. Foley, "On the wavefront-spacing of focused, radially polarized beams", *J. Opt. Soc. Am. A.* 22, pp. 2527–2531 (2005).

T.D. Visser and E. Wolf, "Spectral anomalies near phase singularities in partially coherent focused wavefields", *J. of Opt. A* 5, pp. 371–373 (2003).

Y. Wang, D. Kuebel, T.D. Visser, and E. Wolf, "Creating new von Laue patterns in crystal scattering with partially coherent sources", *Phys. Rev. A* 94, 033812 (2016a).

Y. Wang, H.F. Schouten, and T.D. Visser, "Tunable, anomalous Mie scattering using spatial coherence", *Opt. Lett.* 40, pp. 4779–4782 (2015a).

Y. Wang, H.F. Schouten, and T.D. Visser, "Strong suppression of forward or backward Mie scattering by using spatial coherence", *J. Opt. Soc. Am. A* 33, pp. 513–518 (2016b).

Y. Wang, S. Yan, A.T. Friberg, D. Kuebel, and T.D. Visser, "The electromagnetic field produced by a refractive axicon", (to be submitted) (2017).

Y. Wang, S. Yan, D. Kuebel, and T.D. Visser, "Dynamic control of light scattering using spatial coherence", *Phys. Rev. A* 92, 013806 (2015b).

E. Wolf, *Introduction to the Theory of Coherence and Polarization of Light*, Cambridge University Press, Cambridge (2007).

E. Wolf, "Diffraction of radiation of any state of spatial coherence on media with periodic structure", *Opt. Lett.* 38, pp. 4023–4025 (2013).

E. Wolf and D.F.V. James, "Correlation-induced spectral changes", *Rep. Prog. Phys.* 59, pp. 771–818 (1996).

T. Wulle and S. Herminghaus, "Nonlinear optics of Bessel beams", *Phys. Rev. Lett.* 70, pp. 1401–1405 (1993).

Y.-M. Xie, W. Tan, and Z.-G. Wang, "Anomalous forward scattering of dielectric gain nanoparticles", *Opt. Express* 23, pp. 2091–2100 (2015).

C.J. Zapata-Rodriguez and A. Sanchez-Losa, "Three-dimensional field distribution in the focal region of low-Fresnel-number axicons", *J. Opt. Soc. Am. A.* 23, pp. 3016–3026 (2005).

Summary in Dutch

De Nederlandstalige titel van dit proefschrift luidt "Bessel correlaties en Bessel bundels."

Het eerste hoofdstuk bevat een informele bespreking van twee fundamentele concepten die we veelvuldig gebruiken, namelijk coherentietheorie en verstrooiingstheorie.

Hoofdstuk 2 handelt over hoe de verdeling van het verstrooide veld kan worden gecontroleerd met behulp van een inkomend veld dat ruimtelijk partieel coherent is. We nemen aan dat het medium Gaussisch gecorreleerd is. Gebruik makend van de eerste-orde Born benadering wordt aangetoond dat een Gaussisch gecorreleerd veld een diffuse intensiteitsverdeling geeft, waarbij het maximum steeds in de voorwaartse richting is. Een J_0 Bessel-gecorreleerd veld levert een situatie op die kwalitatief anders is. De intensiteit in de voorwaartse richting kan nu sterk worden onderdrukt.

In het derde hoofdstuk bespreken we een klassiek probleem, namelijk verstrooiing aan een homogene bol, de zogenaamde Mie verstrooiing. In tegenstelling tot hoofdstuk 2 maken we nu geen gebruik van de Born benadering en is het medium niet stochastisch maar deterministisch. Het inkomende veld is wederom J_0 Bessel-gecorreleerd. Het blijkt dat de hoek van maximale verstrooiing ingesteld kan worden door de coherentielengte van het inkomende veld te variëren. De totale intensiteit van het verstrooide veld blijft daarbij gelijk.

Hoofdstuk 4 beschrijft de relatie tussen voorwaartse Mie verstrooiing en reflectie van een veld dat spatieel volledig coherent is, en voorwaartse verstrooiing en reflectie van een Bessel-gecorreleerd veld. De afgeleide vergelijkingen worden gebruikt om te laten zien dat óf het voorwaarts verstrooide veld, óf het gereflecteerde veld meerdere ordes van grootte

onderdrukt kan worden door instelling van de coherentielengte van het inkomende veld.

In hoofdstuk 5 beschrijven we de verstrooiing van partieel coherent licht aan een willekeurige kristalstructuur van identieke puntverstrooiers. We beschouwen daarna het specifieke geval van een orthorhombisch kristal. Het von Laue patroon blijkt sterk afhankelijk te zijn van de coherentie van het invallende veld. Voor een Gaussische correlatie worden de diffractie pieken breder dan in het coherente geval. Wederom blijkt dat een J_0 Bessel-gecorreleerd veld een andere situatie oplevert. In de voorwaartse richting ontstaan gekleurde ellipsvormige von Laue patronen. In reflectie ontstaan quasi-monochromatische ringen die elkaar overlappen.

In hoofdstuk 6 tenslotte, verleggen we de aandacht van Bessel correlaties naar coherente bundels met een intensiteitsprofiel dat beschreven wordt door een Bessel functie. Zulke bundels kunnen worden gegenereerd met een zogenaamd axicon. Dat is een kegelvormige lens met rotatiesymmetrie. We gebruiken drie verschillende formalismes om het veld te beschrijven: geometrische optica, scalaire optica en elektromagnetische optica. In het paraxiale regime blijken, zoals verwacht, de resultaten van een scalaire analyse en die van een elektrodynamische beschrijving van een lineair gepolariseerd veld goed overeen te komen. We analyseren de overgang van het Besselprofiel direct achter de lens, naar een ringvormig profiel in het verre veld. Als het inkomende veld radieel of azimuthaal gepolariseerd is, is een elektromagnetische behandeling noodzakelijk. Het blijkt dat de transversale intensiteitsverdeling sterk afhankelijk is van de polarisatietoestand van de inkomende bundel. Het ringvormige profiel in het verre veld is echter hiervan onafhankelijk.

Dit proefschrift is gebaseerd op een vijftal artikelen. Vier ervan zijn reeds gepubliceerd, het vijfde artikel wordt binnenkort ingediend.

Acknowledgments

First I would like to express my sincere gratitude to my advisor: Prof. Dr. Taco D. Visser for the “tough” training during my PhD study and related research, for his professionality, motivation and broad knowledge. He is an excellent PhD advisor and mentor for my life.

Second I would like to thank my thesis reading committee: Prof. Dr. W.M.G. Ubachs, Prof. Dr. B.J. Hoenders, Prof. Dr. G.J. Gbur, Prof. Dr. P.S. Carney, and Dr. H.F. Schouten, for their insightful comments and encouragements. And special thanks go to Dr. Greg Gbur, for your knowledge and friendship.

Third my sincere thanks go to my co-authors Prof. Dr. Emil Wolf, Dr. Dave Kuebel and Dr. Hugo F. Schouten. Thank you for your well-trained physical thinking and enjoyable collaboration. My special thanks go to the sweet old gentleman and great physicist: Prof. Dr. Emil Wolf.

Then I thank my fellow classmates in the $14103 - 2$ PhD class of the School of Marine Science and Technology, Northwestern Polytechnical University, in Xi’an, China for the three years of wonderful company, especially from Xinxin Guo and Jiaoyang Su.

Last but not least, I would like to thank my family: my parents and my sister for generously supporting me spiritually throughout writing this thesis and for understanding and caring. Thanks for all the people who have influenced me and who encouraged me to be my best.

Yangyundou Wang
March 2017